

Library Copy
A A21L125 R01

c.1.
Copy 43
RM SL53I24

~~CONFIDENTIAL~~

NACA

RESEARCH MEMORANDUM

for the

U. S. Air Force

INVESTIGATION OF THE EFFECTS OF PROPELLER OPERATION

ON THE LOW-SPEED STABILITY AND CONTROL

CHARACTERISTICS OF A 1/6-SCALE MODEL

OF A REVISED CONFIGURATION OF THE

REPUBLIC XF-84H AIRPLANE

By William C. Sleeman, Jr.

Langley Aeronautical Laboratory
Langley Field, Va.

CLASSIFIED DOCUMENT

This material contains information affecting the National Defense of the United States within the meaning of the espionage laws, Title 18, U.S.C., Secs. 793 and 794, the transmission or revelation of which in any manner to an unauthorized person is prohibited by law.

Below 3-7-72

NATIONAL ADVISORY COMMITTEE

FOR AERONAUTICS

WASHINGTON

~~CONFIDENTIAL~~



NATIONAL ADVISORY COMMITTEE FOR AERONAUTICS

CLASSIFICATION CHANGED
 RESEARCH MEMORANDUM
 PREPARED FOR THE
 for the DIRECTOR, OF NASA HQ, DC119
 270 8-21-71, H. G. Weiss,
 U. S. Air Force
 Blm 3-7-72

INVESTIGATION OF THE EFFECTS OF PROPELLER OPERATION
 ON THE LOW-SPEED STABILITY AND CONTROL
 CHARACTERISTICS OF A 1/6-SCALE MODEL
 OF A REVISED CONFIGURATION OF THE
 REPUBLIC XF-84H AIRPLANE
 By William C. Sleeman, Jr.

SUMMARY

An investigation was made to determine the static longitudinal and lateral stability and control characteristics of a 1/6-scale model of the revised Republic XF-84H airplane with and without the propeller operating. The model had a 40° swept wing of aspect ratio 3.45 and was equipped with a thin, three-blade supersonic-type propeller. Modifications incorporated in the revised model included a raised horizontal tail, increased rudder size, wing fences at 65 percent semispan, and a modified wing leading edge outboard of the fences.

The test results for flap-retracted and flap-deflected conditions indicated that the revised configuration should be satisfactory for most normal flight conditions provided the angle of attack does not exceed the angle for pitch-up. An abrupt pitch-up tendency of the model was evident for the zero thrust condition above approximately 15° angle of attack. Although the effects of power were destabilizing, power-on longitudinal stability was satisfactory through the angle-of-attack range for which the model was stable with zero thrust.

Above the angle of attack for pitch-up, an uncontrollable left roll-off tendency would be expected with power on and slats retracted. Projection of wing slats or use of leading-edge chord-extensions with only

the left extension drooped were found beneficial in controlling the roll-off tendency with power on; however the most effective means found was projection of only the left slat.

INTRODUCTION

At the request of the U. S. Air Force, a series of tests were made in the Langley 300 MPH 7- by 10-foot tunnel of a 1/6-scale model of a revised configuration of the Republic XF-84H airplane. The model had a 40° sweptback wing of aspect ratio 3.45 and represented a fighter-type airplane driven by a single supersonic propeller. Results are presented showing the effects of propeller operation on the longitudinal and lateral stability and control characteristics of the model.

Tests of the original configuration (refs. 1, 2, and 3) indicated that improvement in both the power-off and power-on characteristics could be effected by several modifications to the basic model. Revisions accordingly were made to the original configuration and the present investigation was made to determine the characteristics of the revised model.

Aerodynamic characteristics of the model in sideslip and pitch were obtained with the propeller operating at positive thrust and at zero thrust for both the cruising and take-off configurations. Power-on pitch tests were made also to study the lateral-control power available with ailerons and with combined aileron and differential deflection of the lift flaps as means for controlling the large roll-off tendency found at high angles of attack. Analysis and discussion of results of this investigation have been made brief to facilitate publishing the data.

SYMBOLS

The results of this investigation are presented as standard NACA coefficients of forces and moments. The system of axes employed, together with an indication of positive forces, moments, and angular displacements, are presented in figure 1. Moment coefficients are given about the center-of-gravity location shown in figure 2 (15-percent mean aerodynamic chord, on the thrust axis).

- C_L lift coefficient, $Lift/qS$
- C_X longitudinal-force coefficient, X/qS
- C_Y lateral-force coefficient, Y/qS

C_m	pitching-moment coefficient, $M/qS\bar{c}$
C_l	rolling-moment coefficient, L/qSb
C_n	yawing-moment coefficient, N/qSb
X	longitudinal force along X-axis, lb
Y	lateral force along Y-axis, lb
Z	vertical force along Z-axis (Lift = -Z), lb
L	rolling moment about X-axis, ft-lb
M	pitching moment about Y-axis, ft-lb
N	yawing moment about Z-axis, ft-lb
T_c	effective thrust coefficient, $T_e/\rho V^2 D^2$
Q_c	torque coefficient, $Q/\rho V^2 D^3$
V/nD	propeller advance-diameter ratio
η	propulsive efficiency, $T_e V/2\pi n Q$
T_e	effective propeller thrust lb
Q	propeller torque, ft-lb
q	free-stream dynamic pressure, $\frac{1}{2}\rho V^2$, lb/sq ft
V	free-stream velocity, ft/sec
ρ	air density, slugs/cu ft
S	wing area (9.03 on model, excluding area of inlet ducts), sq ft
b	wing span, ft; also propeller blade section chord, in figure 4, ft
\bar{c}	wing mean aerodynamic chord (1.67 on model), ft
D	propeller diameter (2.0 on model), ft

R	propeller radius, ft
r	radius to any propeller blade element, ft
h	propeller blade section maximum thickness, ft
n	propeller rotational speed, rps
α	angle of attack of thrust line, deg
α_g	geometric angle of attack of thrust line, deg
β	angle of sideslip, deg, also propeller blade angle in figure 4, deg
ϵ	effective downwash angle at horizontal tail, deg
σ	tail effectiveness parameter, $\left(\frac{\partial C_m}{\partial i_t} \right) / \left(\frac{\partial C_m}{\partial i_t} \right)_{\alpha = 0^\circ}$
i_t	stabilizer incidence relative to thrust line, positive when trailing edge is down, deg
δ_r	rudder deflection, positive when trailing edge is to left, deg
i_f	offset angle of canopy fin, positive for nose offset to the right, deg
δ_f	wing flap deflection, positive when trailing edge is down, deg
δ_a	aileron deflection, positive when trailing edge is down, deg
δ_1	deflection of wing leading-edge extension between 65 and 94 per- cent semispan (see fig. 3)
δ_2	deflection of wing leading edge between 48 and 65 percent semispan

Subscripts:

β partial derivative of a coefficient with respect to sideslip,
for example, $C_{l_\beta} = \partial C_l / \partial \beta$

L and R left and right aileron or flap

MODEL AND APPARATUS

The model used in this investigation was a 1/6-scale model of a revised configuration of the Republic XF-84H airplane. The wing had 40° sweepback of the quarter-chord line, aspect ratio 3.45, taper ratio 0.578, and had NACA 64A010 airfoil sections normal to the quarter-chord line. A two-view drawing of the model is presented as figure 2 and geometric characteristics of the revised configuration are given in table I. The model was supplied by Republic Aviation Corporation and was not checked for accuracy.

Differences in the model and airplane shape are indicated in figure 2 by dashed lines. Since no attempt was made to simulate air flow through the model, the inlets and jet exit were faired over as shown. Duplication of scale design features of the nonrotating propeller spinner nose was not considered feasible on the model and therefore a hemispherical spinner nose was used.

Details of modifications incorporated in the revised configuration are given in figures 2 and 3. Some additional wing modifications which were studied briefly (spoilers and chord-extensions) are also shown in figure 3. The following modifications were on the model for all tests except where indicated otherwise: (1) raised horizontal tail mounted on revised vertical tail with large rudder, (2) wing fences at 65 percent semispan, and (3) modified wing leading edge (see fig. 3) from 65 to 94 percent semispan.

The proposed revised configuration is supposed to incorporate a triangular canopy fin as shown in figure 2. This fin is to be aligned with the thrust axis for flap-retracted conditions and offset 10° when the flaps are deflected 20° . This canopy fin was not on the model for pitch tests at zero sideslip.

Information on the aforementioned wing modifications is given in figure 3. Tests were made with a 16-inch-long spoiler placed at several positions on the right wing only, and placed normal to the airfoil surface. A triangular leading-edge chord-extension was placed on both wings for a few lateral-control tests and the effects of droop on the left extension were studied.

Effects on lateral-stability parameters of two pylon-mounted wing tanks of fineness ratio 9.2 were studied briefly. The spanwise location of the tanks was approximately 22 percent semispan and the length of the tanks was 1.28 wing semispans.

Geometric characteristics of the solid steel model propeller are given in figure 4. The blade angle used in all tests was 16.5° at 0.75R

and was selected on the basis of simulating the thrust-torque relationship for the airplane at maximum power and high thrust. The propeller was driven by a 47-horsepower electric motor in the model. The rotational speed of the propeller was determined by observation of a stroboscopic-type frequency indicator which indicated the output frequency of a small alternator connected to the motor shaft. The accuracy of the frequency indicator was within ± 0.05 percent.

TESTS AND RESULTS

Test conditions.- Tests were made in the Langley 300 MPH 7- by 10-foot tunnel at dynamic pressures of 4, 6, and 8 pounds per square foot for power-on tests. Tests with $T_c = 0$ and with the propeller off were made at dynamic pressures of 12 and 40 pounds per square foot, respectively. These test conditions correspond to airspeeds from approximately 40 to 126 miles per hour and to test Reynolds numbers of approximately 0.64×10^6 to 2.0×10^6 based on the wing mean aerodynamic chord of 1.67 feet.

The wing-off tests and propeller calibrations were made with the model mounted on a single centrally located vertical support strut. All other tests were made with the model supported by its wings through a twin-strut system. The presence of the wing support struts prevented the use of the main landing wheels, and tests of the flap-deflected configurations (landing and take-off condition) therefore were made with only the nose wheel extended.

In order to avoid possible confusion regarding test configurations when differential flap deflections are used, the configuration will be designated as clean or take-off. In the basic clean configuration the landing gear and flaps were retracted and in the basic take-off condition the flaps were deflected 20° and the nose wheel extended. The wing slats were retracted in all instances with the exception of a few tests as indicated in the figures. The maximum differential flap deflection contemplated is $\pm 10^\circ$ for each flap from the initial deflection.

Test procedure.- Propeller calibrations presented in figure 5 were made with the propeller on the clean fuselage (wing, canopy, dorsal, empennage, and tail skid removed). The propeller was calibrated by measuring the resultant longitudinal force, minimum motor current, and rolling moment of the model at 0° angle of attack for a range of propeller speed. Effective propeller thrust was computed from the following relationship:

$$T_e = X_R - X_0$$

where X_R is the longitudinal force obtained with the propeller operating and X_0 is the longitudinal force of the model with the propeller removed.

Torque coefficients presented in figure 5 were obtained from measured rolling moments and these results were in excellent agreement with those determined by use of a calibration of motor torque as a function of minimum motor current.

A number of power-on tests simulated a constant-power flight condition in which the propeller speed and angle of attack of the model were adjusted to correspond to the relationship of T_c and C_L given in figure 6. The power condition of figure 6 represents a military power rating of approximately 7070 horsepower at sea-level altitude for an airplane gross weight of 16,000 pounds. The angle-of-attack range obtained for the constant-power tests was limited by maximum operating conditions of the model motor since the angle of attack and propeller thrust were proportional for constant-power operation.

For the constant-thrust tests, the propeller speed was held constant while the angle of attack or sideslip of the model was varied. The propeller and spinner were replaced by a dummy spinner for the propeller-off tests. The vertical tail was on the model for the horizontal tail-off pitch tests of the model. Both the horizontal and vertical tails were removed for the tail-off tests in sideslip.

Lateral-stability parameters were obtained from pitch tests at $\pm 5^\circ$ sideslip angle by assuming a linear variation between these points.

Corrections.- Jet boundary corrections to the angles of attack, longitudinal force coefficients, and tail-on pitching-moment coefficients were obtained from reference 4. The following corrections were added to the data:

$$\Delta\alpha = 1.02C_{L_W}(\text{deg})$$

$$\Delta C_X = -0.0155C_{L_W}^2$$

$$\Delta C_m = 0.0143C_{L_W}$$

where

$$C_{L_W} = C_L - (\Delta C_L)_{\text{propeller thrust}}$$

~~CONFIDENTIAL~~

$$(\Delta C_L)_{\text{propeller thrust}} = T_c \left(\frac{2D^2}{S} \right) \sin \alpha_g$$

Blockage corrections have not been applied to the data.

No systematic evaluation of support tares has been made and corrections for support interference have not been applied to the data. Results of a few tare tests, however, have indicated that the wing support tares were small and associated primarily with a small change in longitudinal trim. Single support tares were evaluated for the propeller calibrations and were found to be negligible for resultant longitudinal force coefficients.

Results.- The figures presenting the results are as follows:

	Figure
Basic longitudinal results:	
Clean configuration	7
Take-off and landing configuration	8 and 9
Characteristics at constant thrust	10
Downwash and tail effectiveness	11
Lateral trim at zero sideslip:	
Clean configuration	12 to 17
Take-off configuration	18 to 20
Directional trim at zero sideslip:	
Basic model, take-off configuration	21
Canopy fin on, take-off configuration	22
Power A, clean configuration	23
Characteristics in pitch at $\pm 5^\circ$ sideslip:	
Clean configuration	24
Take-off configuration	25
Characteristics in sideslip:	
Clean configuration	26 and 27
Take-off configuration	28 and 29
Wing-off test	30 to 33
Summary of results	34 and 35

DISCUSSION

The discussion of results will be based primarily on the summary of trim characteristics and lateral-stability parameters presented in figures 34 and 35.

Longitudinal stability and trim.- The variation of stabilizer angle for trim with trimmed lift coefficient is presented in figure 34(a) for flaps retracted and deflected; the results were obtained from the test data of figures 7 to 9. Longitudinal stability with the propeller operating at zero thrust was quite high through most of the lift range and the static margin was approximately $0.25\bar{c}$ for all $T_c = 0$ conditions. At lift coefficients near maximum lift an abrupt instability is indicated for the zero thrust conditions and in all instances this instability occurred at approximately $\alpha = 15^\circ$ (see figs. 7(a), 8(a), and 9). This pitch-up tendency appears to be associated with effects of an unfavorable downwash gradient on the tail contribution to stability (fig. 11). Pitching-moment results obtained with the propeller operating at a constant value of thrust ($T_c = 0.81$, fig. 10) also show a marked pitch-up tendency near $\alpha = 15^\circ$ for both the flap-deflected and flap-retracted conditions.

Application of full constant power caused a progressive loss in stability with lift coefficient (fig. 34(a)). Although the overall power-on stability was low at the highest test lift coefficients, no abrupt pitch-up tendency was indicated up to the highest test angle of attack attained. It should be noted however that the constant-power data were not obtained above 15° angle of attack and in all other cases, the pitch-up tendency occurred at angles of attack between 14° and 16° . The absence of longitudinal instability up to $\alpha = 15^\circ$ for the clean configuration with full constant power demonstrated the benefits of the modifications used in the revised configuration since the original model (ref. 2) became unstable at about $\alpha = 9^\circ$ with constant power.

Lateral trim characteristics.- Power-on lateral trim results with full corrective control deflection are summarized in figure 34(b) for $T_c = 0.81$. The effect of differential flap deflection with full aileron deflection is shown for the clean configuration. Although the control effectiveness is almost doubled at low angles of attack when the flaps were deflected differentially, only a small increase in maximum trimmed angle is achieved with the slats retracted. Projection of both slats afforded a significant increase in control effectiveness and maximum trim angle for the clean configuration, whereas projection of only the left slat was found the most effective means for controlling the roll-off tendency with power on.

The addition of leading-edge chord-extensions with droop ($\delta_1 = \delta_2$) on both wings had no beneficial effect on rolling moments (fig. 20). Deflection of only the left extension arrangement (figs. 20 and 34(b)) extended the maximum trim angle up to about 19° angle of attack.

Although the lateral-control results with power on are restricted to only one thrust coefficient, these results demonstrate the existing lateral-control problems for this configuration. Some additional information is presented in figure 33 for a range of thrust coefficients at

constant angles of attack. With the model at $\alpha = 0^\circ$ (fig. 33, tail-off), the wing removes a substantial amount of the rolling moment due to torque. At the highest angle of attack, however, an unfavorable wing contribution added to torque effects (at low values of T_c) and produced a roll-off tendency which was as severe at very low thrust as that which existed at higher thrust.

The large rolling moment at high angles of attack for the $T_c = 0$ condition ($\delta_a = 0^\circ$, fig. 12(a) and 33) was not present with the propeller removed (ref. 1) or with the propeller windmilling (zero torque condition, see ref. 3). It appears that the stall behavior on this wing was very sensitive to conditions of flow asymmetry caused by even small amounts of slipstream rotation. Since the Reynolds number of these tests was low, it might be expected, therefore, that some scale effect between the model and airplane behavior would be present. This scale effect on lateral control with power on would probably cause the airplane to retain lateral trim to a somewhat higher angle of attack than indicated in the model tests. The very large adverse power effects on the lateral trim at zero sideslip found in the model results indicate that an uncontrollable roll-off would be expected for the airplane at moderately high angles of attack with power on and using only the ailerons and differential flaps for control.

Directional control characteristics.- Results of tests with the rudder deflected are summarized in figure 34(c) as rudder deflection required to trim to zero yawing moment. The results through the sideslip range show the effect of power for the clean and take-off configurations with the canopy fin on the model. The limiting sideslip conditions were encountered in the take-off configuration with power on at negative sideslip, and at positive sideslip with the propeller operating at zero thrust. The maximum values of sideslip which could be maintained for these conditions with a rudder deflection range of 15° to -35° was approximately 9° positive and 11° negative sideslip, respectively.

Characteristics of the model at zero sideslip for the take-off configuration are also given in figure 34(c) for a range of thrust coefficients. These results show that sufficient rudder power is present with or without the canopy fin through the test thrust range. The canopy fin would however be expected to provide additional rudder power for sideslip as indicated in figure 29.

The effect of the horizontal tail on rudder effectiveness as shown in figure 30 amounts to roughly a 10-percent increase in rudder power through the angle-of-attack range. The contribution of the vertical tail to $C_{n\beta}$ was increased about 12 percent by the presence of the horizontal tail (see fig. 31).

Lateral-stability parameters.- Effects of constant-power propeller operation on lateral-stability parameters are presented in figures 24 and 25 for the clean and take-off configuration. Data presented for the zero thrust conditions were obtained with the rudder and ailerons neutral, whereas data for the power-on conditions were obtained with these controls deflected to bring the model more nearly in trim at high angles of attack.

Positive dihedral effect over a $\pm 5^\circ$ sideslip range is indicated (fig. 35) for the power and flap conditions investigated through the test lift range; however, application of power reduced C_{l_β} . Test data obtained through the sideslip range (figs. 26 to 29) indicate that application of power also tends to further reduce the dihedral effect at positive sideslip angles and in some cases neutral or negative dihedral effect would be expected (see fig. 29).

Directional stability was high without power throughout most of the lift range (fig. 35). Application of constant power caused the directional stability to increase sharply with lift coefficient and to become very high at high lift for both flap conditions tested.

Addition of wing tanks had little effect on the lateral-stability parameters of the model in the take-off configuration with power on.

CONCLUSIONS

Results of a low-speed investigation of the effects of propeller operation on the static stability and control characteristics of a 1/6-scale model of the revised Republic XF-84H airplane have indicated the following conclusions:

1. The revised configuration should be satisfactory for most normal flight conditions providing the angle of attack does not exceed the angle for pitch-up (15° on model). Above the angle of attack for pitch-up, an uncontrollable left roll-off tendency would be expected with power on and slats retracted.

2. Effects of propeller operation on longitudinal stability were destabilizing; however, with the large power-off static margin ($0.25\bar{c}$) at lift coefficients below unity the power-on characteristics were satisfactory through the angle-of-attack range (up to $\alpha = 15^\circ$) for which the model was stable with zero thrust.

3. The use of differential flap operation with the ailerons about doubled the rolling effectiveness with power on at low angles of attack;

however, no significant gain in maximum angle of attack for trim was obtained with this lateral control arrangement.

4. Projection of both wing slats for the clean configuration was found beneficial for controlling the roll-off tendency with power on; however, the most effective means found was projection of only the left slat.

5. The use of leading-edge chord-extensions with only the left extension drooped was found beneficial in delaying the left roll-off tendency for the model in the take-off configuration with power on.

6. Adequate directional control for take-off was indicated and the maximum range of sideslip angles which could be maintained by full rudder deflection was approximately 9° to -11° sideslip for the most adverse power and flap conditions studied.

7. The model had positive dihedral effect and directional stability with and without power for $\pm 5^{\circ}$ sideslip range throughout the lift range.

Langley Aeronautical Laboratory,
National Advisory Committee for Aeronautics,
Langley Field, Va., September 4, 1953.

William C. Sleeman Jr.

William C. Sleeman, Jr.
Aeronautical Research Scientist

Approved: *Thomas A. Harris*

Thomas A. Harris
Chief of Stability Research Division

bss

REFERENCES

1. Weil, Joseph, Sleeman, William C., Jr., and Byrnes, Andrew L., Jr.: Investigation of the Effects of Wing and Tail Modifications on the Low-Speed Stability Characteristics of a Model Having a Thin 40° Swept Wing of Aspect Ratio 3.5. NACA RM L53C09, 1953.
2. Sleeman, William C. Jr., and Byrnes, Andrew L., Jr.: Low-Speed Longitudinal Stability Characteristics of a 1/6-Scale Model of the Republic XF-84H Airplane With the Propeller Operating. NACA RM SL53F26, U. S. Air Force, 1953.
3. Sleeman, William C., Jr., and Morrison, William D., Jr.: Low-Speed Investigation of the Static Lateral Stability and Control Characteristics of a 1/6-Scale Model of the Republic XF-84H Airplane With the Propeller Operating. NACA RM SL53G10, U. S. Air Force, 1953.
4. Gillis, Clarence L., Polhamus, Edward C., and Gray, Joseph L., Jr.: Charts for Determining Jet-Boundary Corrections for Complete Models in 7- by 10-Foot Closed Rectangular Wind Tunnels. NACA WR L-123, 1945. (Formerly NACA ARR L5G31.)

TABLE I.- SUMMARY OF BASIC MODEL GEOMETRY

Wing:

Area (not including inlet area), sq ft	9.03
Span, ft	5.59
Sweepback of quarter-chord line, deg	40
Aspect ratio	3.45
Taper ratio	0.578
Dihedral	-3°30'
Incidence	2°30'
Geometric twist, deg	0
Mean aerodynamic chord, ft	1.67
Airfoil section (normal to quarter-chord line)	NACA 64A010
Root chord, ft	2.063
Tip chord, ft	1.195

Flap:

Type	plain trailing edge
Area (one flap), sq ft	0.420
Span, ft	1.009
Hinge line, percent c	75
Maximum deflection, deg	40

Aileron:

Area (one aileron), sq ft	0.38
Span, ft	1.24
Hinge line, percent c	75
Maximum deflection (normal to hinge line), deg	±18

Leading-edge slat:

Span of one slat (normal to model center line), ft	1.33
Ratio of slat chord to wing chord (normal to quarter-chord line)	0.140
Inboard edge (from model center line), ft	1.347
Forward extension of slat, percent c	8.4
Downward extension of slat, percent c	7.24

Horizontal tail:

Type	All-movable
Area, sq ft	1.55
Span, ft	2.36
Sweepback of quarter-chord line, deg	40
Taper ratio	1.0
Dihedral, deg	0
Chord, ft	0.67
Maximum deflection, deg	+6 to -15
Airfoil section	NACA 64A009

TABLE I.- SUMMARY OF BASIC MODEL GEOMETRY - Concluded

Vertical tail:

Area, sq ft	1.79
Span, ft	1.83
Sweepback of quarter-chord line, deg	41.56
Aspect ratio	1.84
Taper ratio	0.38
Mean aerodynamic chord, ft	1.05
Maximum deflection, deg	15 to -35
Airfoil section (normal to quarter-chord line).	NACA 64 ₍₁₀₎ A011

~~CONFIDENTIAL~~

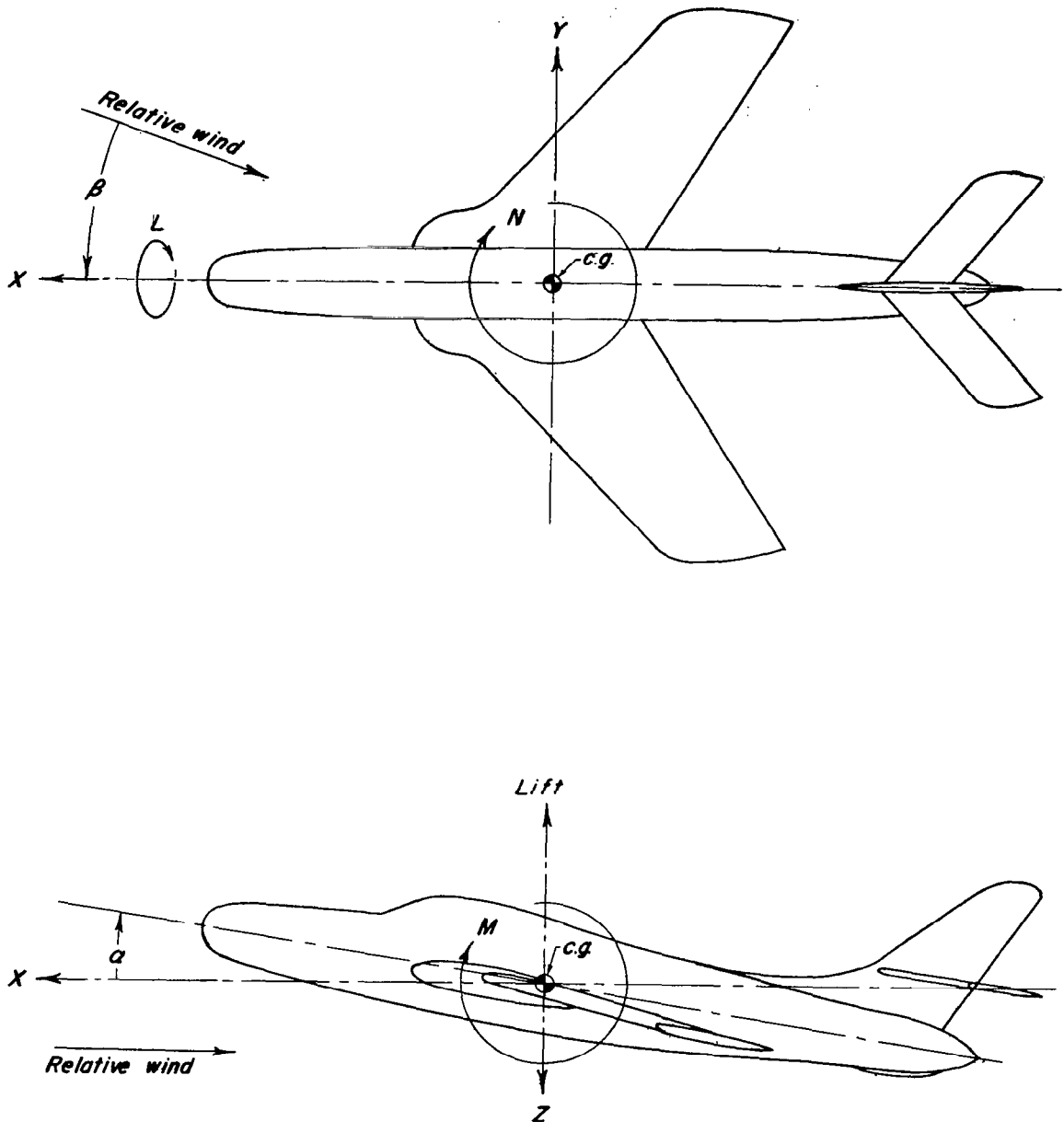


Figure 1.- System of axes; positive values of forces, moments, and angles are indicated by arrows.

~~CONFIDENTIAL~~

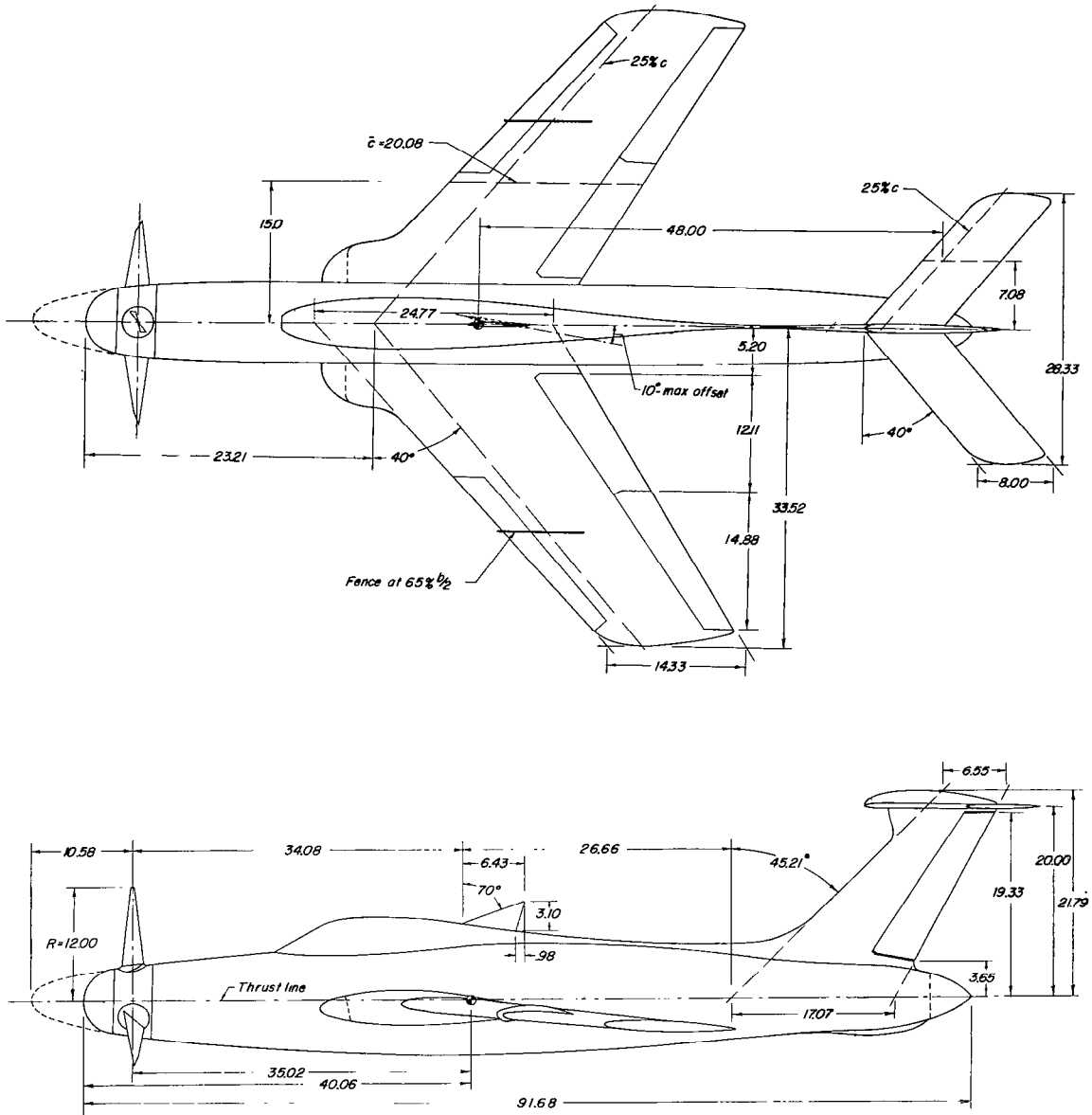


Figure 2.- Two-view drawing of the revised 1/6-scale model of the Republic XF-84H airplane. Broken lines at spinner, inlets, and jet exit indicate shape for full-scale airplane. All dimensions are in inches.

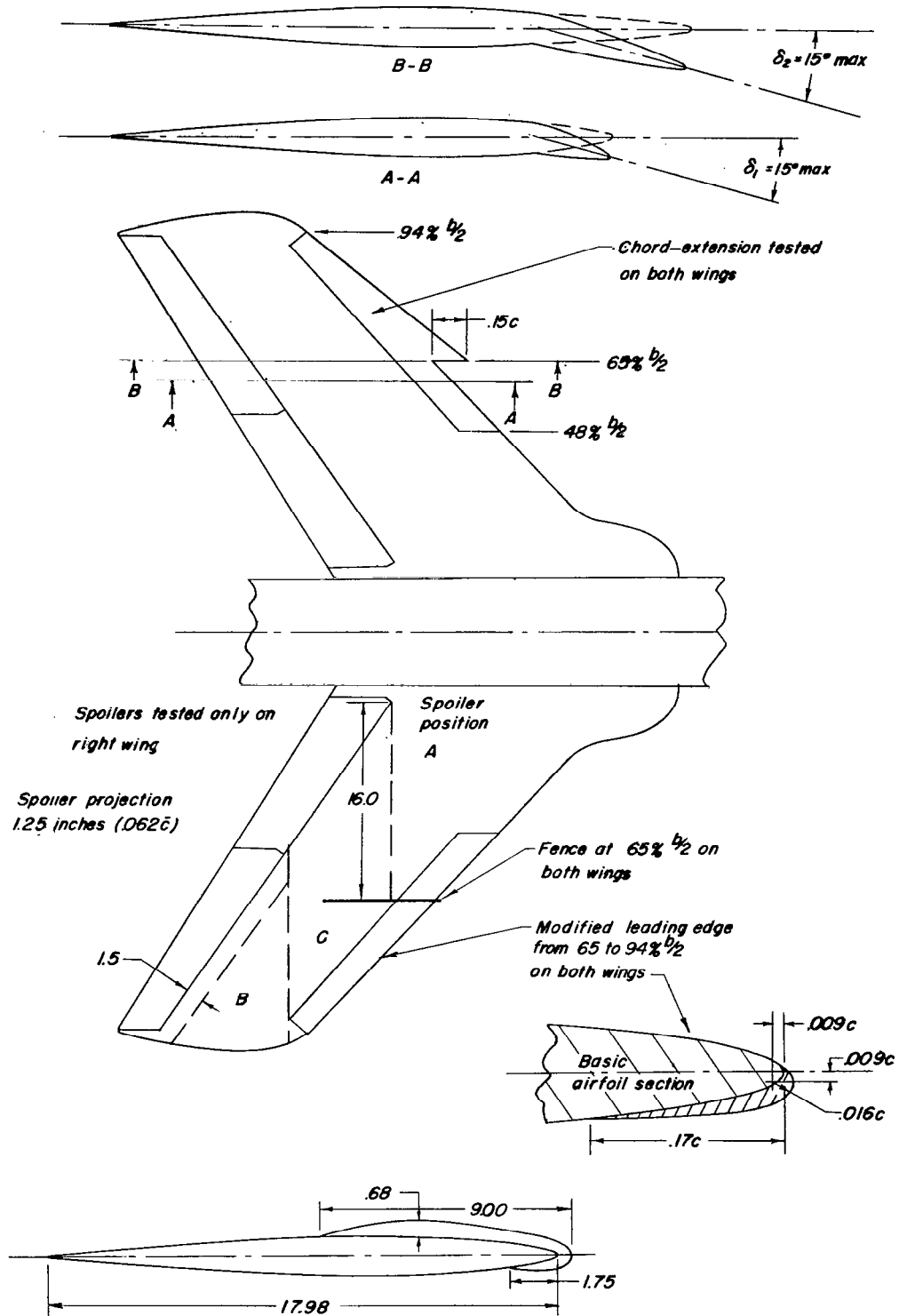


Figure 3.- Details of wing modifications tested. Dimensions are in inches.

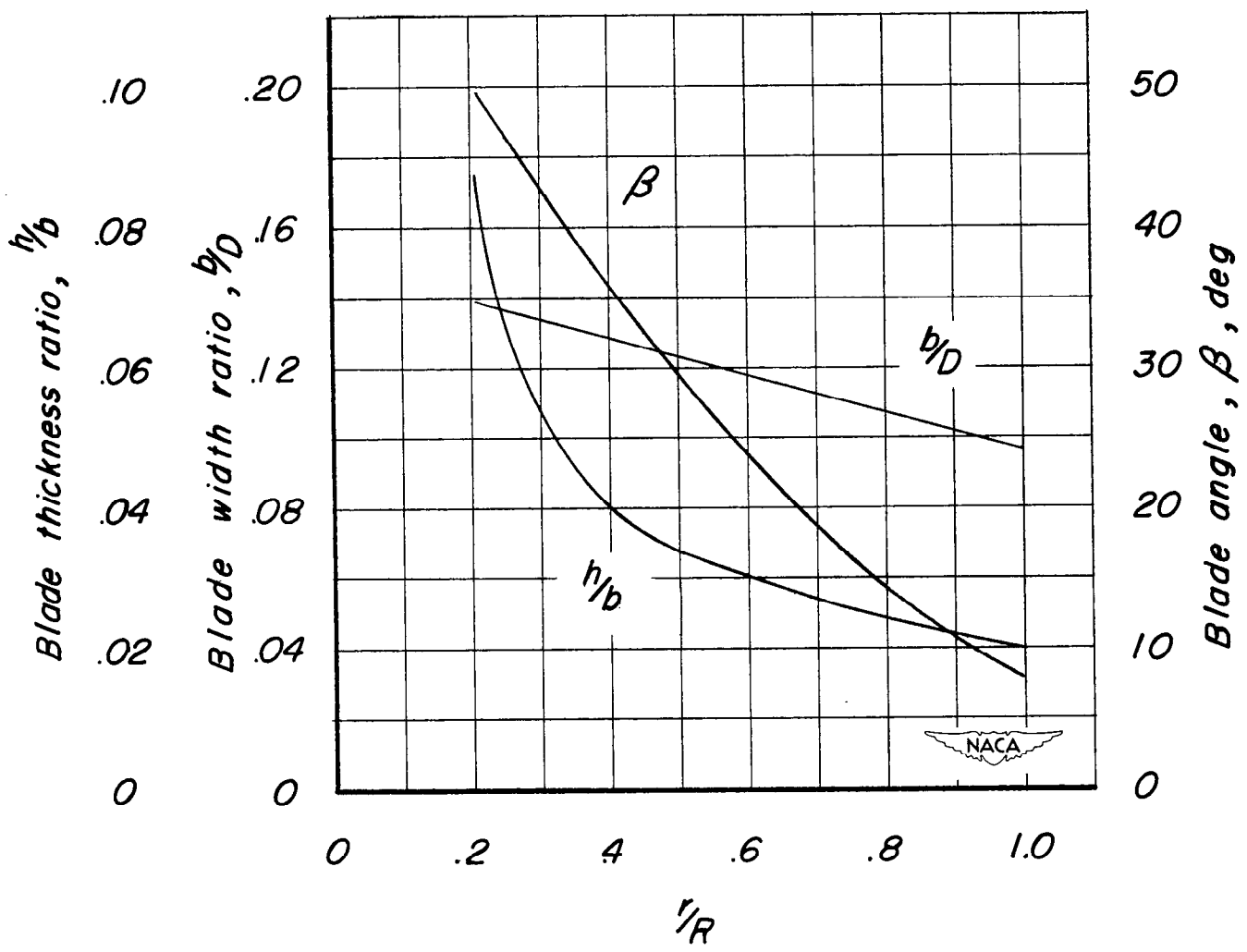


Figure 4.- Blade form characteristics of the model propeller.

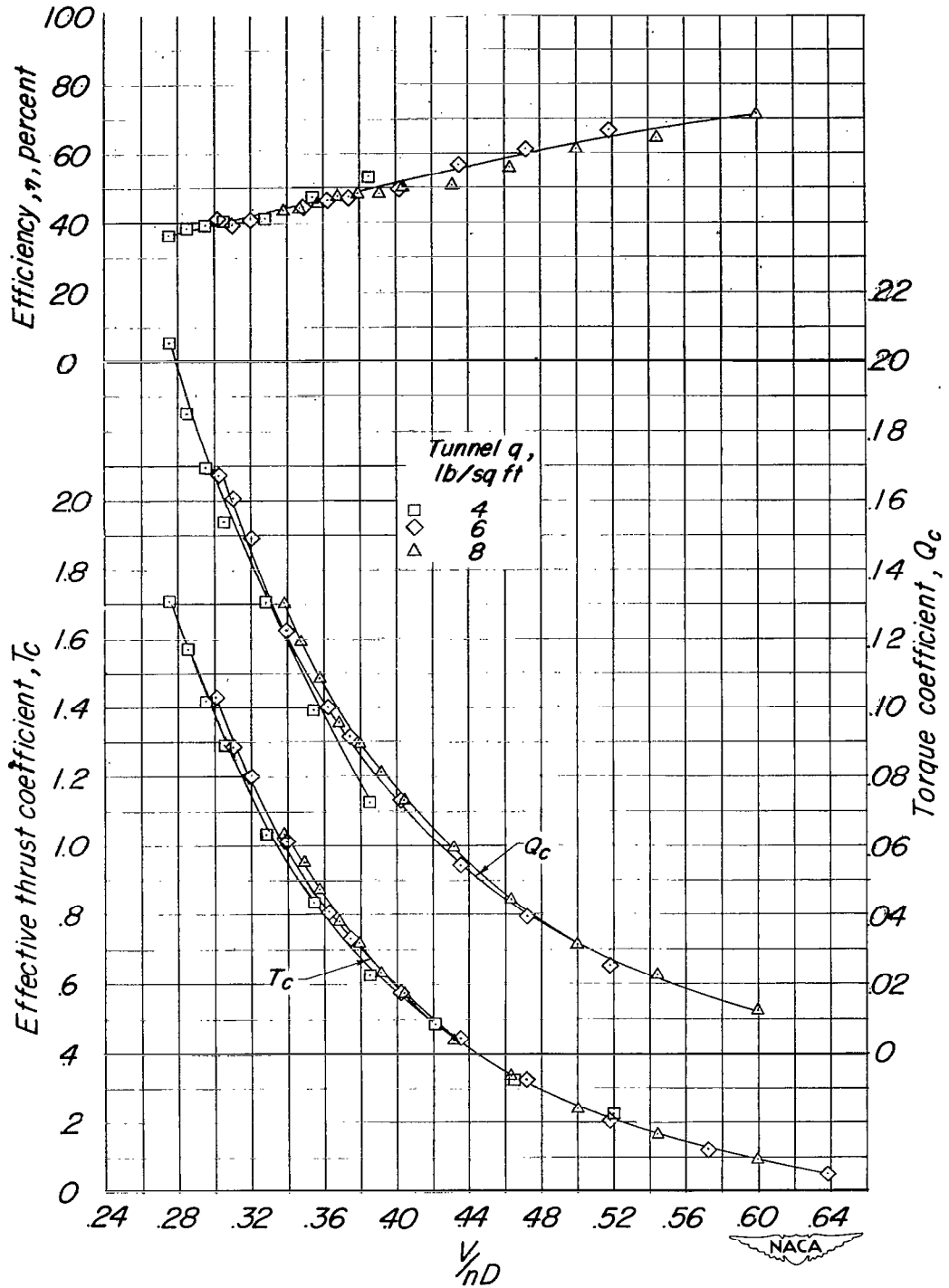


Figure 5.- Characteristics of the model propeller as determined from calibrations with the propeller on the basic fuselage. Wing, tail, canopy, and external protuberances removed. $\beta = 16.5^\circ$.

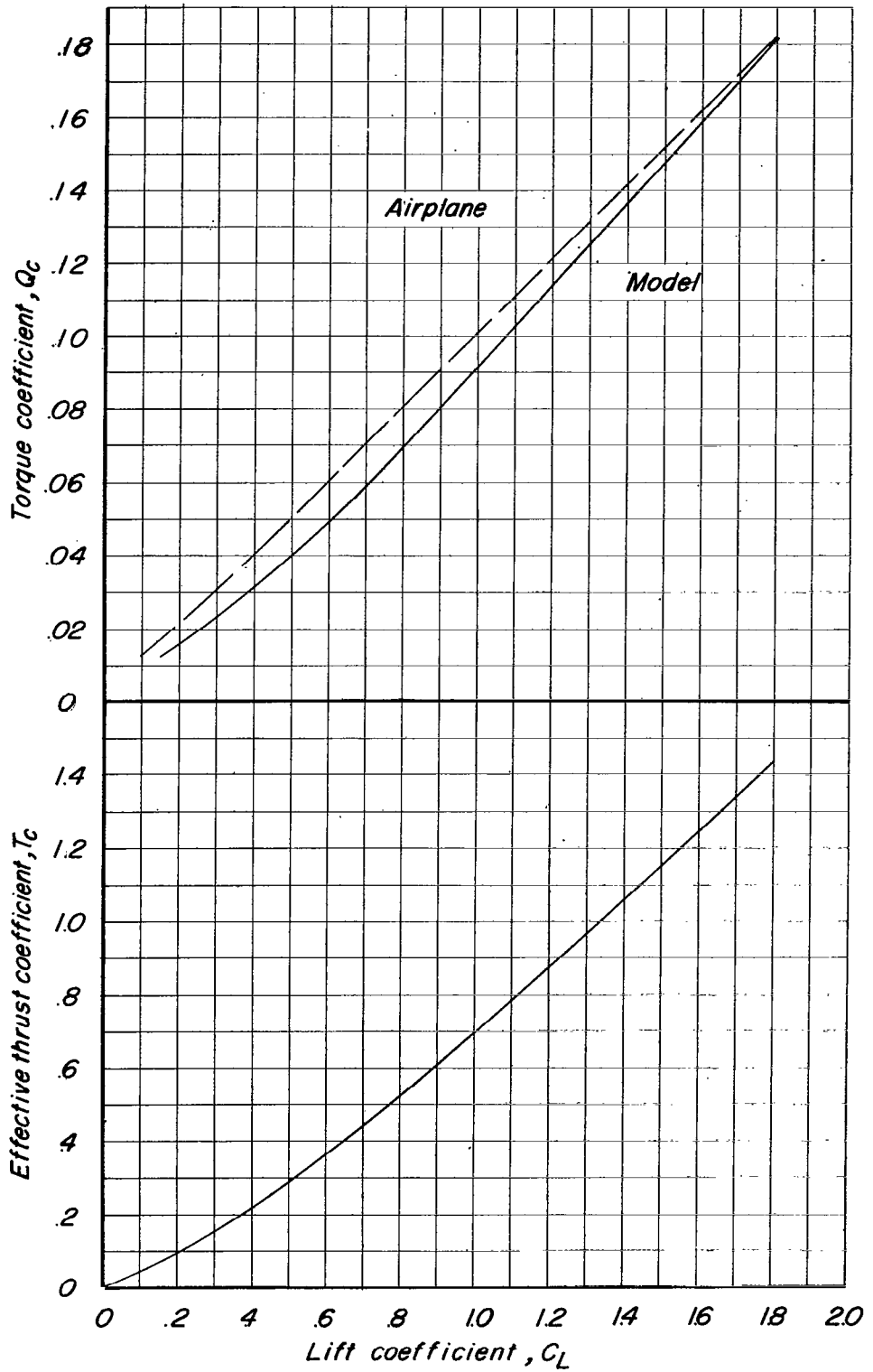
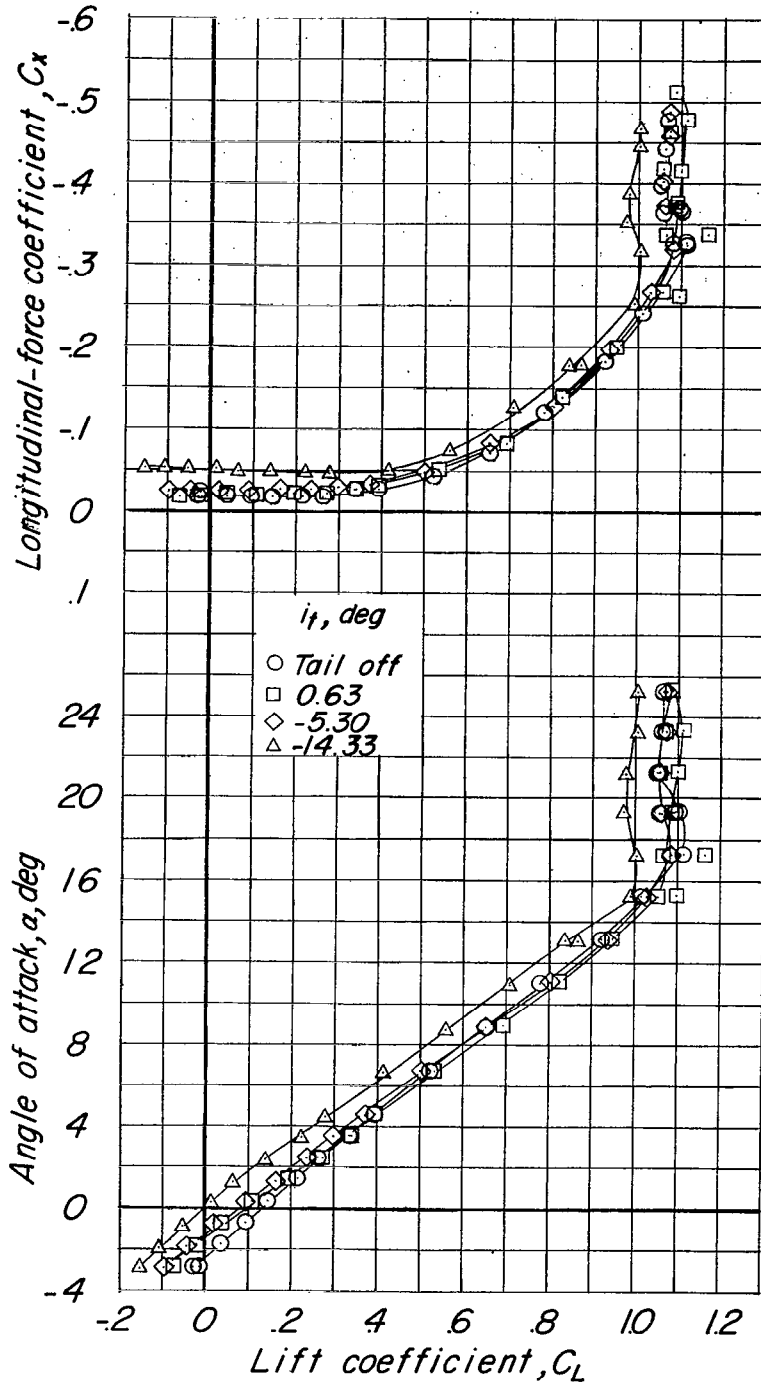
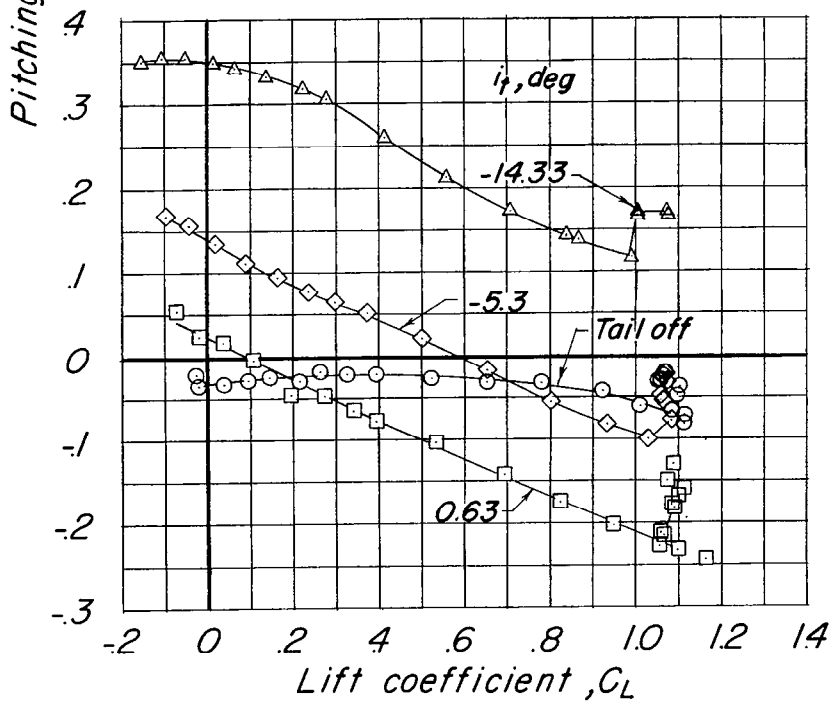
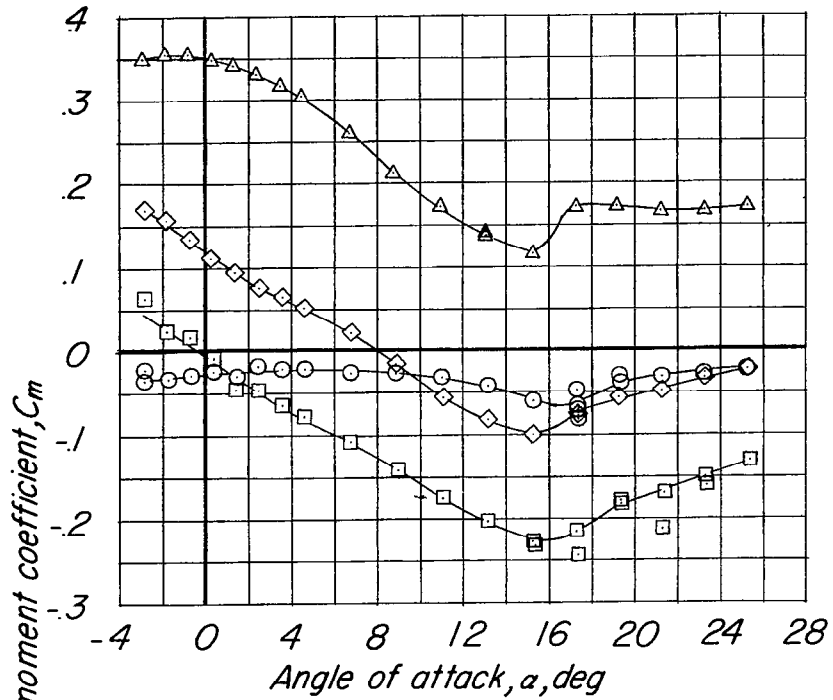


Figure 6.- Variation of thrust and torque coefficients with lift coefficient for the constant power conditions investigated.



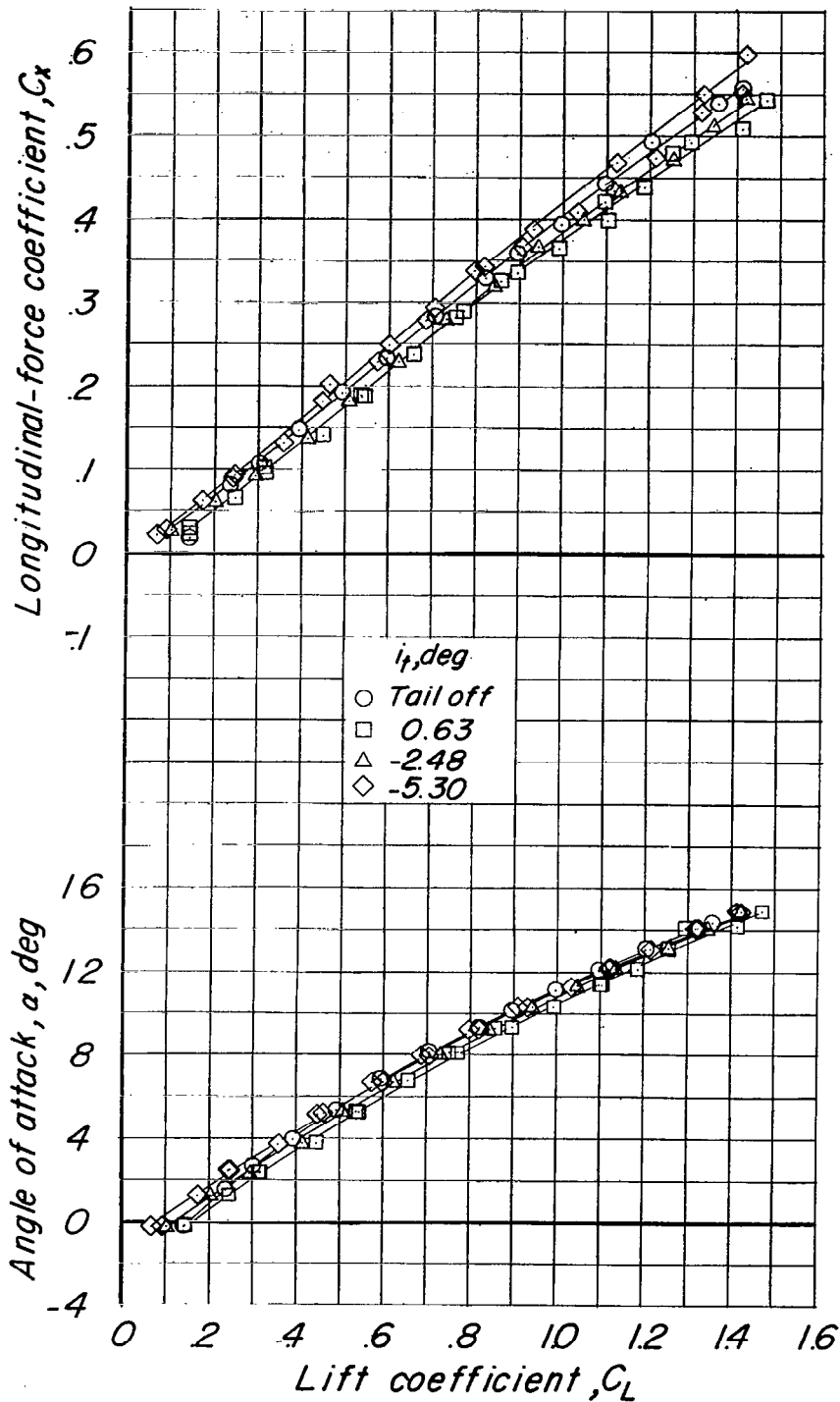
(a) $T_c = 0$; $q = 12$ lb/sq ft.

Figure 7.- Effect of stabilizer deflection on the longitudinal characteristics of the model in the clean configuration. $\delta_f = \delta_a = \delta_r = 0^\circ$.



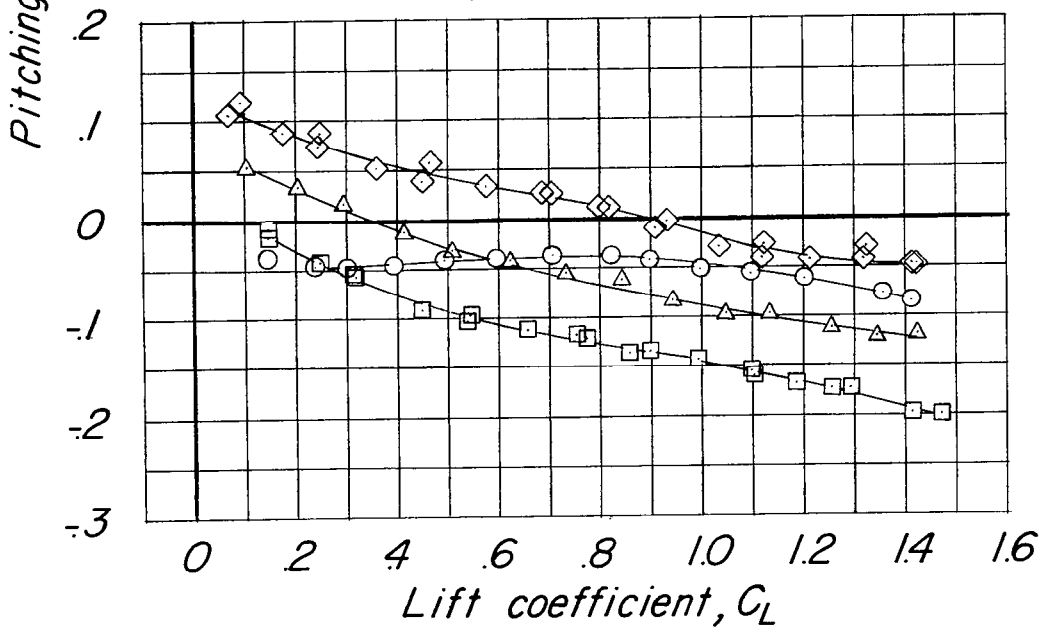
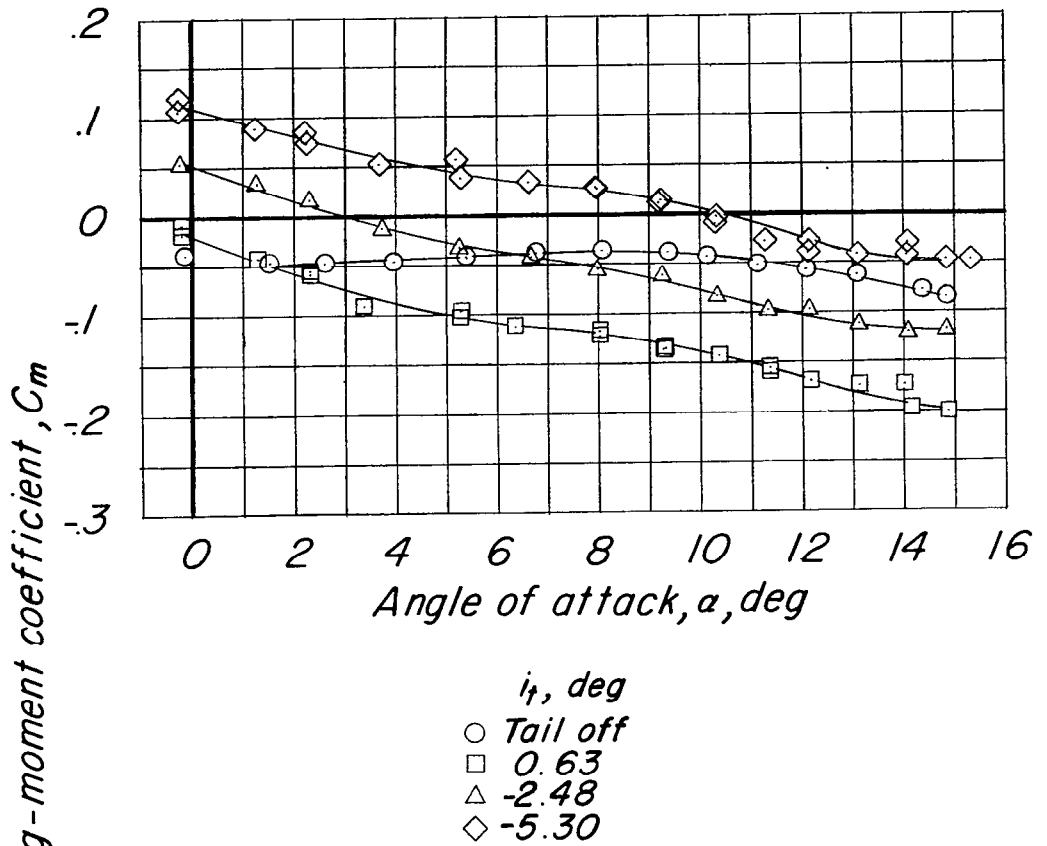
(a) Concluded.

Figure 7.- Continued.



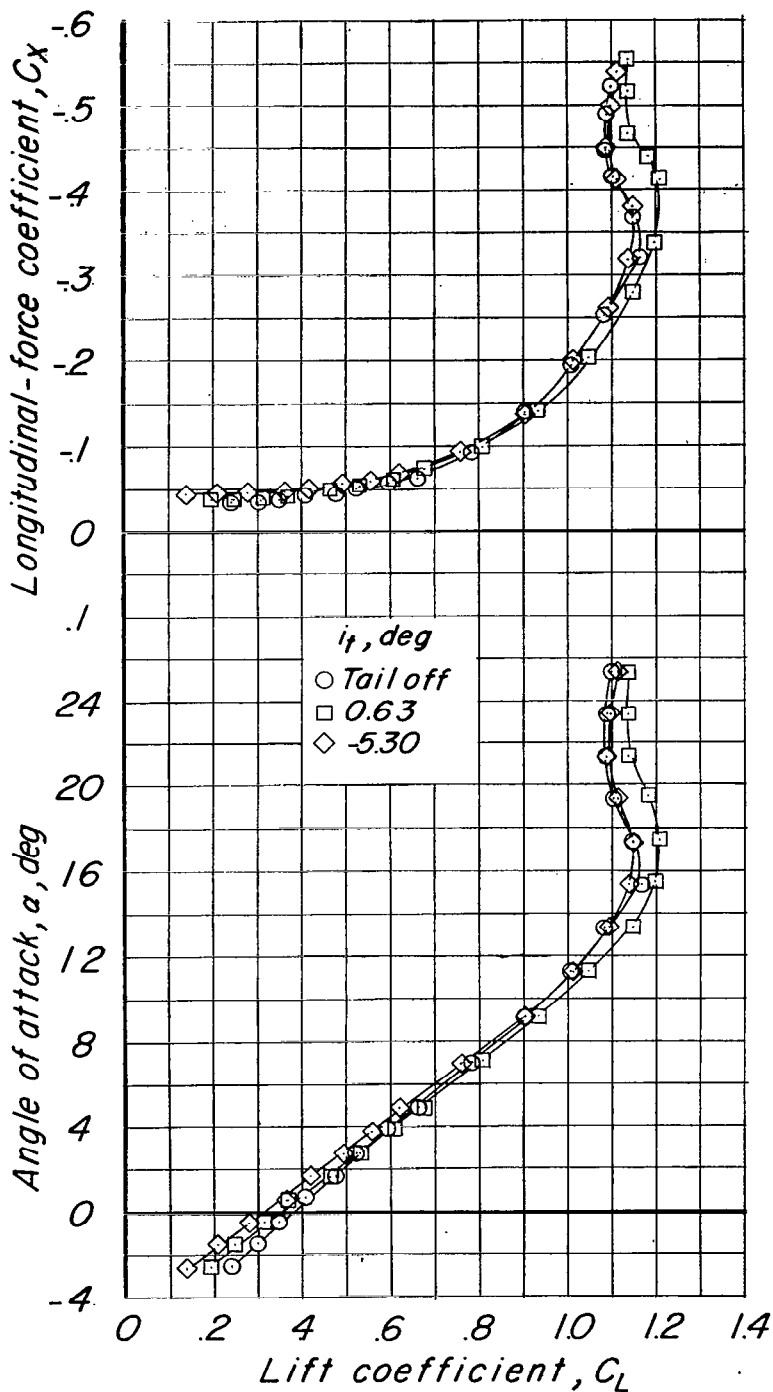
(b) Power; $q = 8 \text{ lb/sq ft.}$

Figure 7.- Continued.



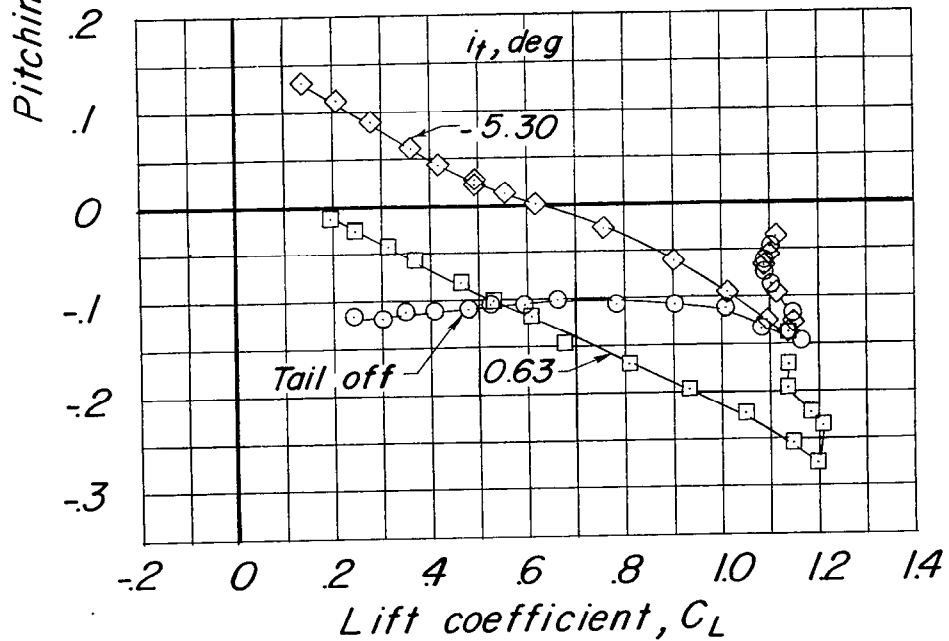
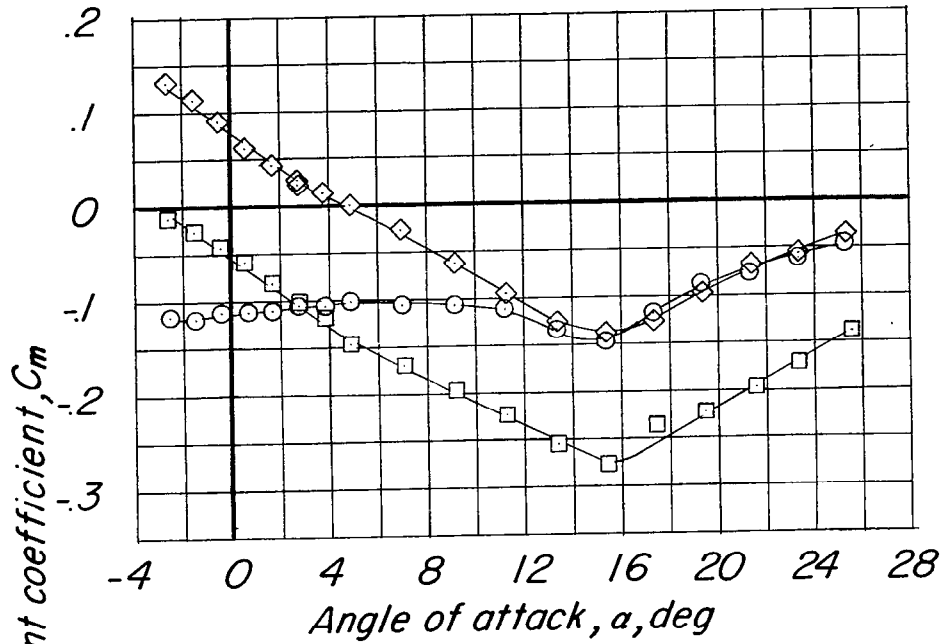
(b) Concluded.

Figure 7.- Concluded.



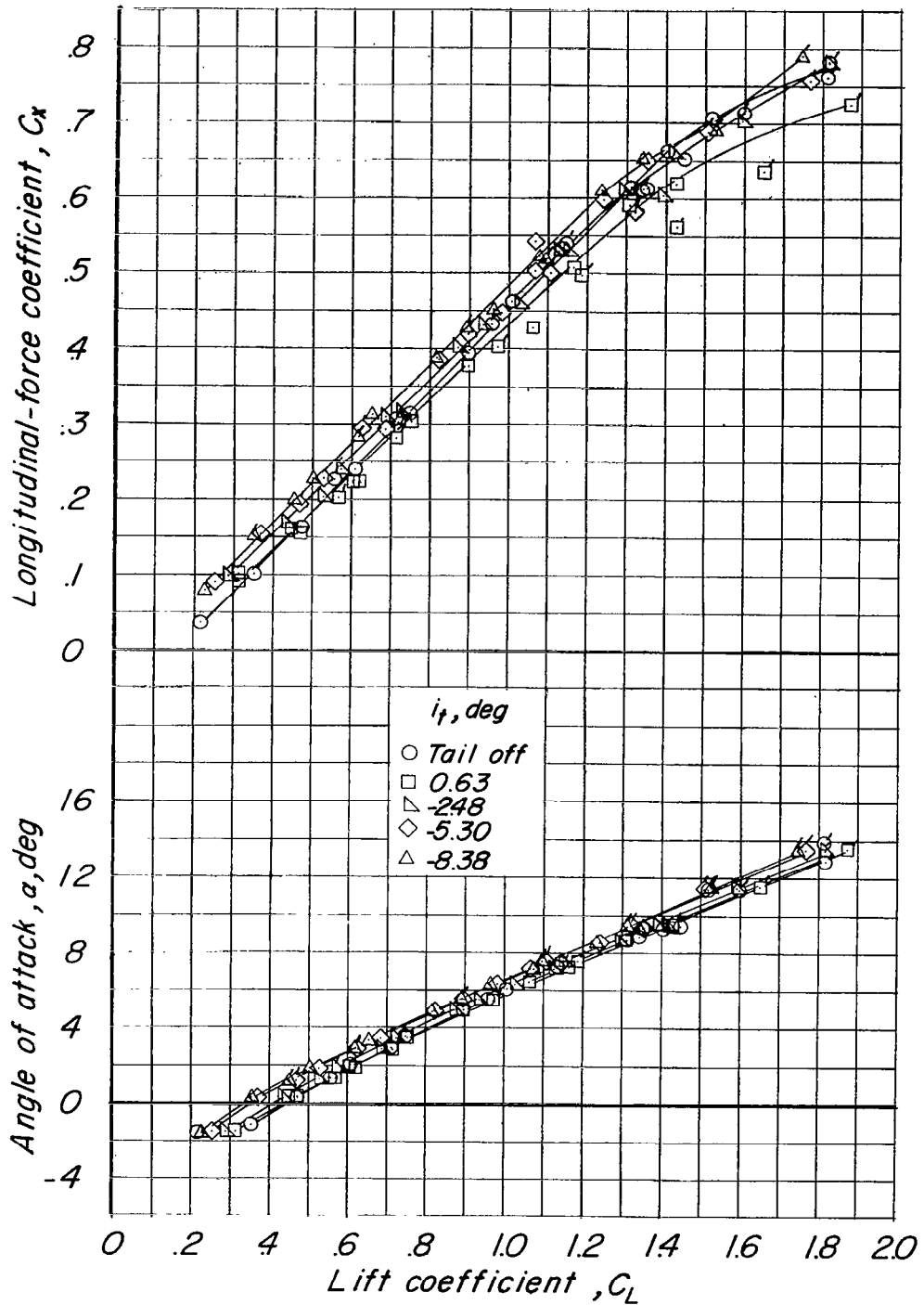
(a) $T_c = 0$; $q = 12$ lb/sq ft.

Figure 8.- Effect of stabilizer deflection on the longitudinal characteristics of the model in the take-off configuration. $\delta_f = 20^\circ$; $\delta_a = \delta_r = 0^\circ$.



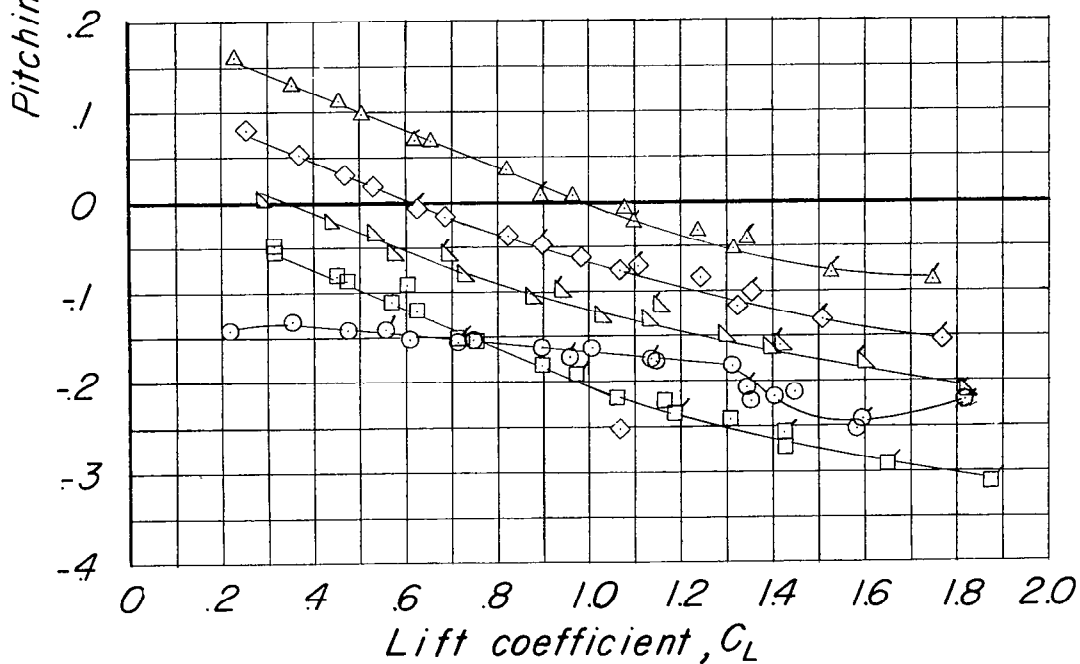
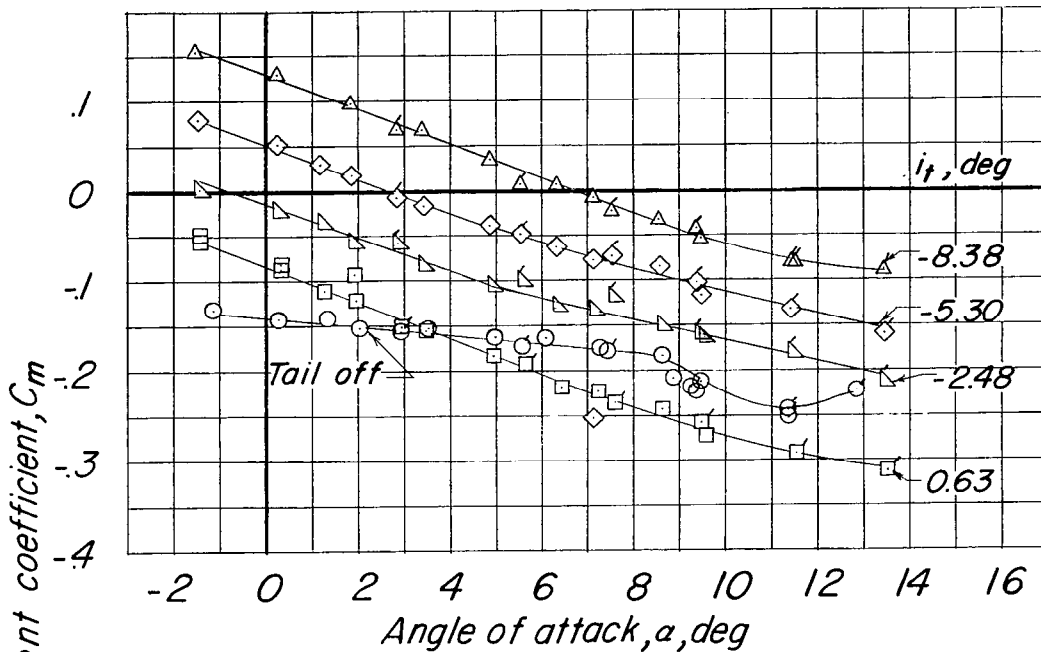
(a) Concluded.

Figure 8.- Continued.



(b) Power A. $q = 8$ and 6 lb/sq ft. Flagged symbols indicate data at $q = 6$ lb/sq ft.

Figure 8.- Continued.



(b) Concluded.

Figure 8.- Concluded.

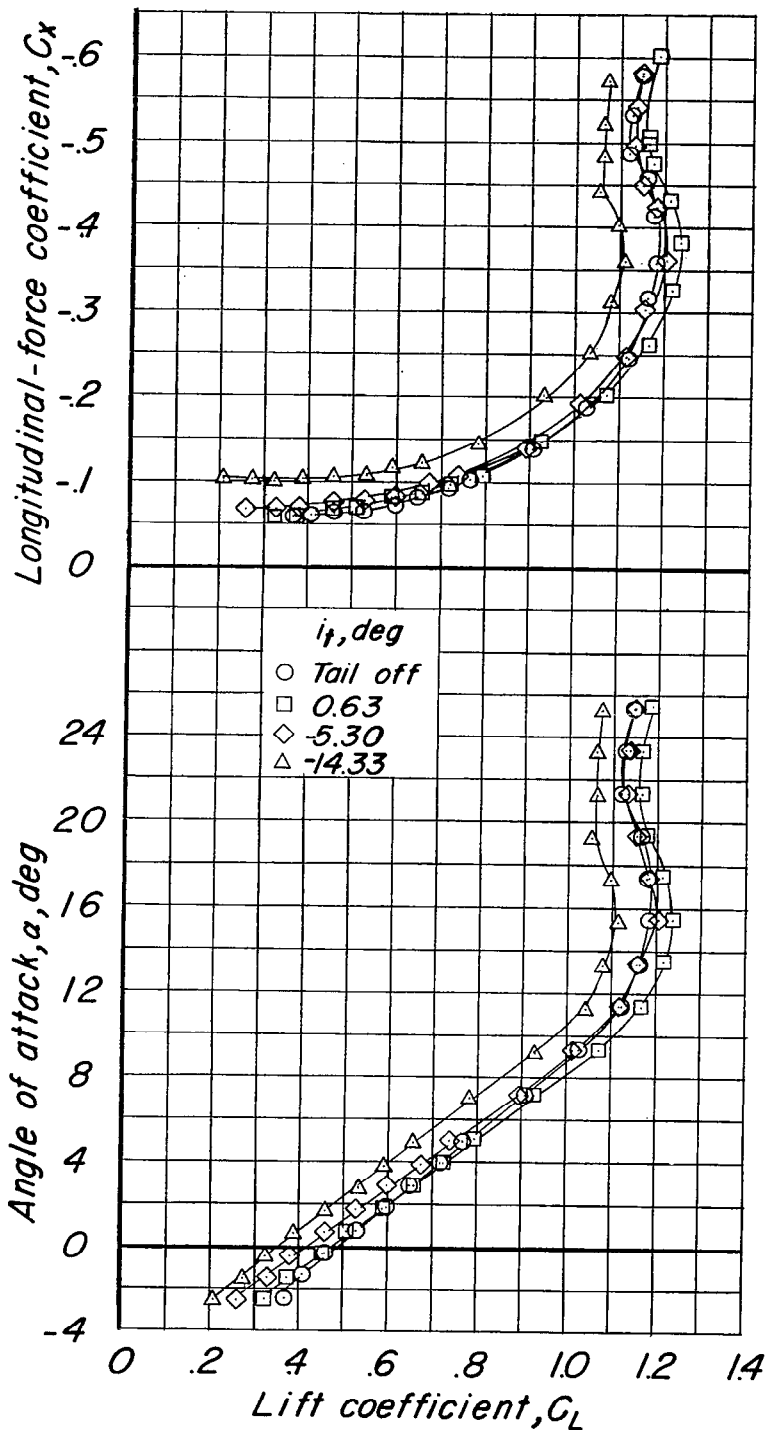


Figure 9.- Effect of stabilizer deflection on the longitudinal characteristics of the model in the landing condition. $T_c = 0$; $\delta_f = 40^\circ$; $\delta_a = \delta_r = 0^\circ$; $q = 12$ lb/sq ft.

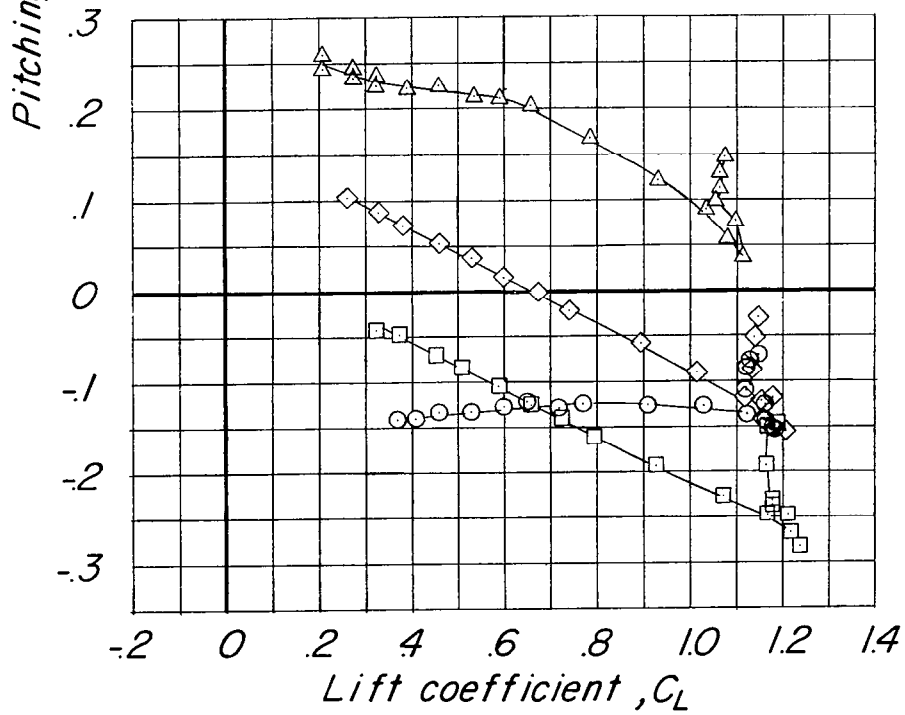
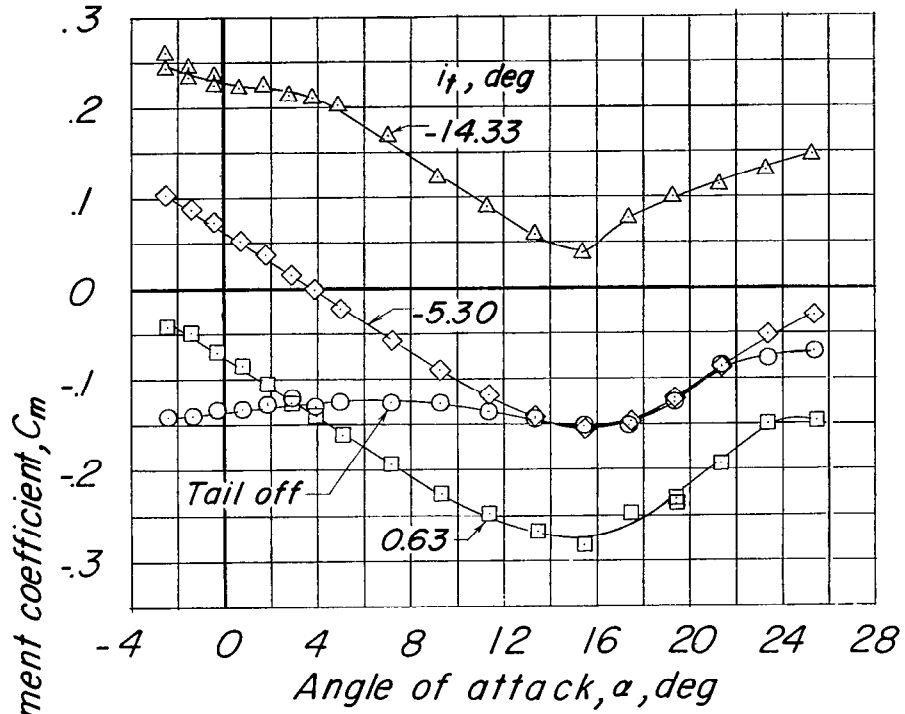


Figure 9.- Concluded.

~~CONFIDENTIAL~~

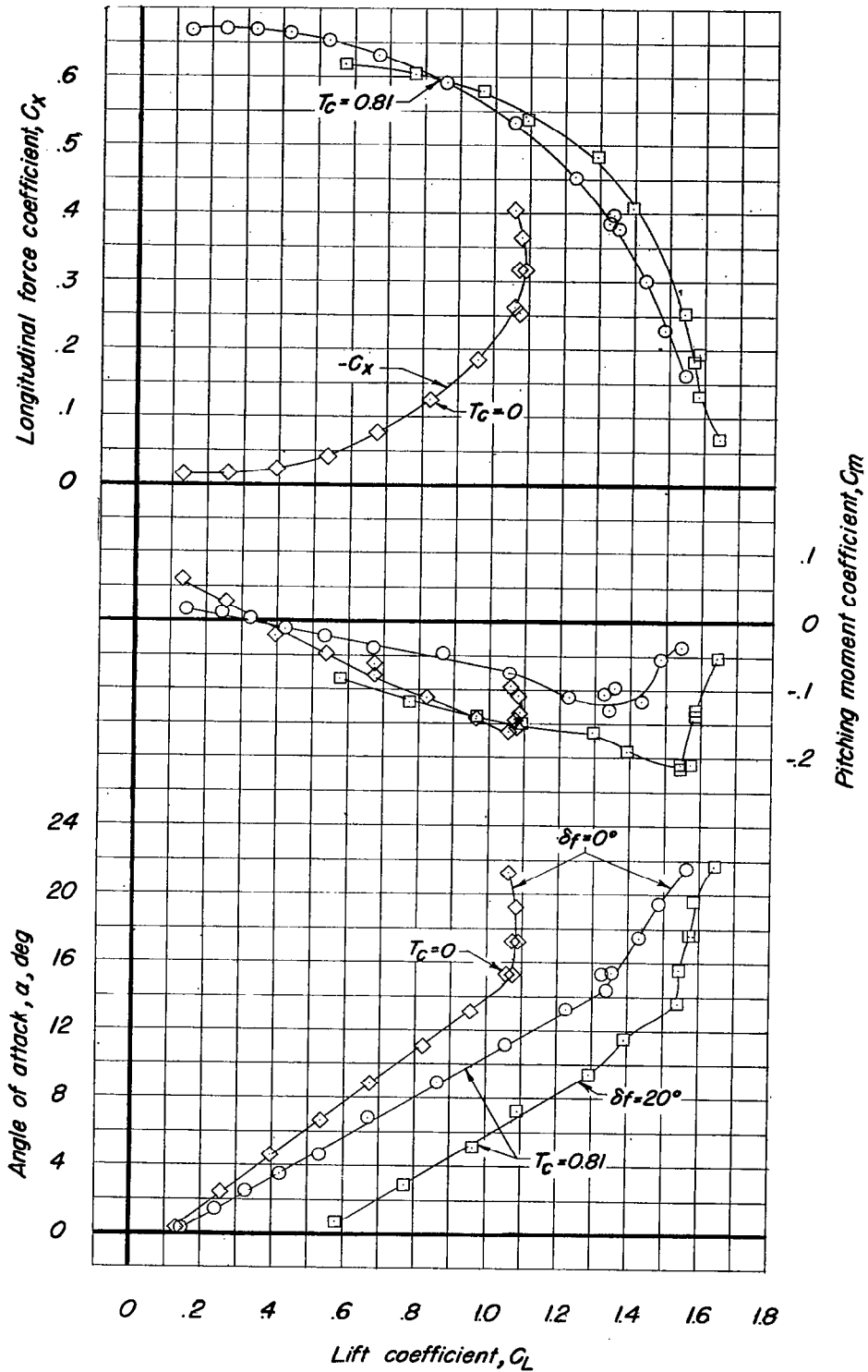
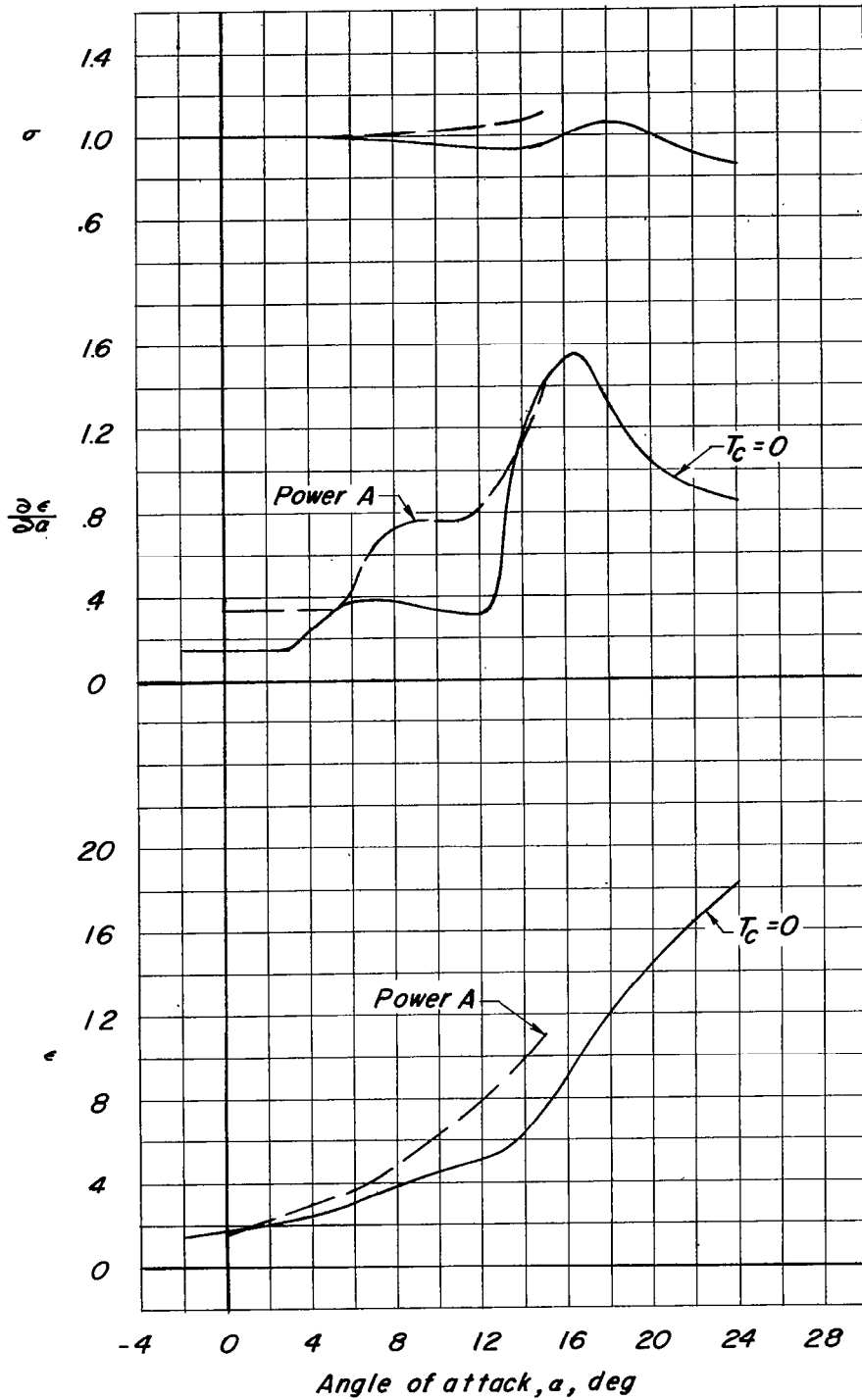


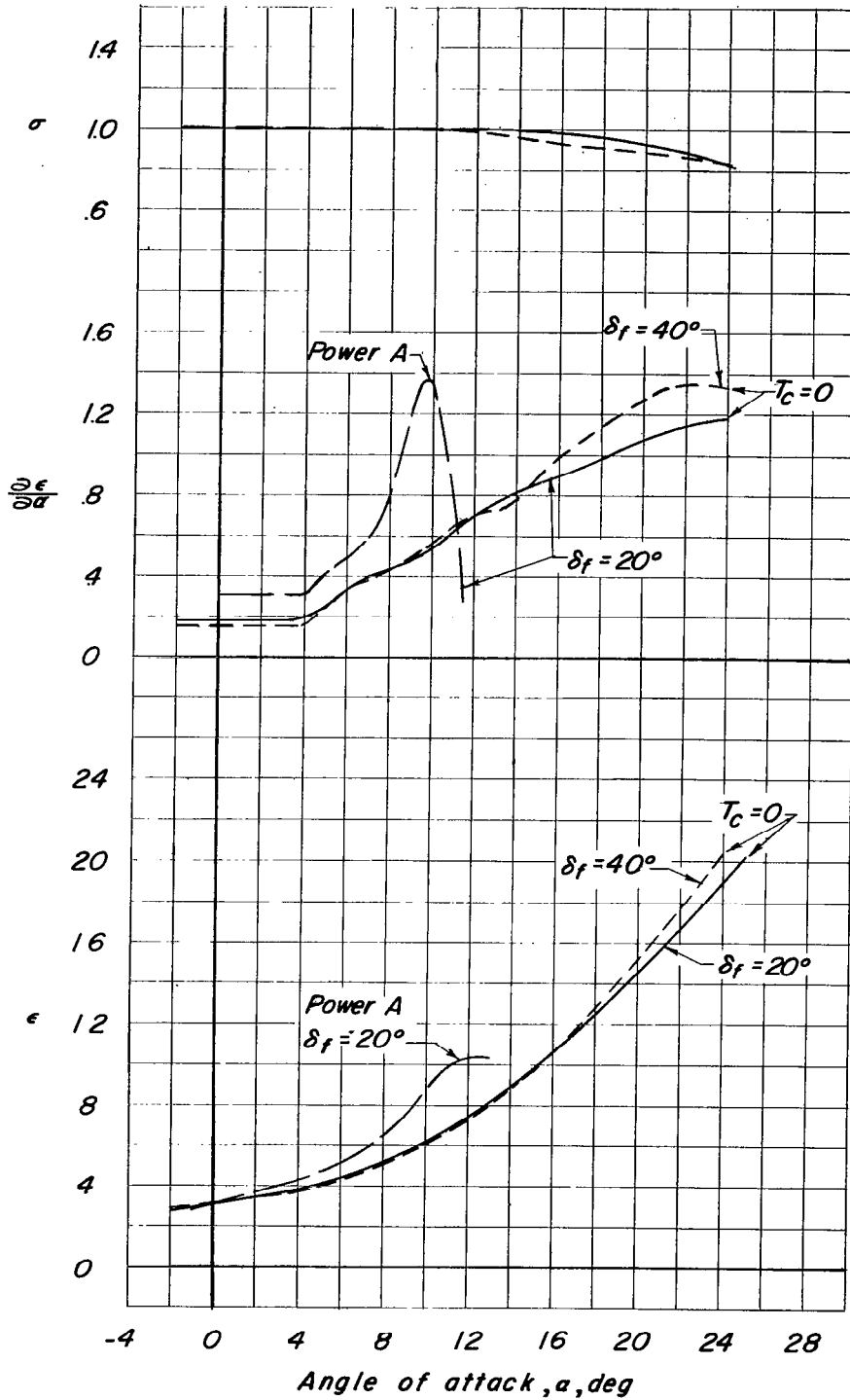
Figure 10.- Longitudinal characteristics of the model with the propeller operating at constant thrust. $\delta_a = \delta_r = 0^\circ$; $i_t = -2.48^\circ$.

~~CONFIDENTIAL~~



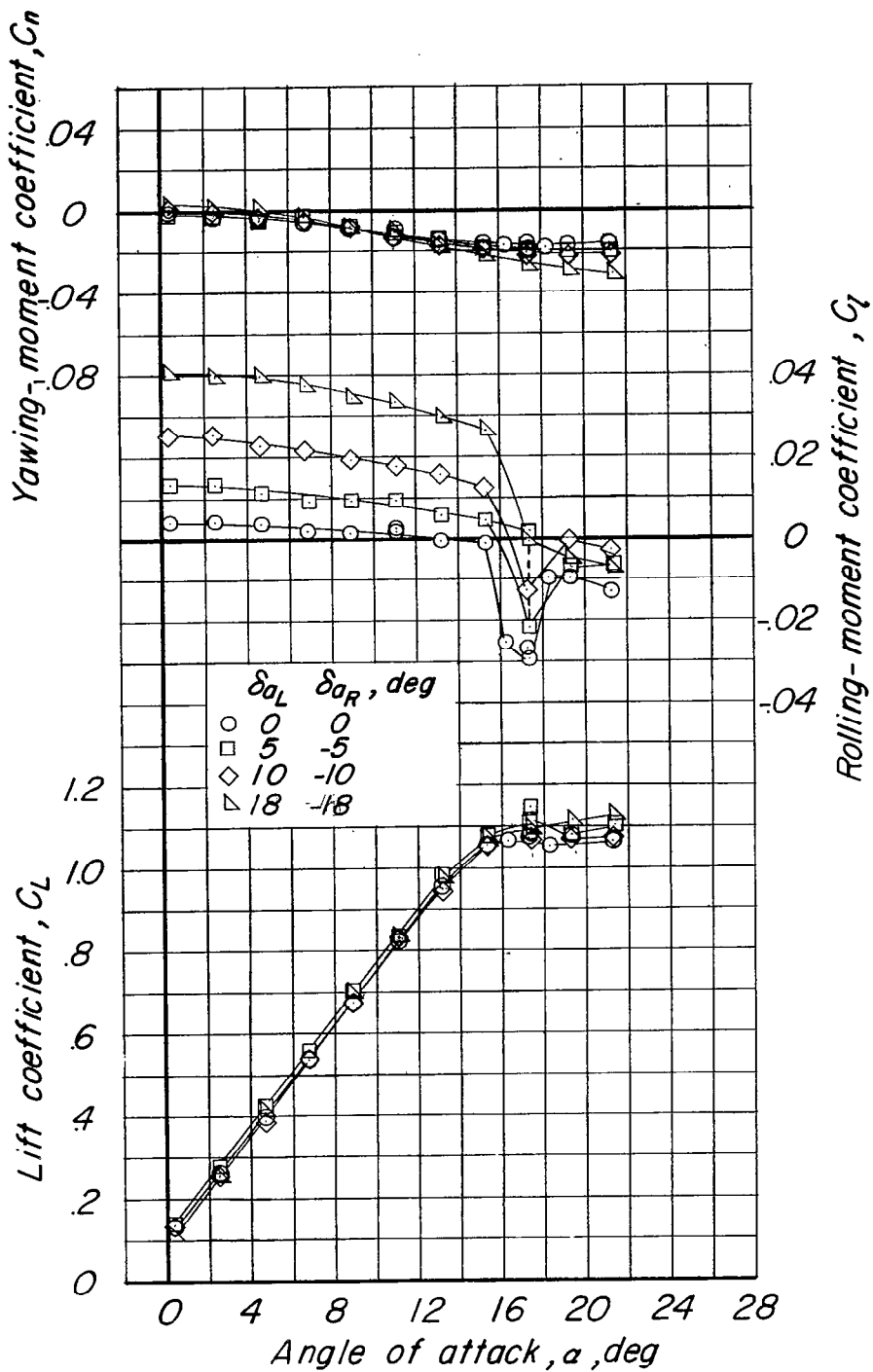
(a) Flaps retracted.

Figure 11.- Summary of downwash and tail effectiveness results.
 $\delta_a = \delta_r = 0^\circ$.



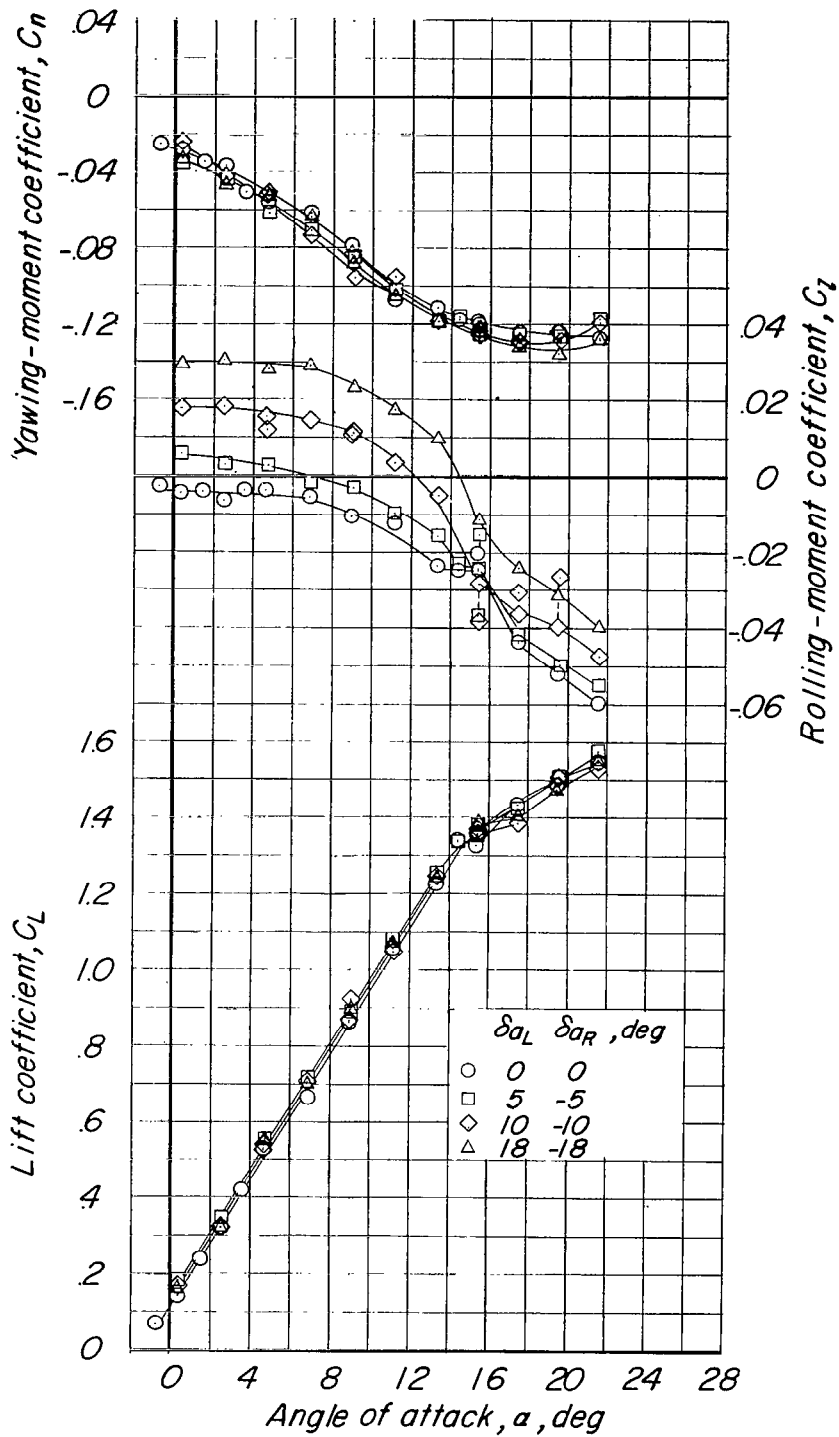
(b) Flaps deflected.

Figure 11.- Concluded.



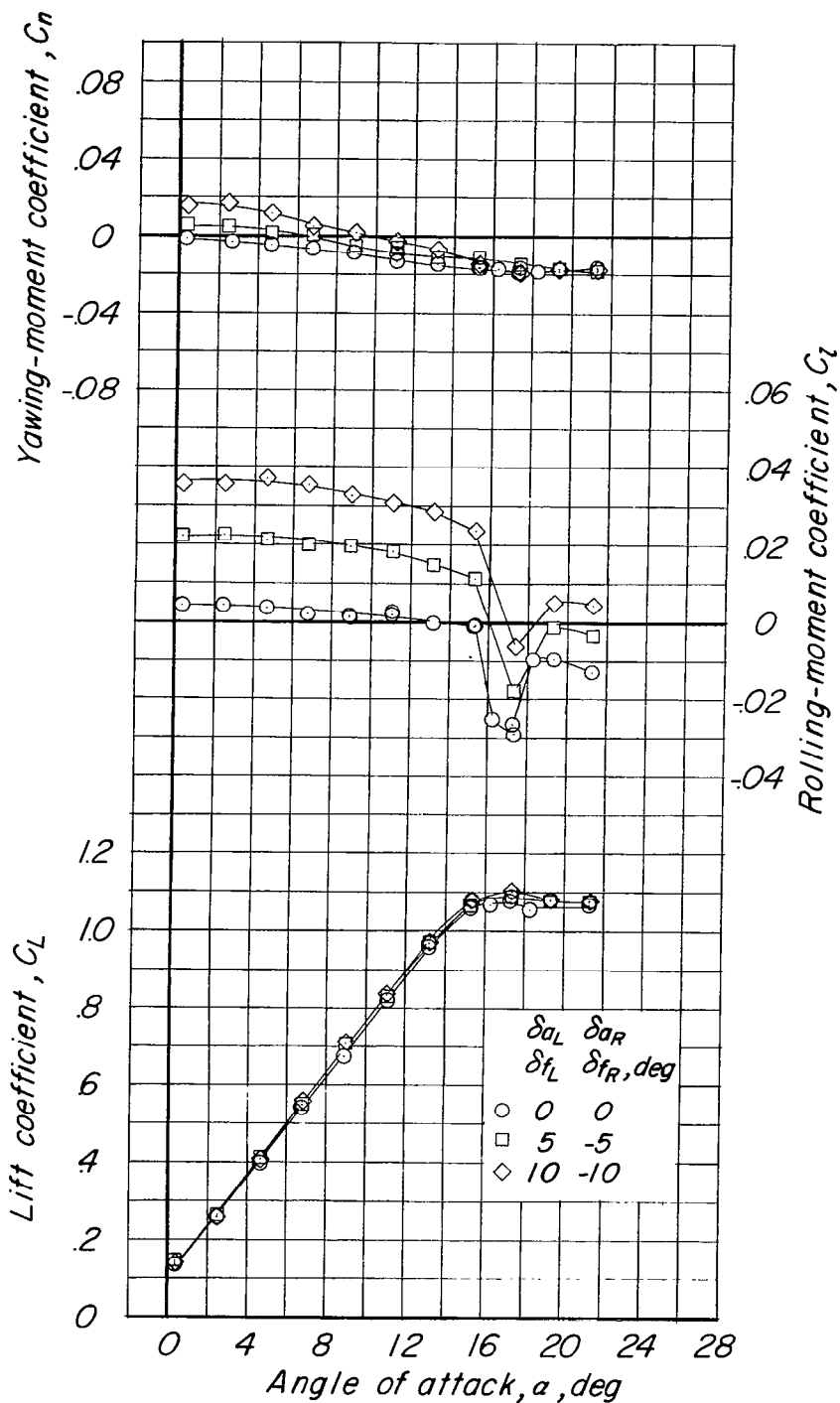
(a) $T_c = 0$; $q = 12$ lb/sq ft.

Figure 12.- Effect of aileron deflection on the aerodynamic characteristics of the model in the clean configuration. $\delta_f = \delta_r = 0^\circ$; $i_t = -2.48^\circ$.



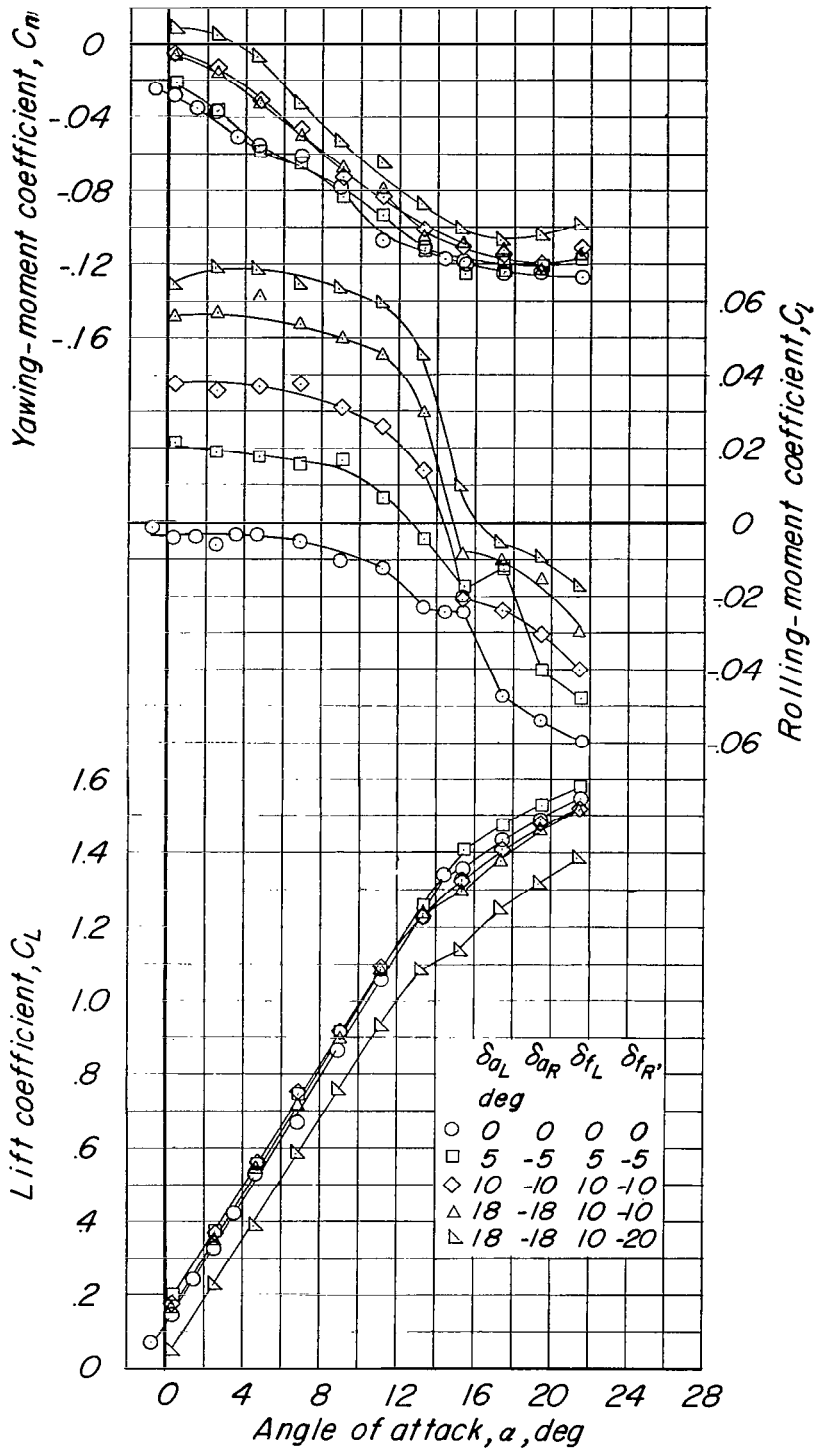
(b) $T_c = 0.81$; $q = 8 \text{ lb/sq ft.}$

Figure 12.- Concluded.



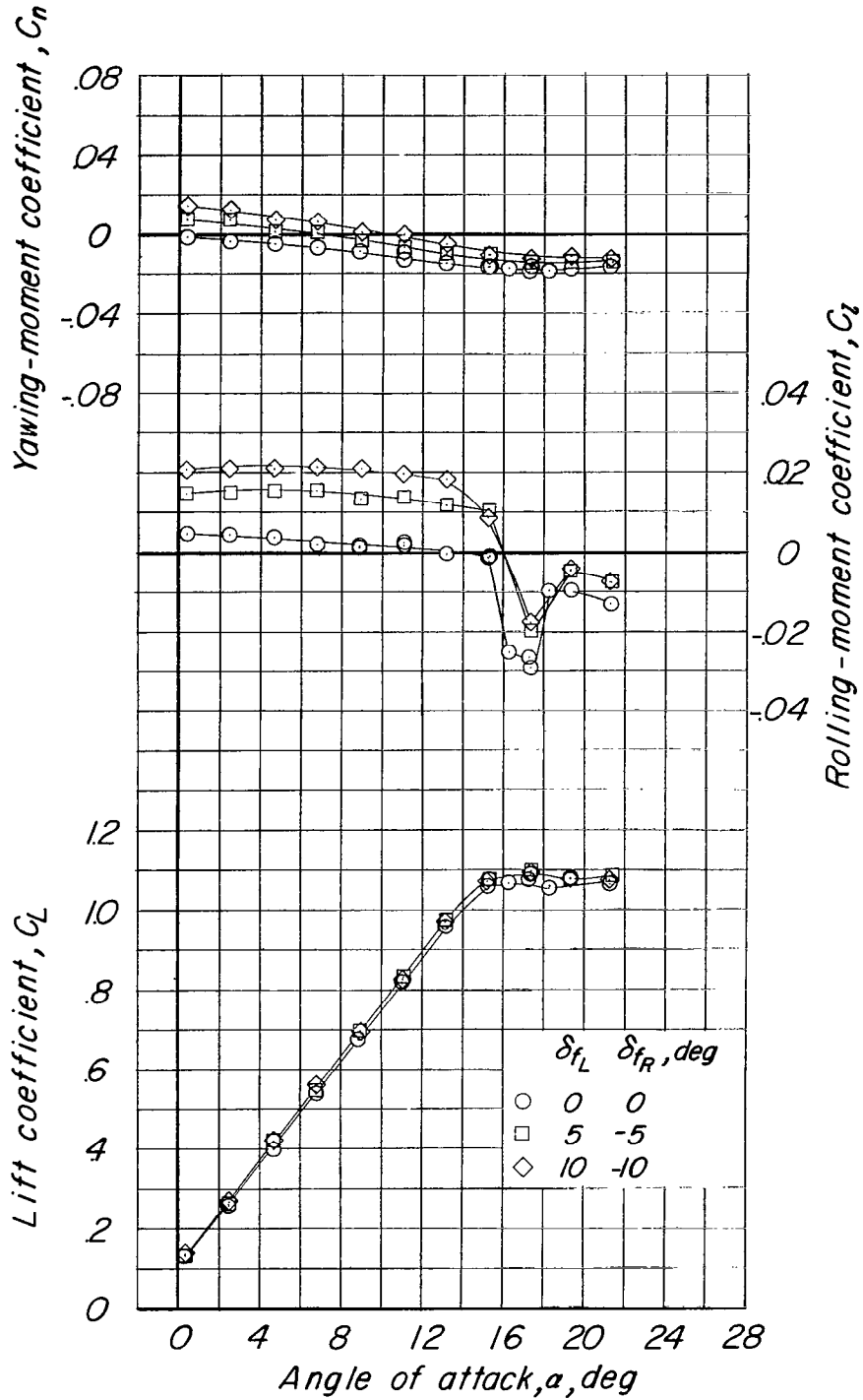
(a) $T_c = 0$; $q = 12$ lb/sq ft.

Figure 13.- Effect of aileron and differential flap deflection on the aerodynamic characteristics of the model in the clean configuration. $\delta_r = 0^\circ$; $i_t = -2.48^\circ$.



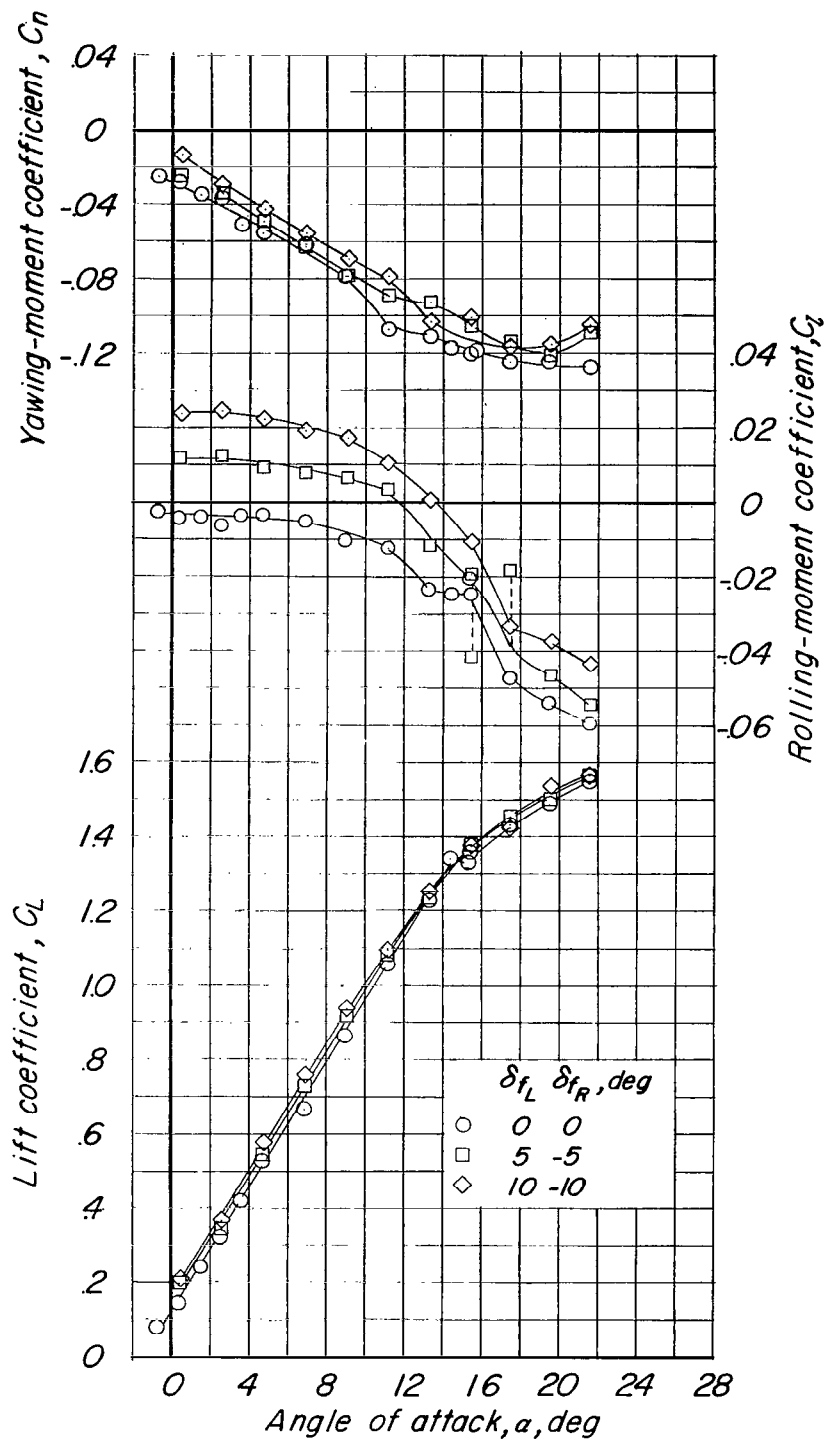
(b) $T_c = 0.81$; $q = 8$ lb sq ft.

Figure 13.- Concluded.



(a) T_c = 0; q = 12 lb/sq ft.

Figure 14.- Effect of differential flap deflection on the aerodynamic characteristics of the model in the clean configuration. δ_a = δ_r = 0°; i_t = -2.48°.



(b) $T_c = 0.81$; $q = 8$ lb/sq ft.

Figure 14.- Concluded.

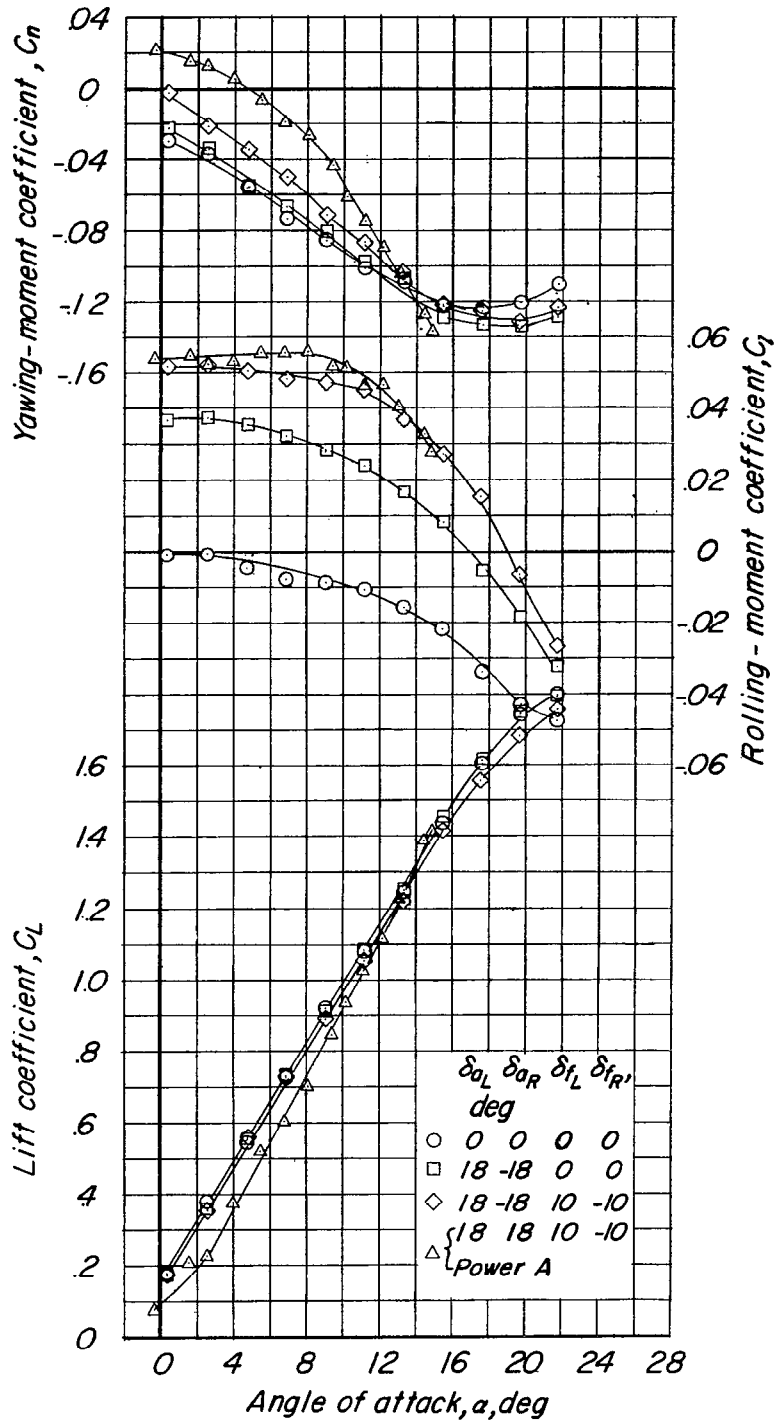


Figure 15.- Effect of full corrective aileron and differential flap deflection on the power-on aerodynamic characteristics of the model with slats extended. Clean configuration; wing fence and modified leading edge off; $T_c = 0.81$; $\delta_r = 0^\circ$; $i_t = -2.48^\circ$; $q = 8$ lb/sq ft.

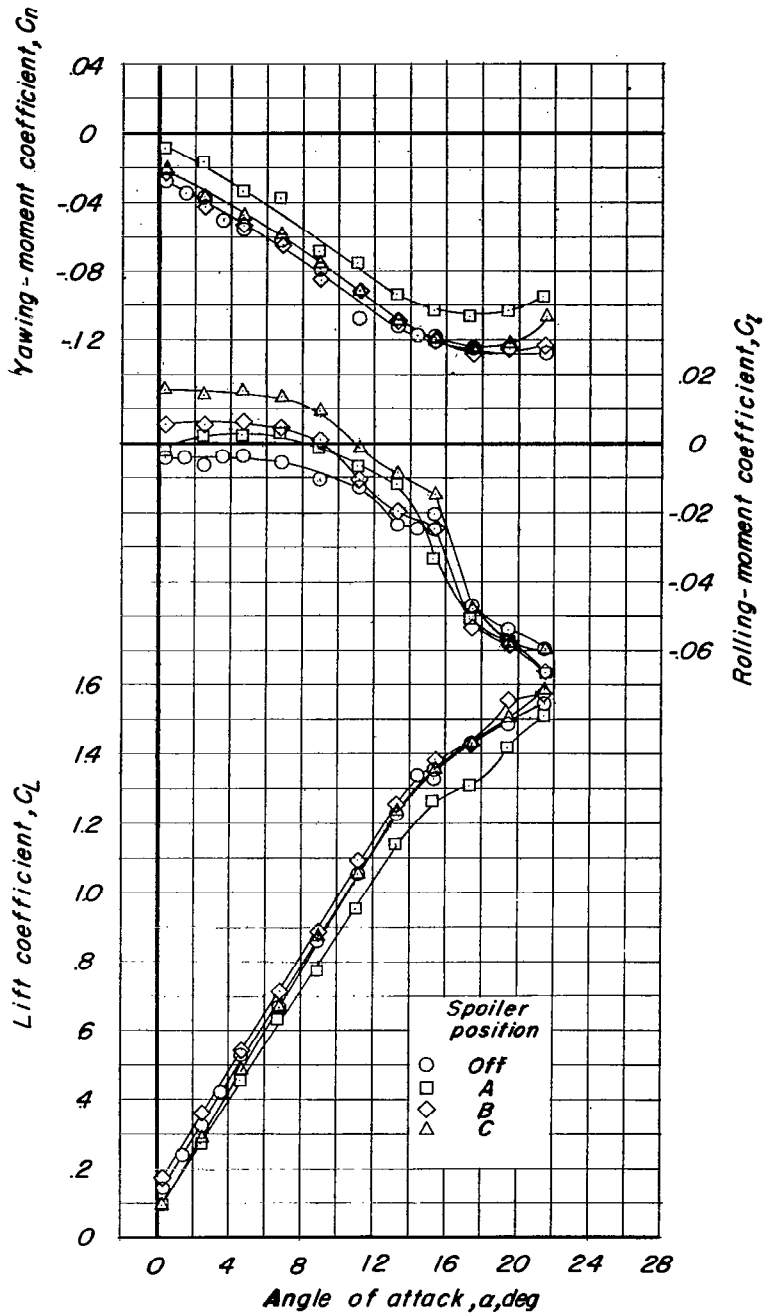


Figure 16.- Effect of spoiler location on the right wing. Clean configuration; $T_c = 0.81$; $\delta_f = \delta_a = \delta_r = 0^\circ$; $i_t = 2.48^\circ$; $q = 8 \text{ lb/sq ft}$.

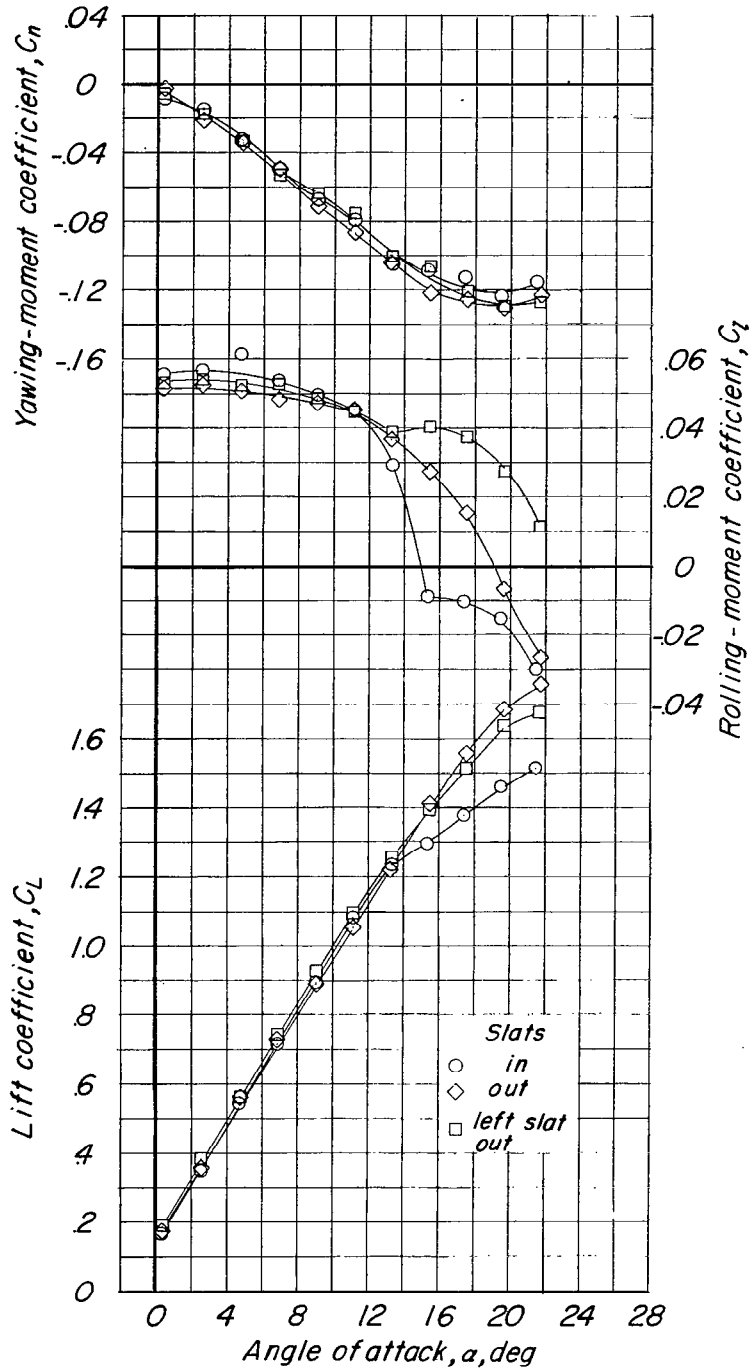


Figure 17.- Effect of projecting the left slat on the power-on aerodynamic characteristics of the model with full corrective aileron and differential flap deflection. Clean configuration; wing fence and modified leading edge off; $T_c = 0.81$; $\delta_{f_L} = 10^\circ$; $\delta_{f_R} = -10^\circ$; $\delta_{a_L} = 18^\circ$; $\delta_{a_R} = -18^\circ$; $\delta_r = 0^\circ$; $i_t = -2.48^\circ$; $q = 8 \text{ lb/sq ft}$.

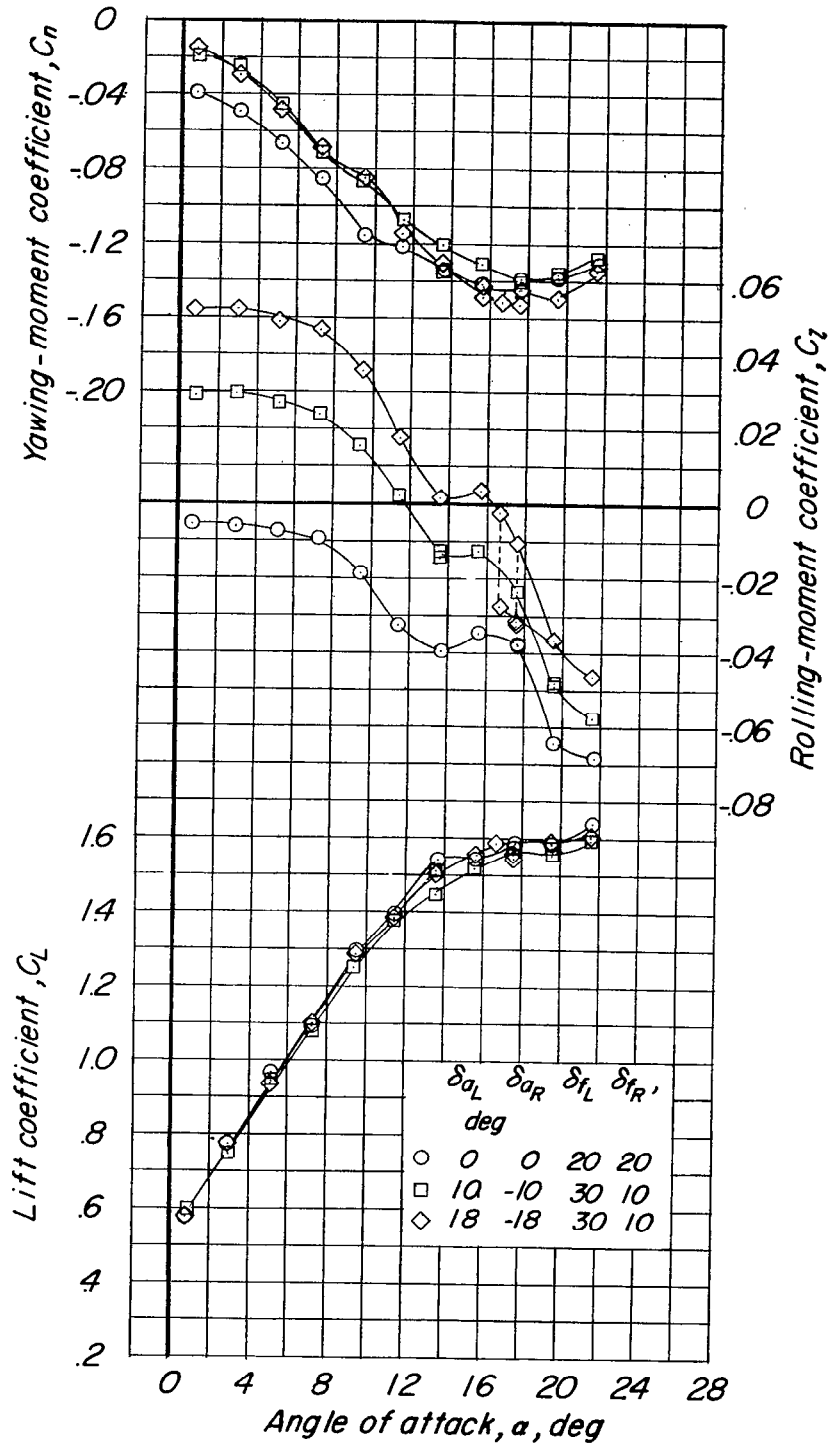
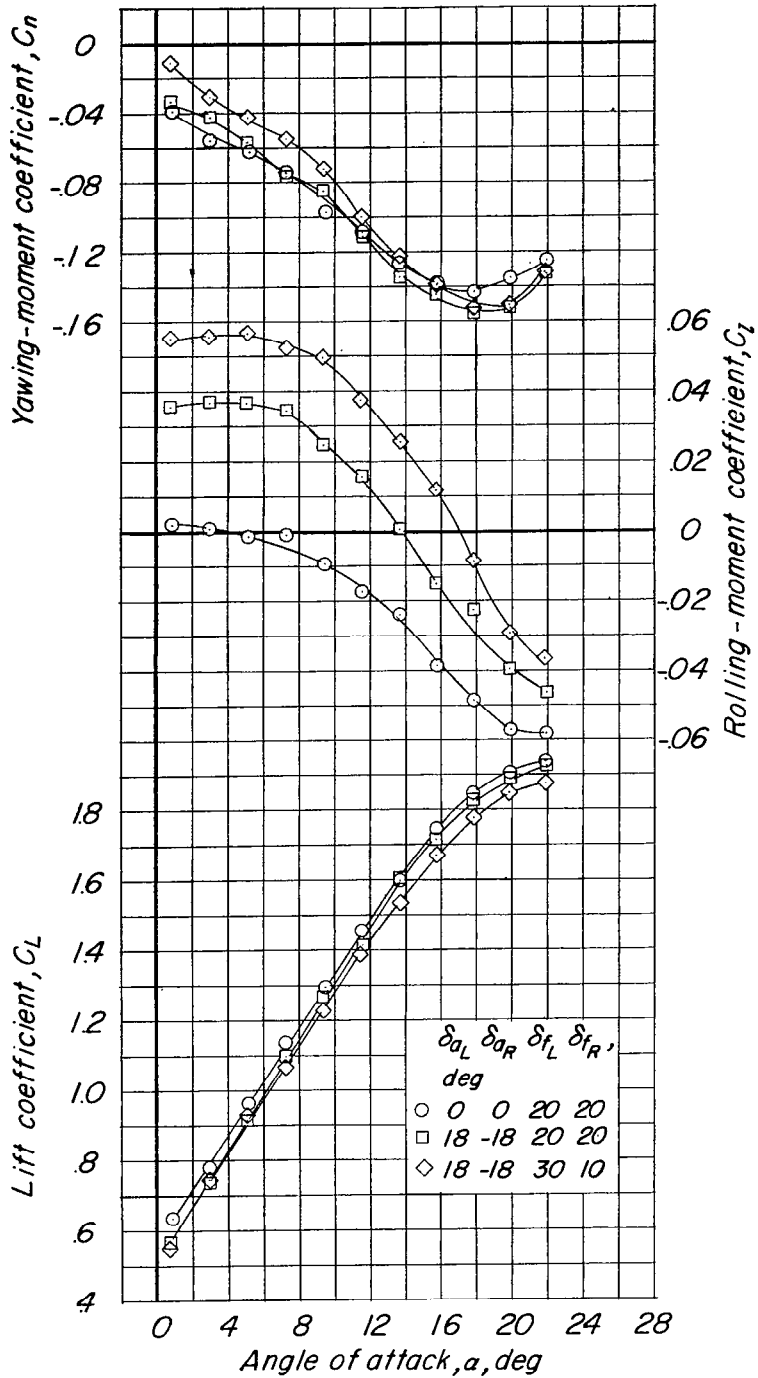
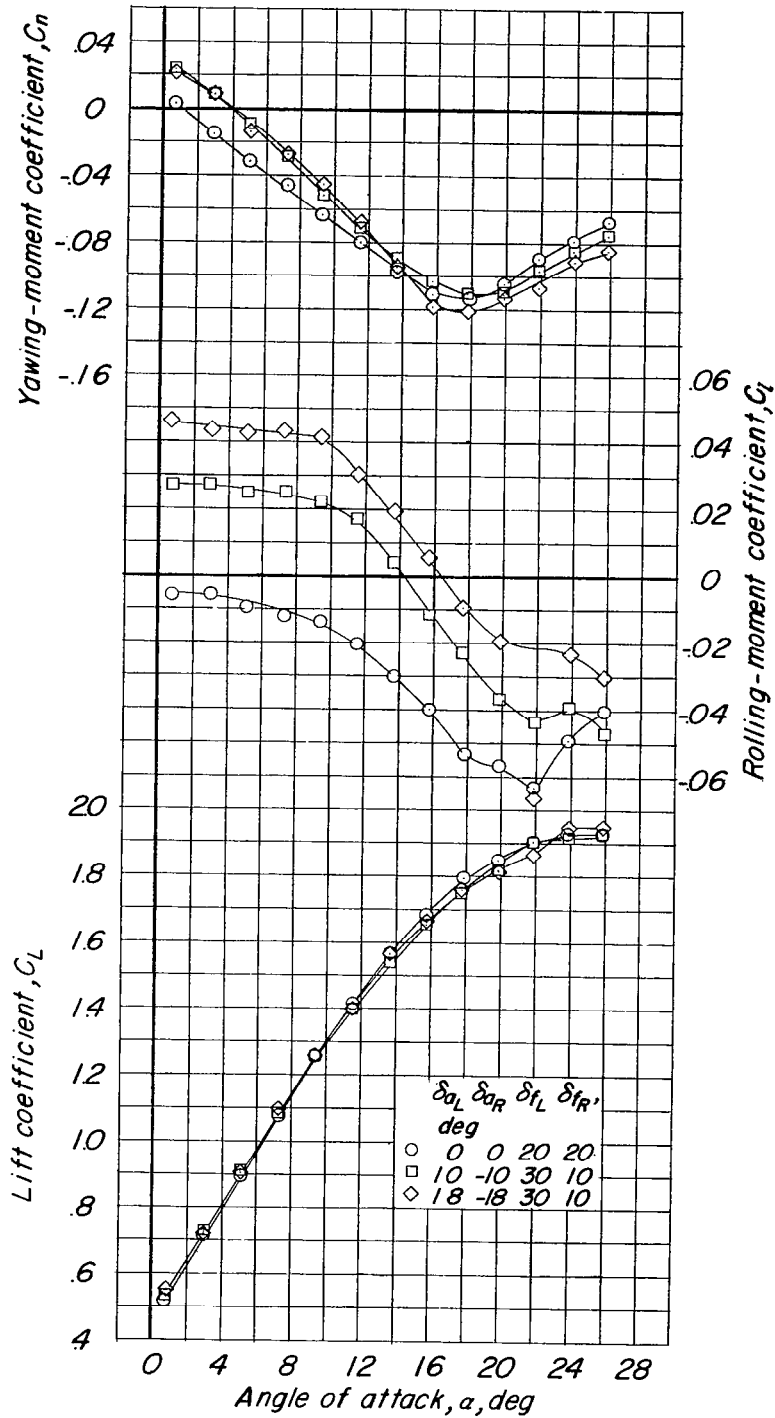


Figure 18.- Effect of aileron and differential flap deflection on the power-on aerodynamic characteristics of the model in the take-off configuration. $T_c = 0.81$; $\delta_r = 0^\circ$; $i_t = -2.48^\circ$; $q = 8$ lb/sq ft.



(a) Wing fence and modified leading edge on.

Figure 19.- Effect of full aileron and differential flap deflection on the power-on aerodynamic characteristics of the model with the slats extended. Take-off configuration; $T_c = 0.81$; $\delta_r = 0^\circ$; $i_t = -2.48^\circ$; $q = 8 \text{ lb/sq ft}$.



(b) Wing fence and modified leading edge off.

Figure 19.- Concluded.

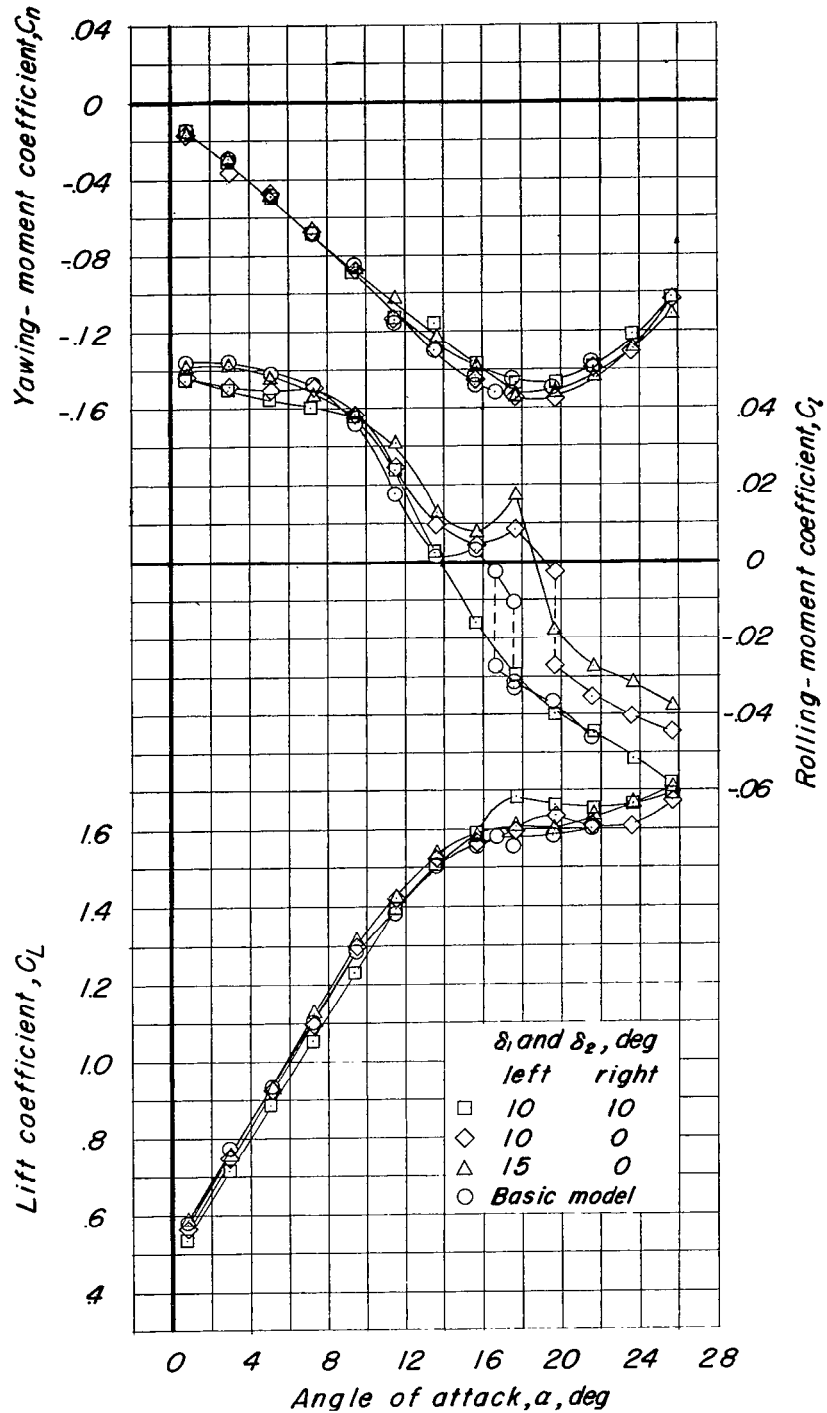
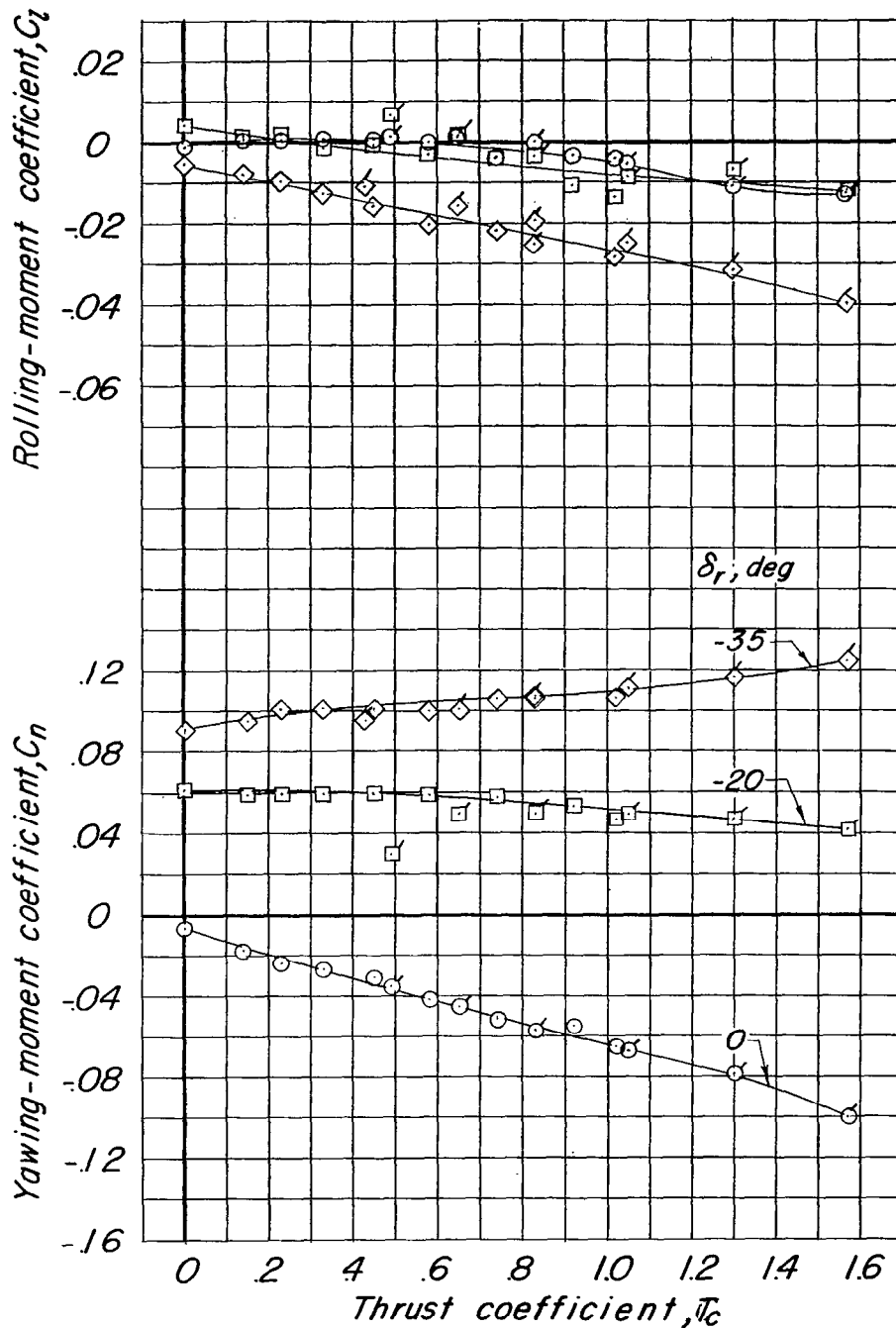
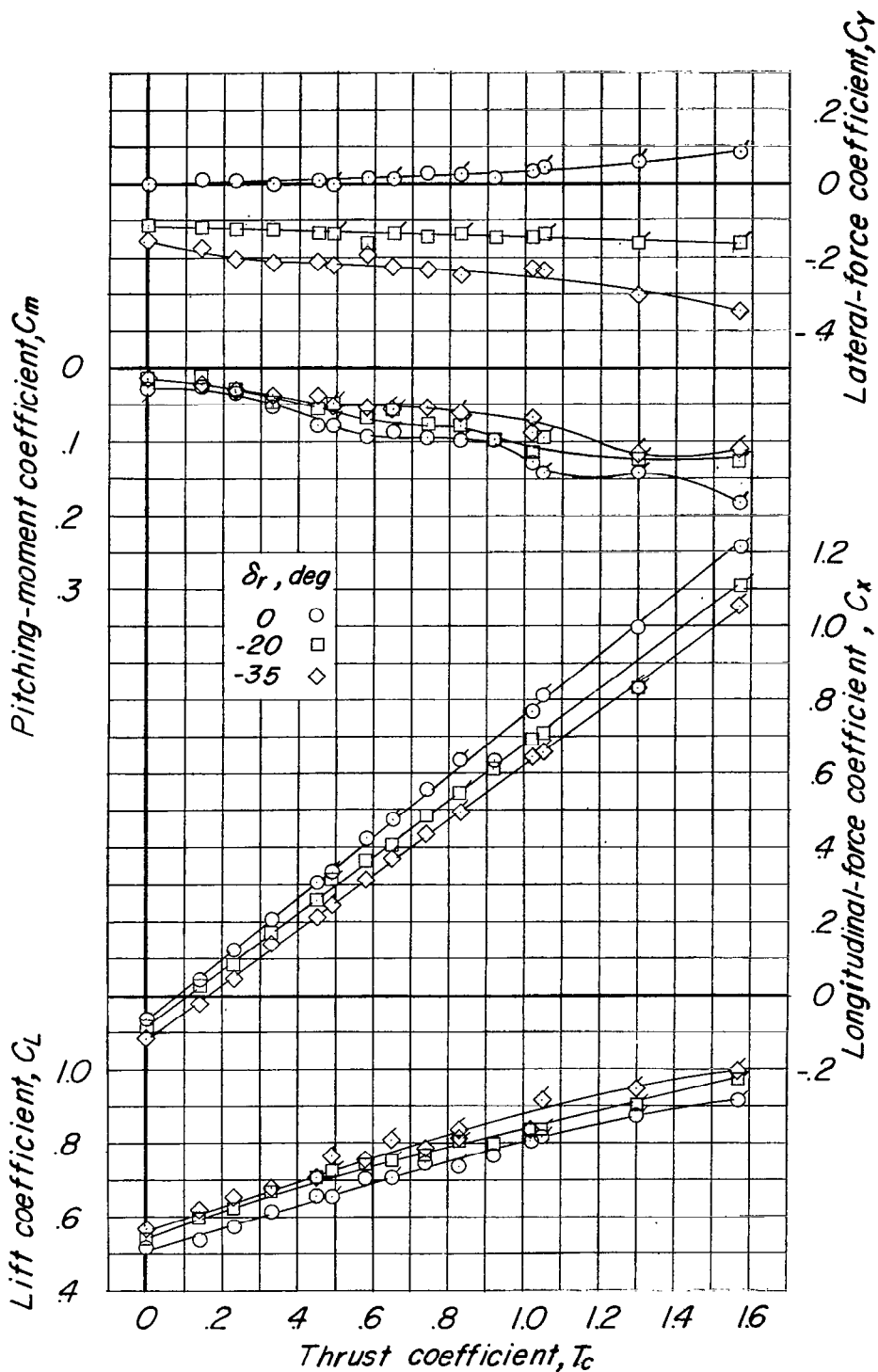


Figure 20.- Effect of droop angle of the leading-edge chord-extension on the left wing. Take-off configuration; wing fence and modified leading edge off; $T_c = 0.81$; $\delta_r = 0^\circ$; $i_t = 2.48^\circ$; $\delta_{f_L} = 30^\circ$; $\delta_{f_R} = 10^\circ$; $\delta_{a_L} = 18^\circ$; $\delta_{a_R} = -18^\circ$; $q = 8$ lb/sq ft.



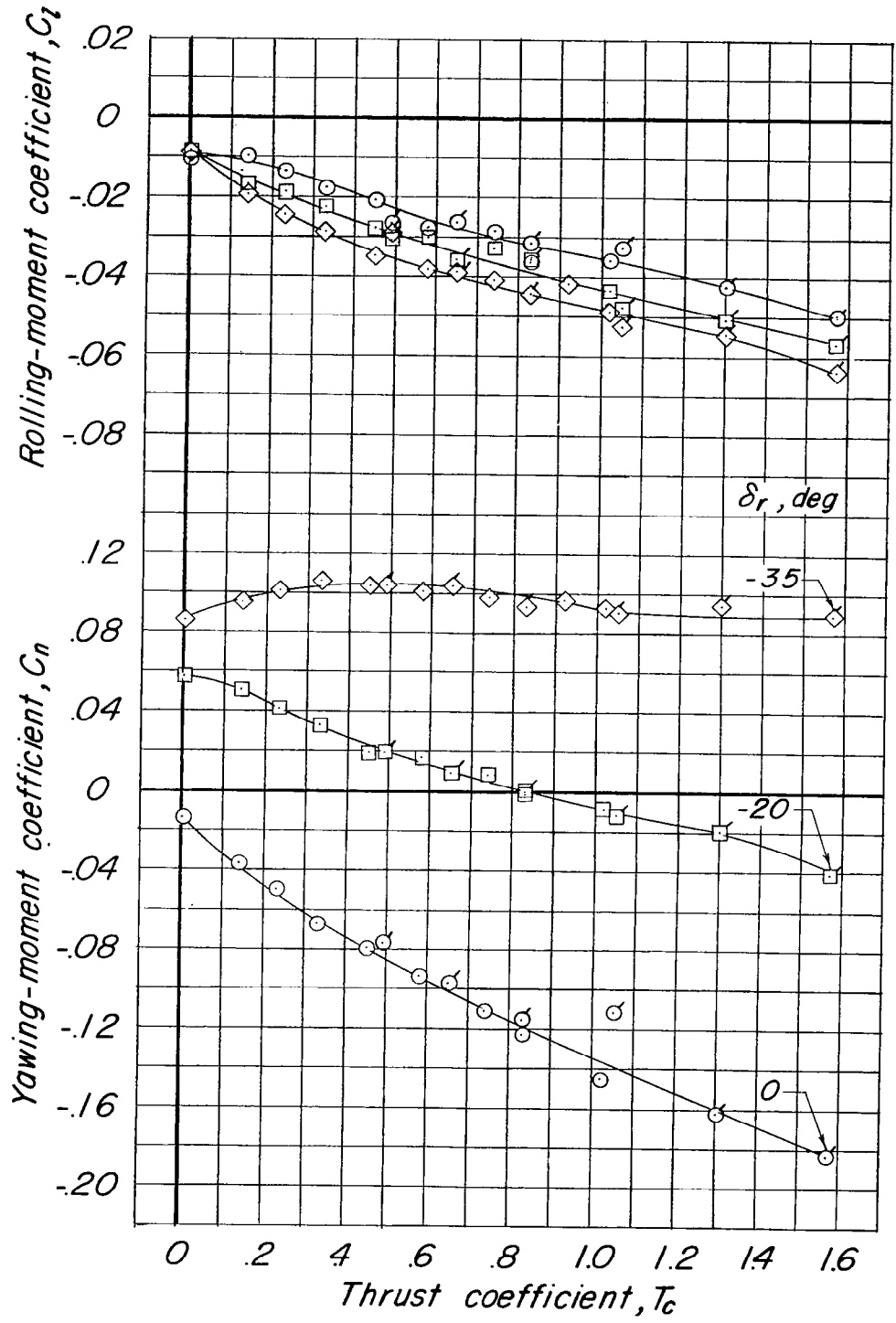
(a) $\alpha = 3^\circ$.

Figure 21.- Variation of aerodynamic characteristics at zero sideslip with thrust coefficient for several rudder deflections. Take-off configuration; $\delta_f = 20^\circ$; $\delta_a = 0^\circ$; $i_t = -2.48^\circ$; $q = 6$ and 4 lb/sq ft. Flagged symbols indicate data at $q = 4$ lb/sq ft.



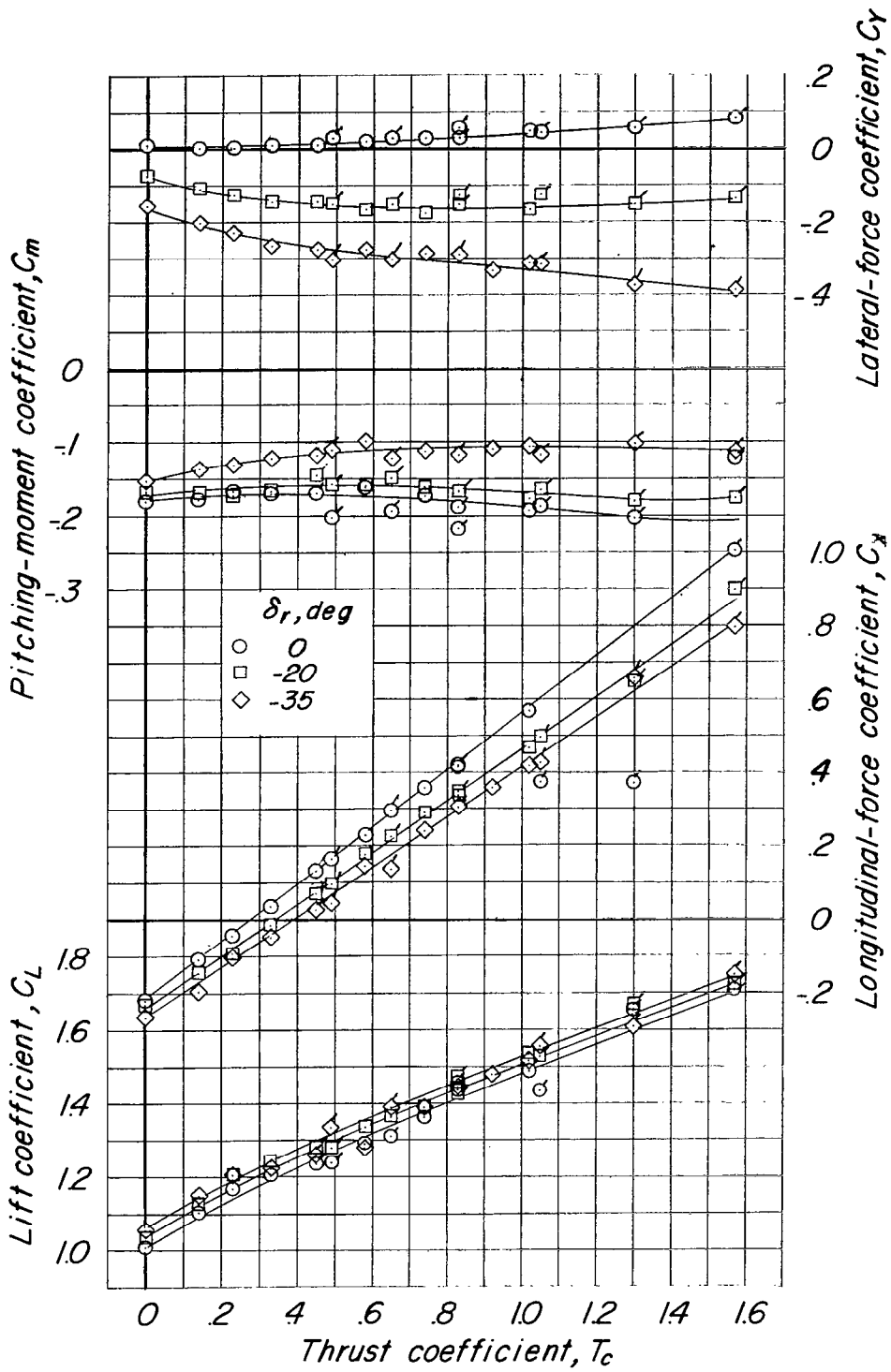
(a) Concluded.

Figure 21.- Continued.



(b) $\alpha = 11.4^\circ$.

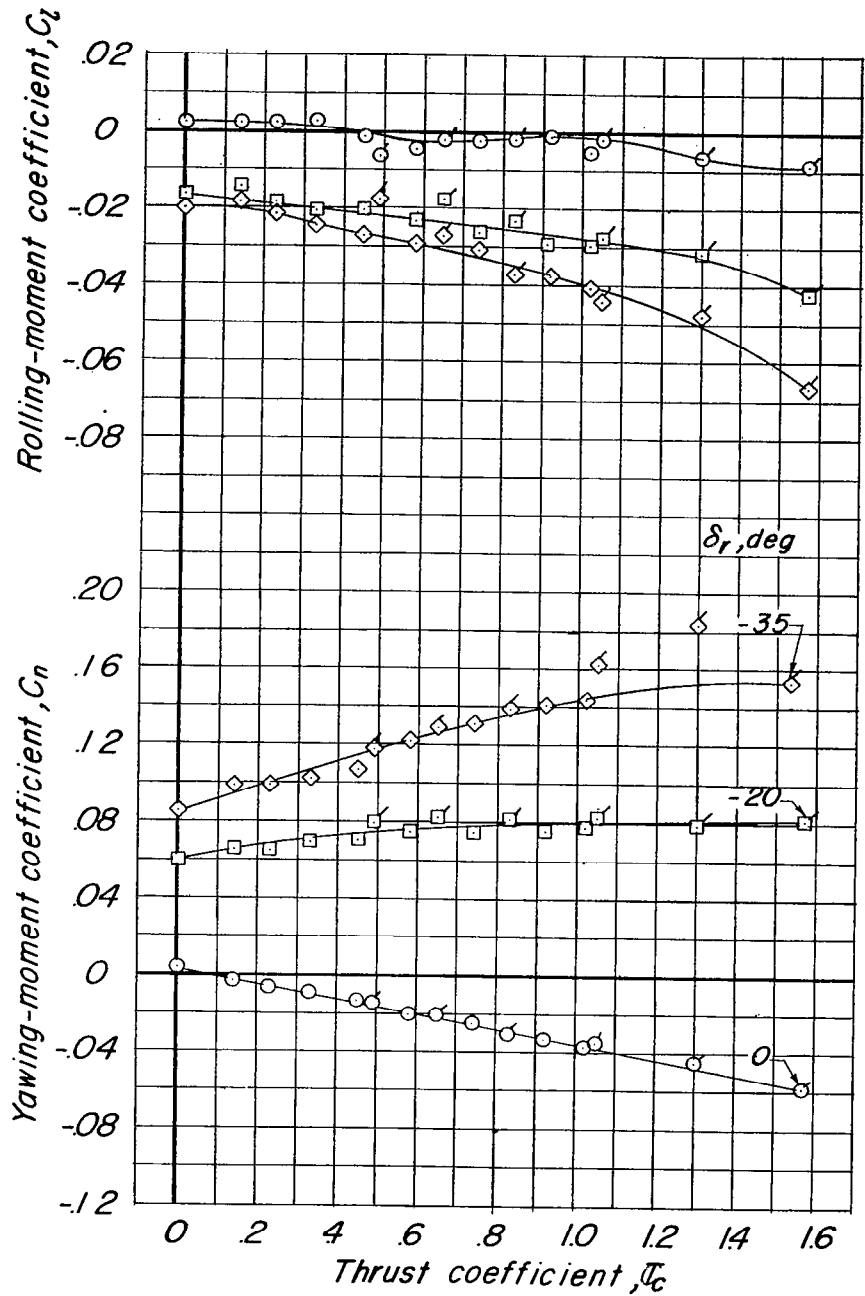
Figure 21.- Continued.



(b) Concluded.

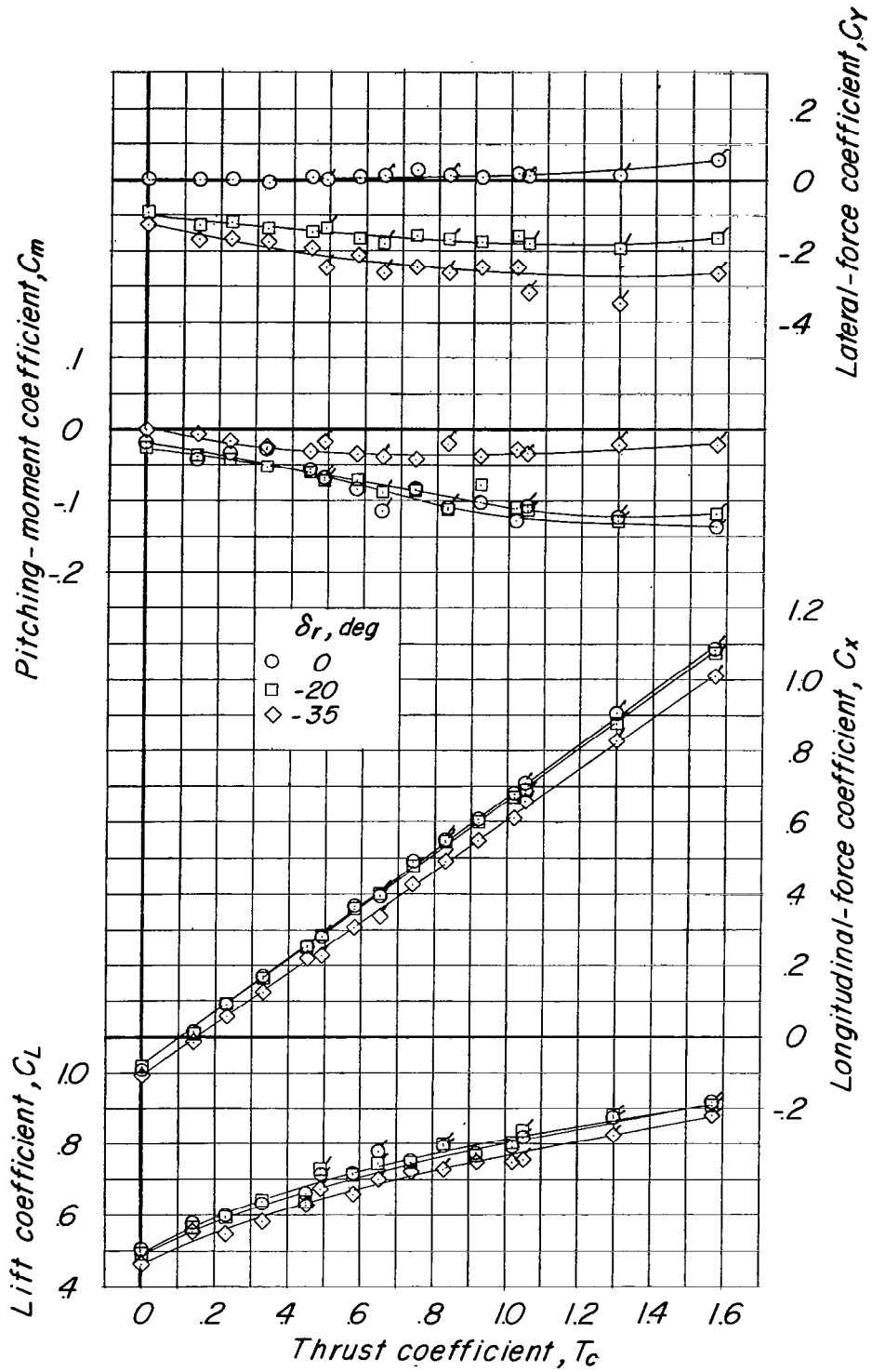
Figure 21.- Concluded.

~~CONFIDENTIAL~~



(a) $\alpha = 3^\circ$.

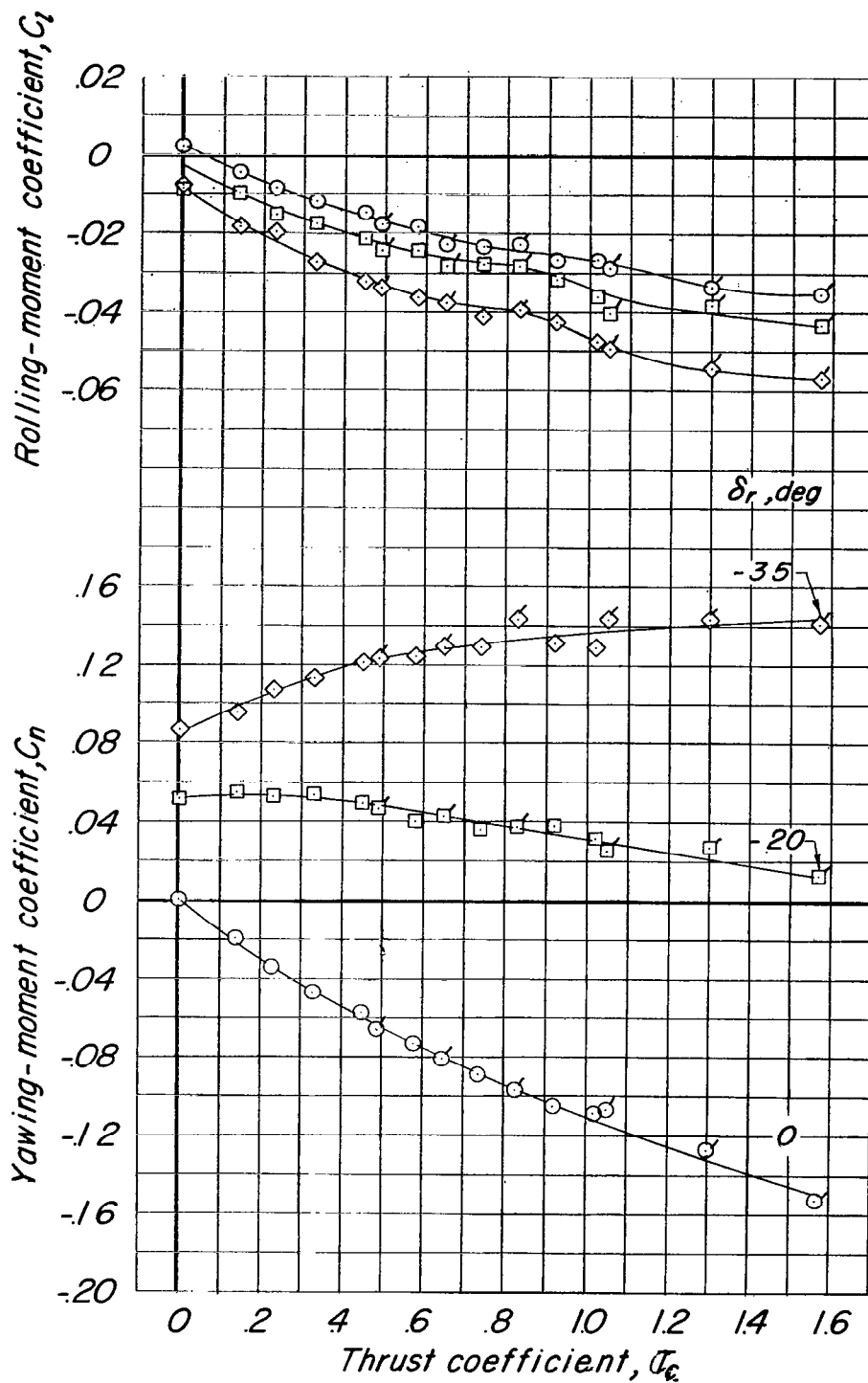
Figure 22.- Variation of aerodynamic characteristics at zero sideslip with thrust coefficient for several rudder deflections with the canopy fin on. Take-off configuration; canopy fin offset 10° ; $\delta_f = 20^\circ$; $\delta_a = 0^\circ$; $i_t = -2.48^\circ$; $q = 6$ and 4 lb/sq ft. Flagged symbols indicate data at $q = 4$ lb/sq ft.



(a) Concluded.

Figure 22.- Continued.

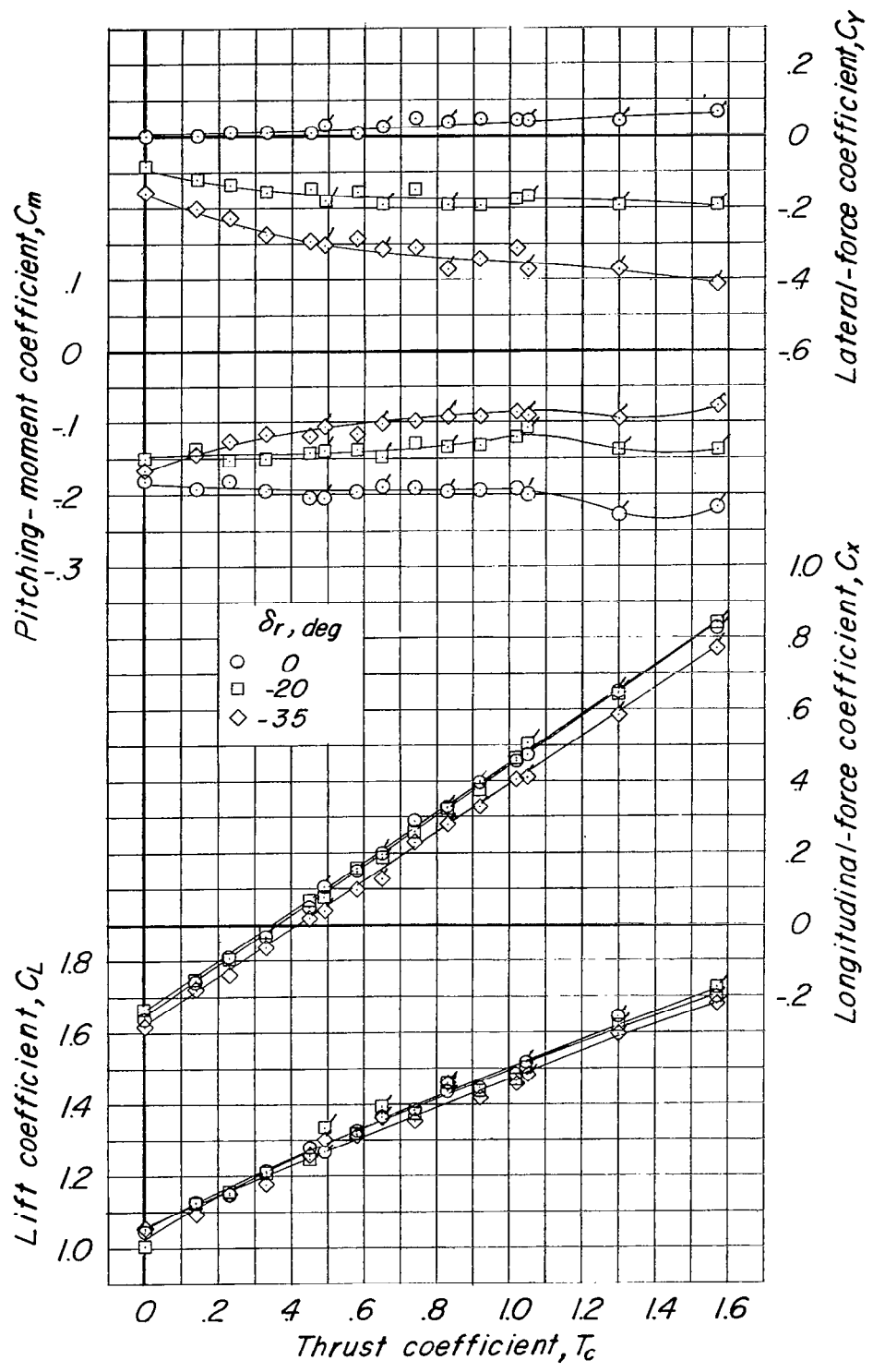
~~CONFIDENTIAL~~



(b) $\alpha = 11.4^\circ$.

Figure 22.- Continued.

~~CONFIDENTIAL~~



(b) Concluded.

Figure 22.- Concluded.

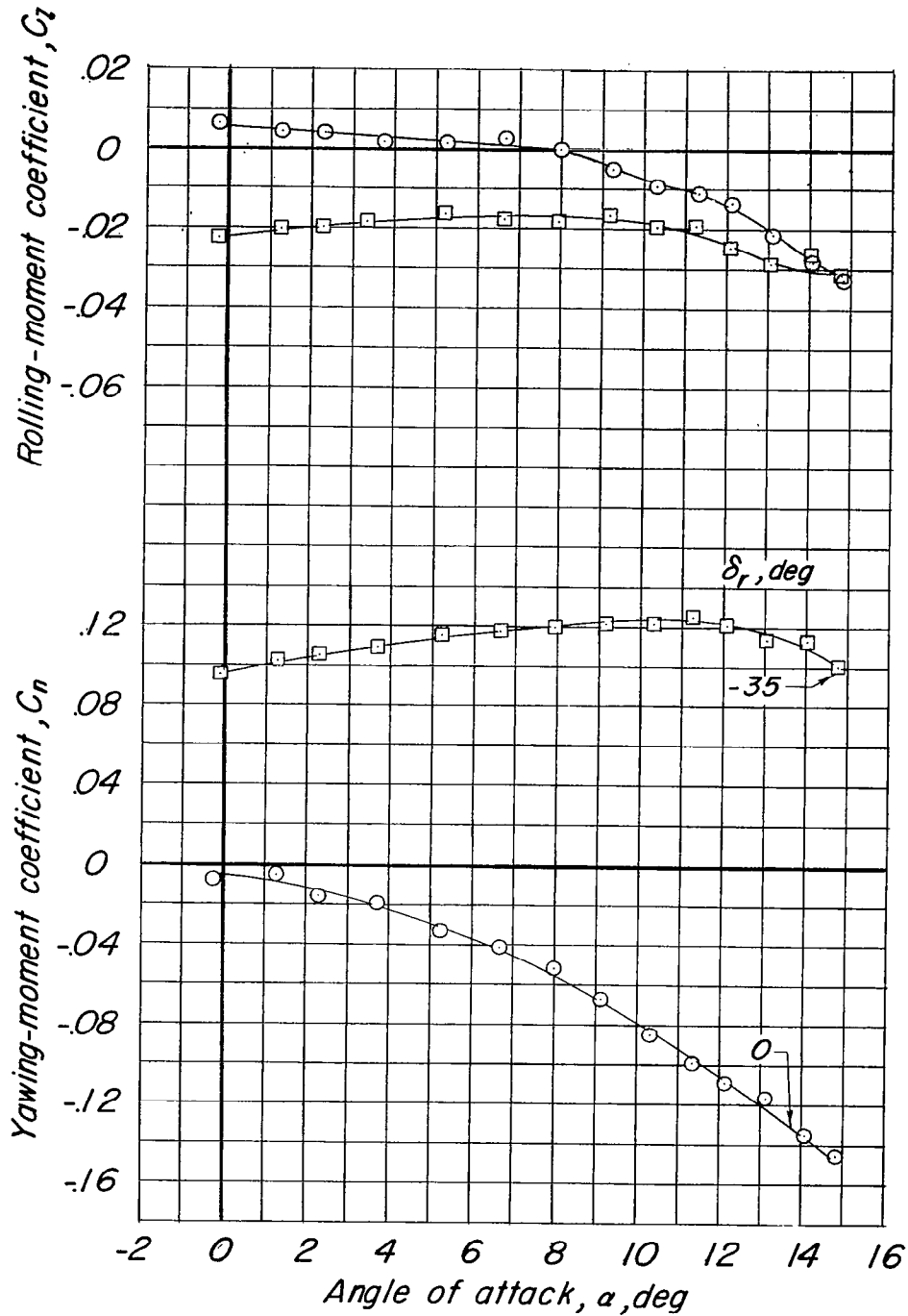
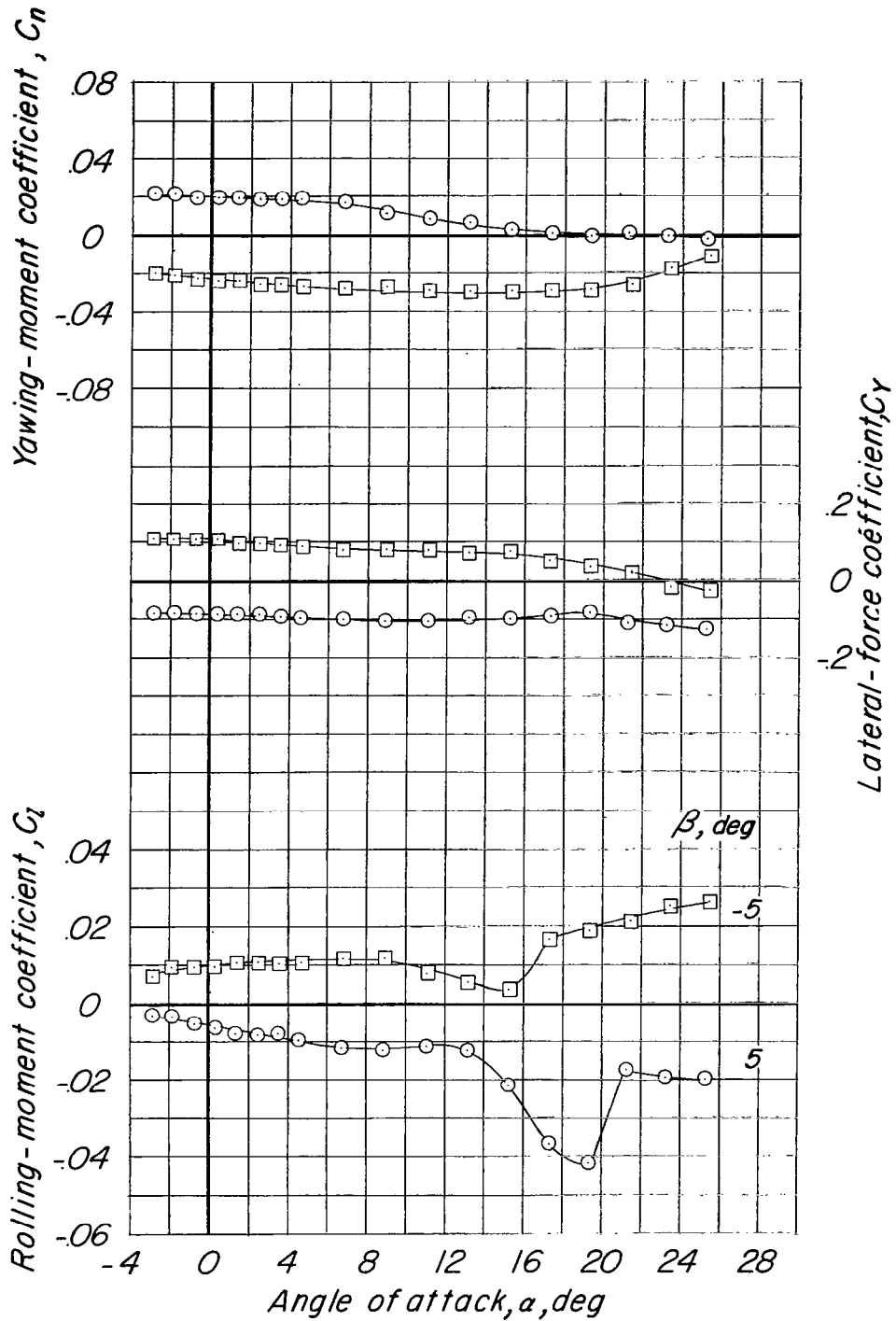
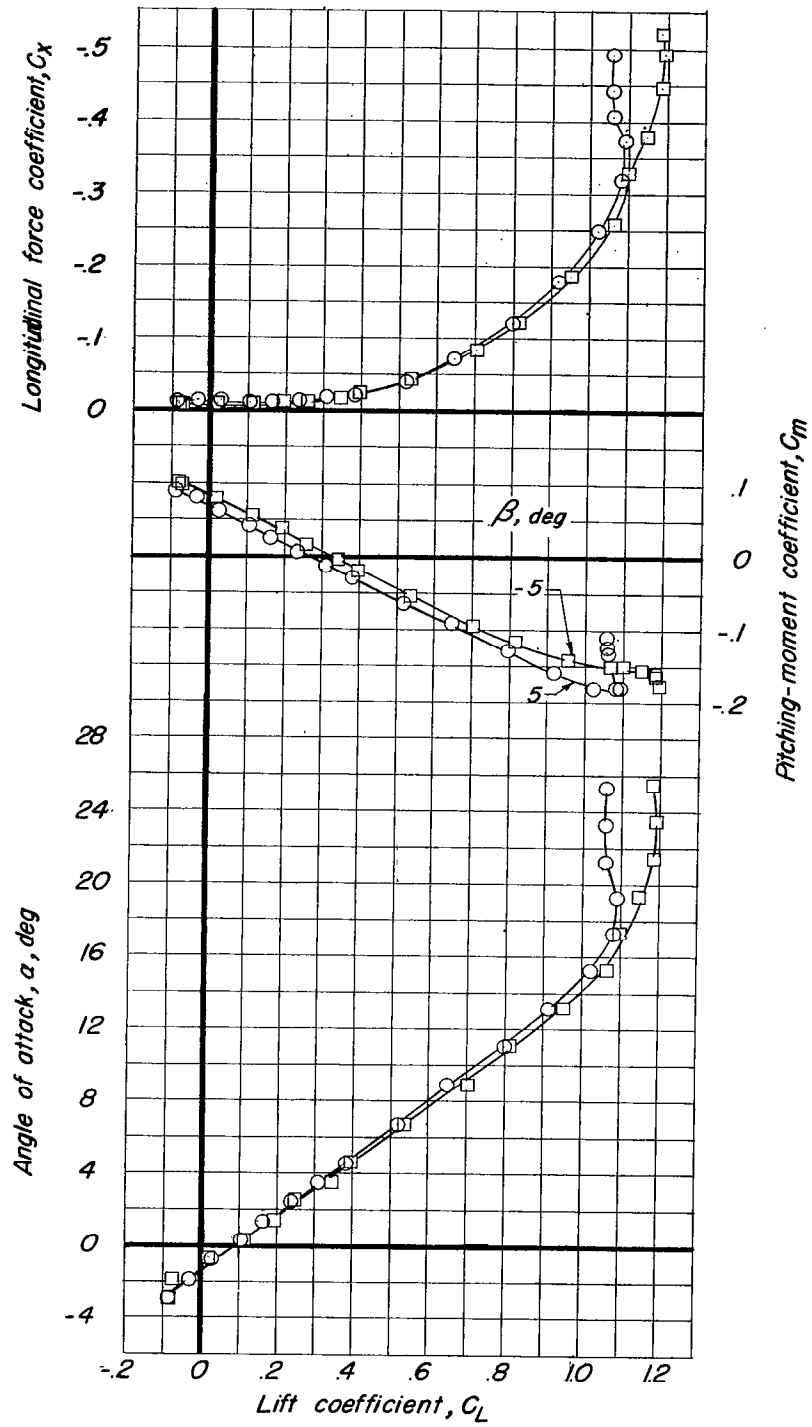


Figure 23.- Effect of rudder deflection on the lateral characteristics in pitch. Clean configuration; power A; $\delta_f = 0^\circ$; $\delta_a = 0^\circ$; $i_t = -2.48^\circ$; $q = 8$ lb/sq ft. Longitudinal characteristics for $\delta_r = 0^\circ$ presented in figure 7(b).



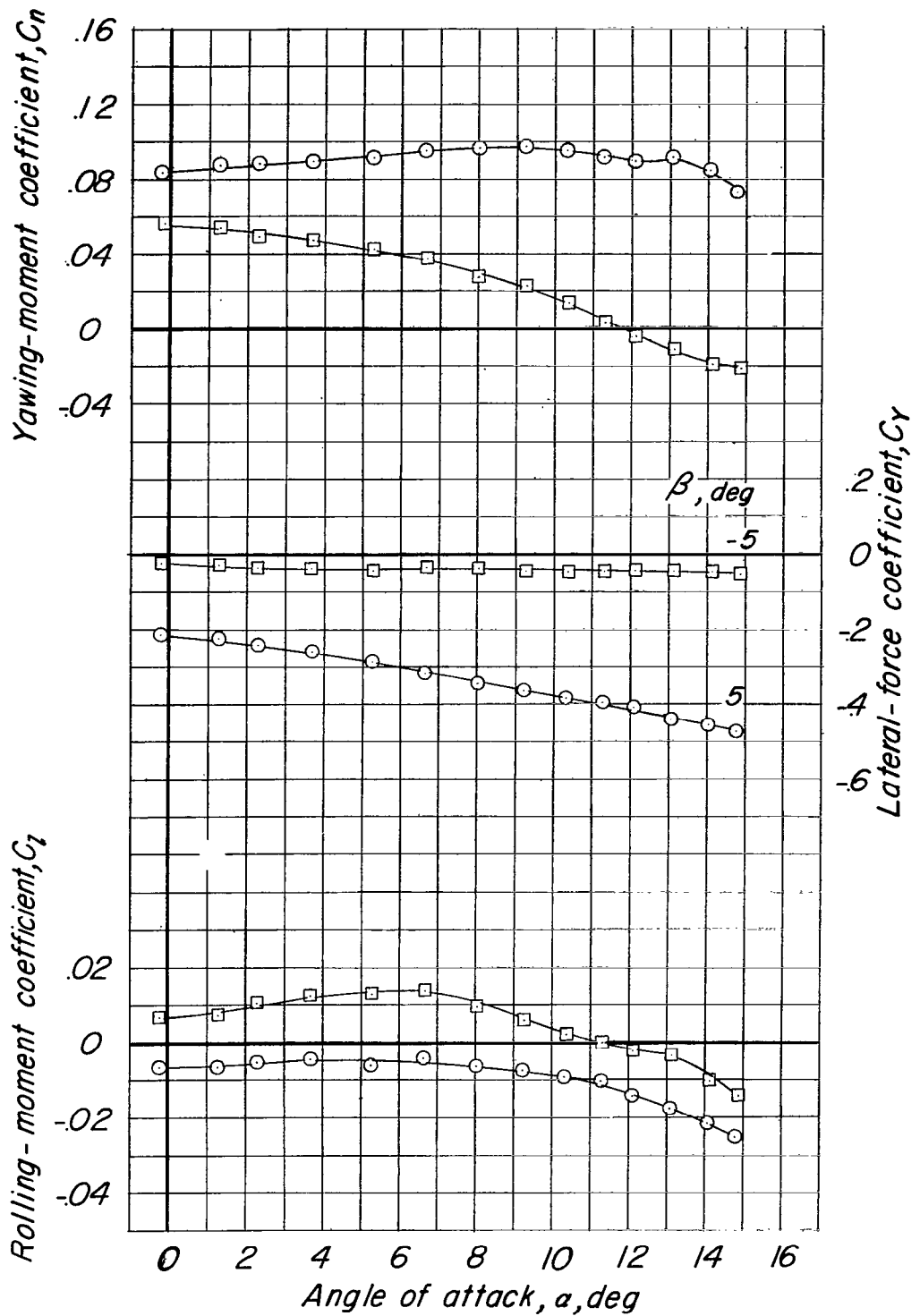
(a) $T_c = 0$; $\delta_f = \delta_a = \delta_r = 0^\circ$; $q = 12 \text{ lb/sq ft.}$

Figure 24.- Aerodynamic characteristics in pitch at $\pm 5^\circ$ sideslip. Clean configuration; zero canopy fin offset; $i_t = -2.48^\circ$.



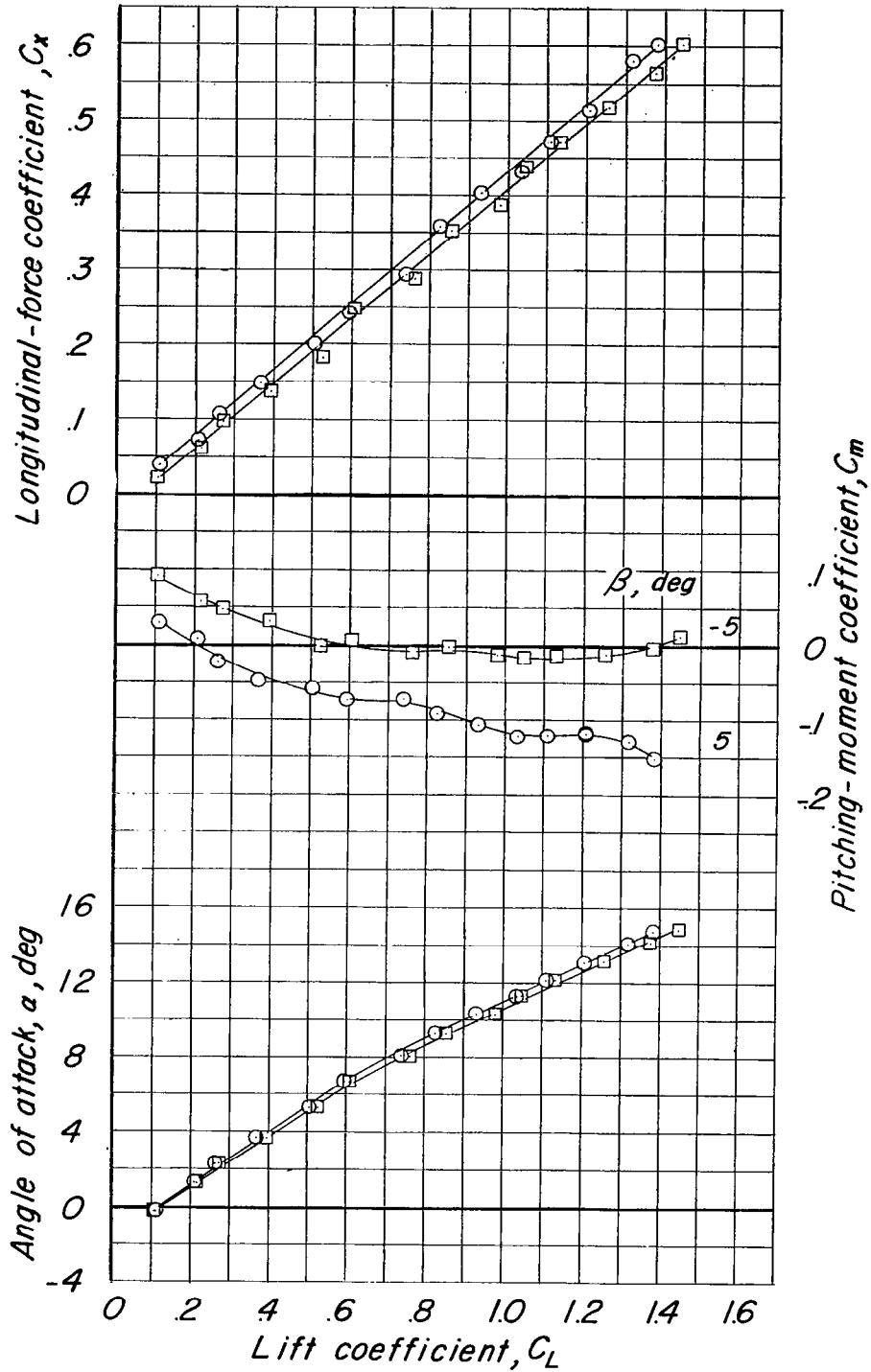
(a) Concluded.

Figure 24.- Continued.



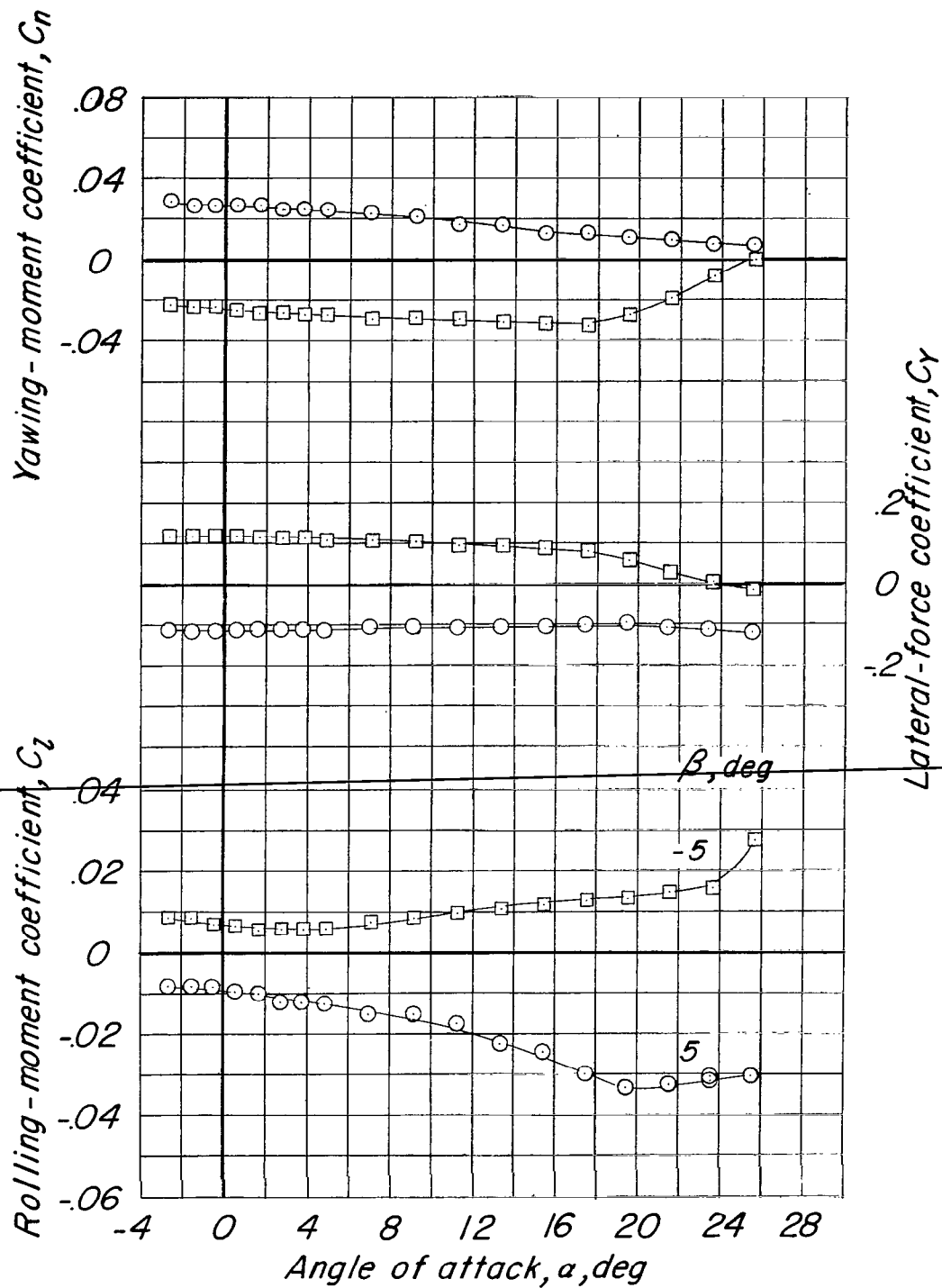
(b) Power A; $\delta_{f_L} = \delta_{a_L} = 5^\circ$; $\delta_{f_R} = \delta_{a_R} = -5^\circ$; $\delta_r = -20^\circ$; $q = 8$ lb/sq ft.

Figure 24.- Continued.



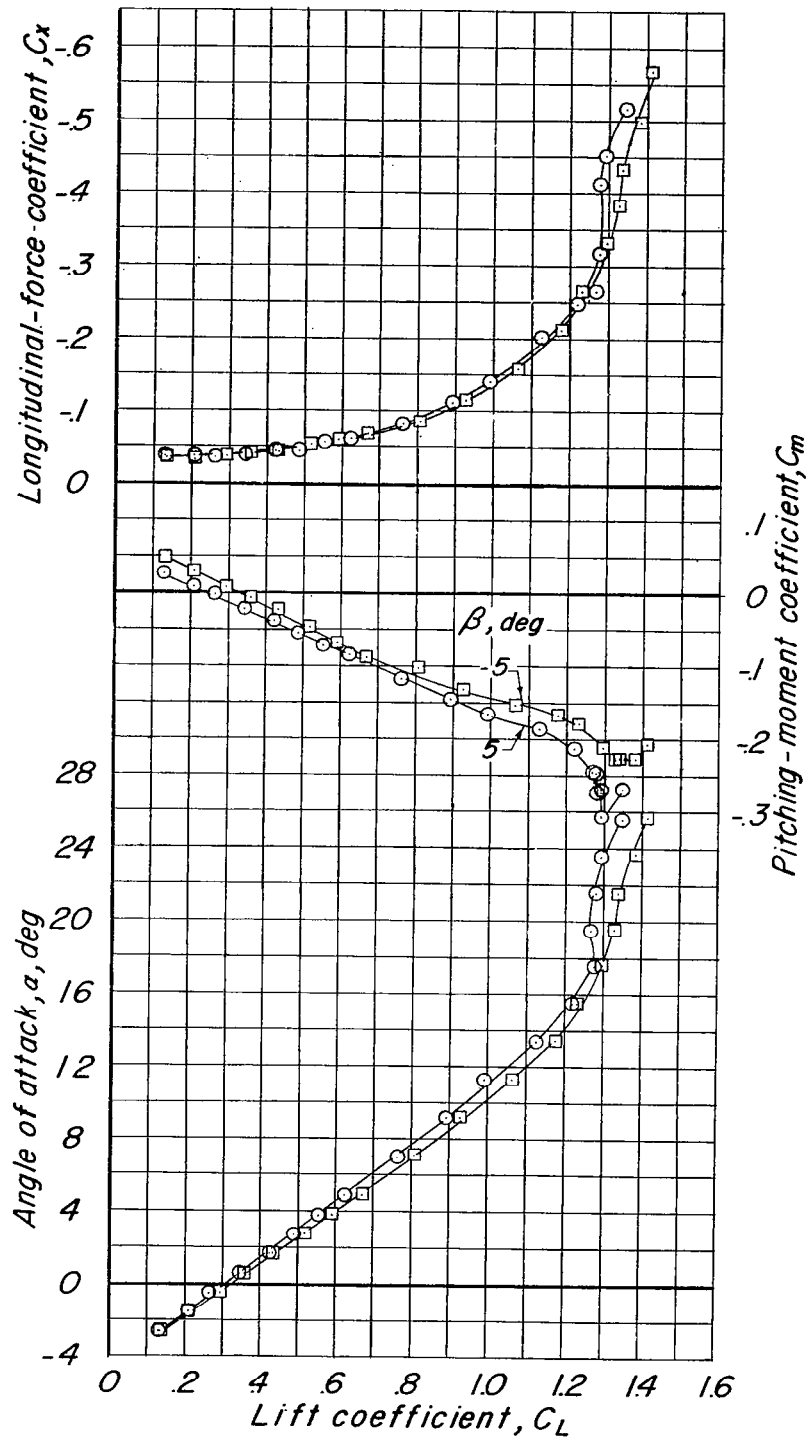
(b) Concluded.

Figure 24.- Concluded.



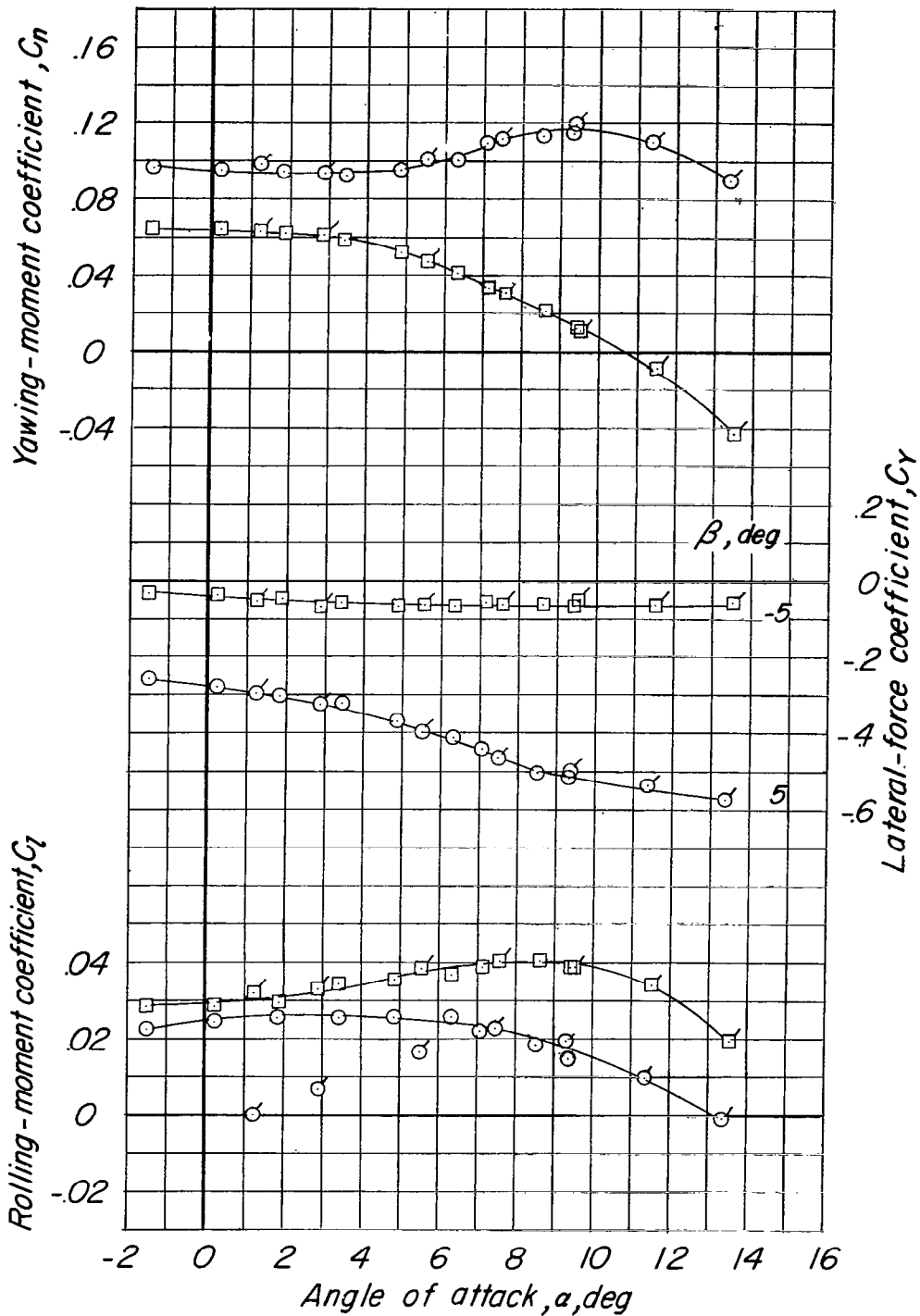
(a) $T_c = 0$; $\delta_f = 20^\circ$; $\delta_a = \delta_r = 0^\circ$; $q = 12$ lb/sq ft.

Figure 25.- Aerodynamic characteristics in pitch at $\pm 5^\circ$ sideslip. Take-off configuration; 10° canopy fin offset; $i_t = -2.48^\circ$.



(a) Concluded.

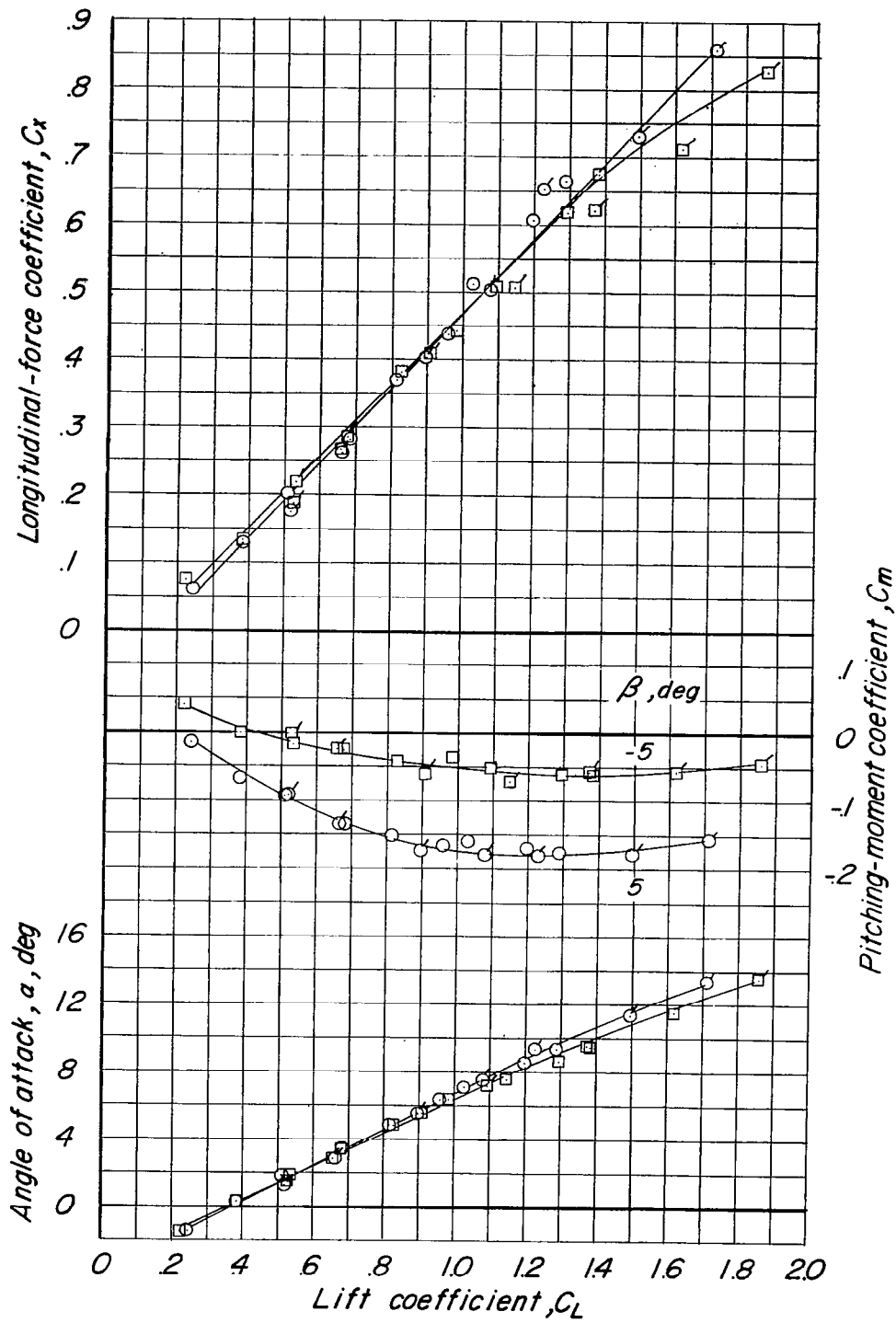
Figure 25.- Continued.



(b) Power A; $\delta_{f_L} = 30^\circ$; $\delta_{f_R} = 10^\circ$; $\delta_{a_L} = 18^\circ$; $\delta_{a_R} = -18^\circ$; $\delta_r = -20^\circ$;
 $q = 8$ and 6 lb/sq ft. Flagged symbols indicate data at $q = 6$ lb/sq ft.

Figure 25.- Continued.

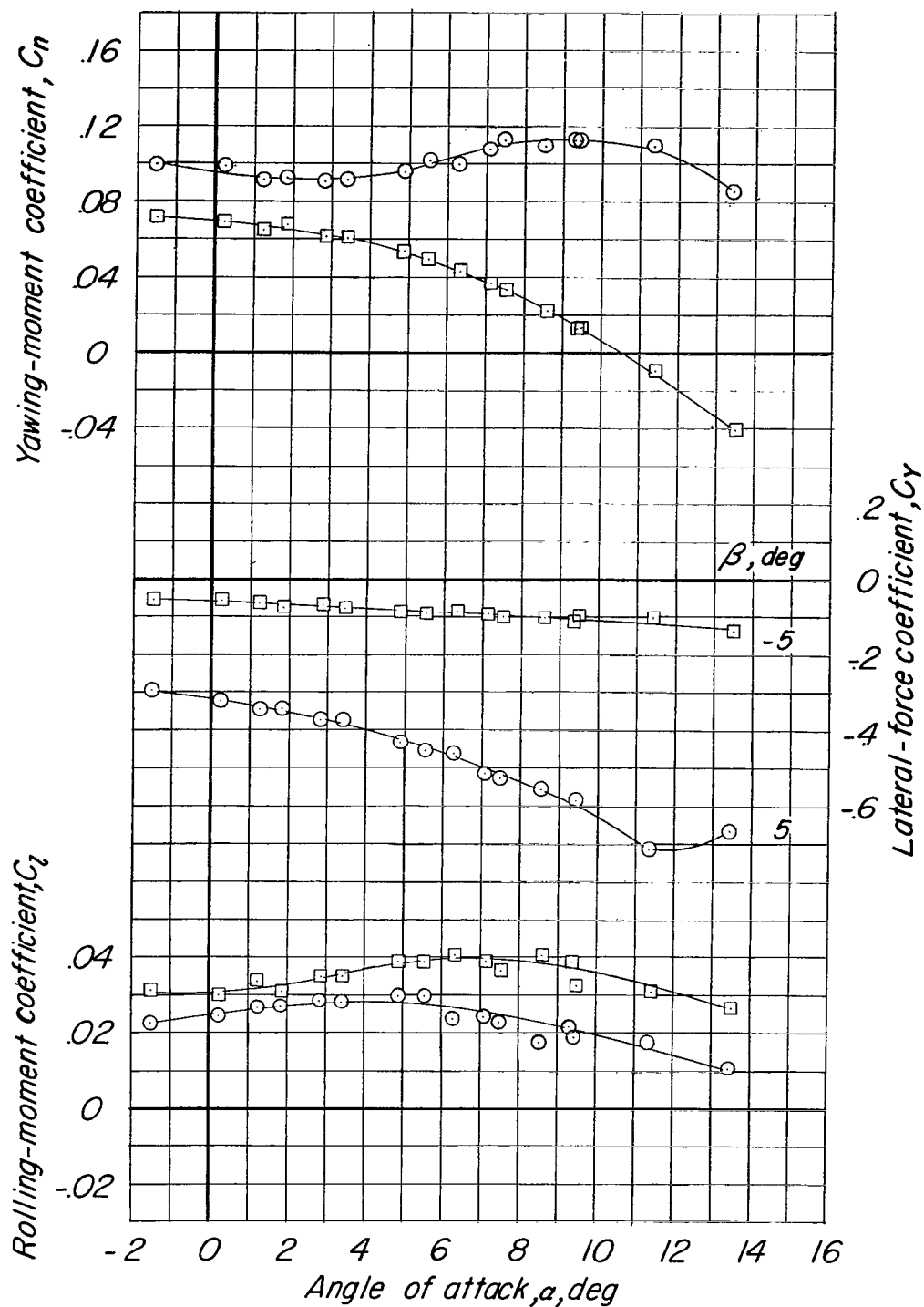
~~CONFIDENTIAL~~



(b) Concluded.

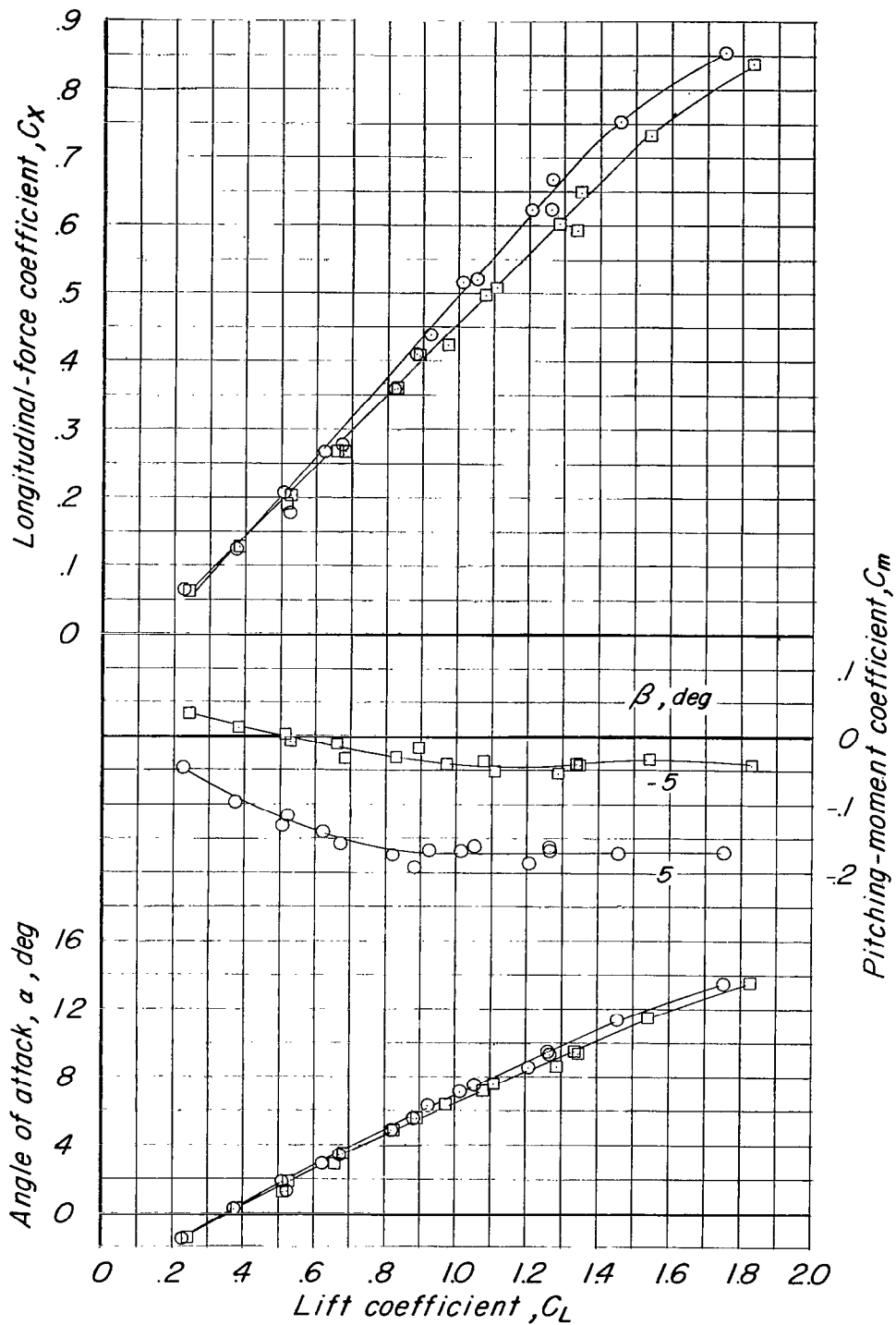
Figure 25.- Continued.

~~CONFIDENTIAL~~



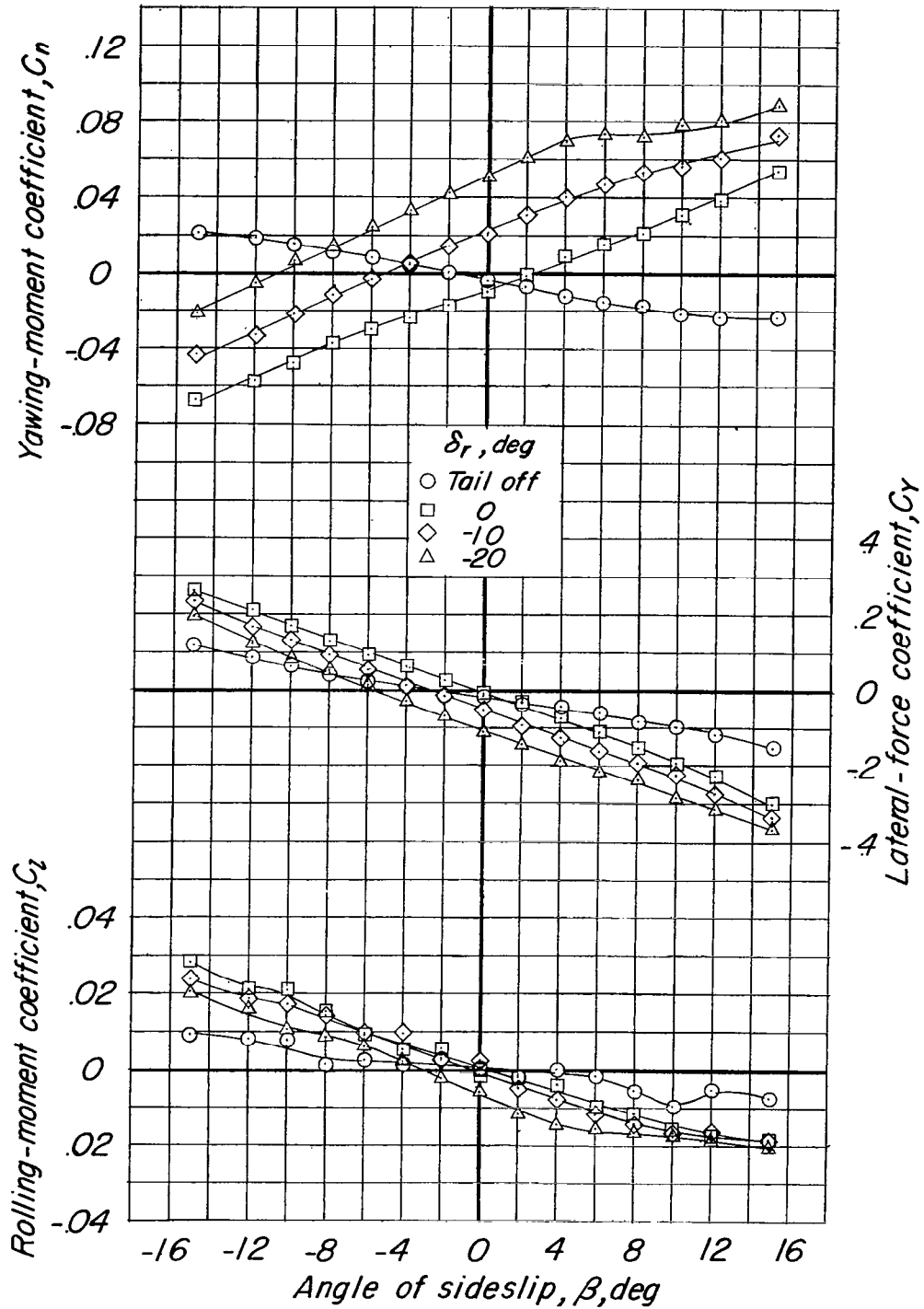
(c) Tanks on; power A; $\delta_{fL} = 30^\circ$; $\delta_{fR} = 10^\circ$; $\delta_{aR} = 18^\circ$; $\delta_r = -20^\circ$; $q = 8$ and 6 lb/sq ft. Flagged symbols indicate data at $q = 6$ lb/sq ft.

Figure 25.- Continued.



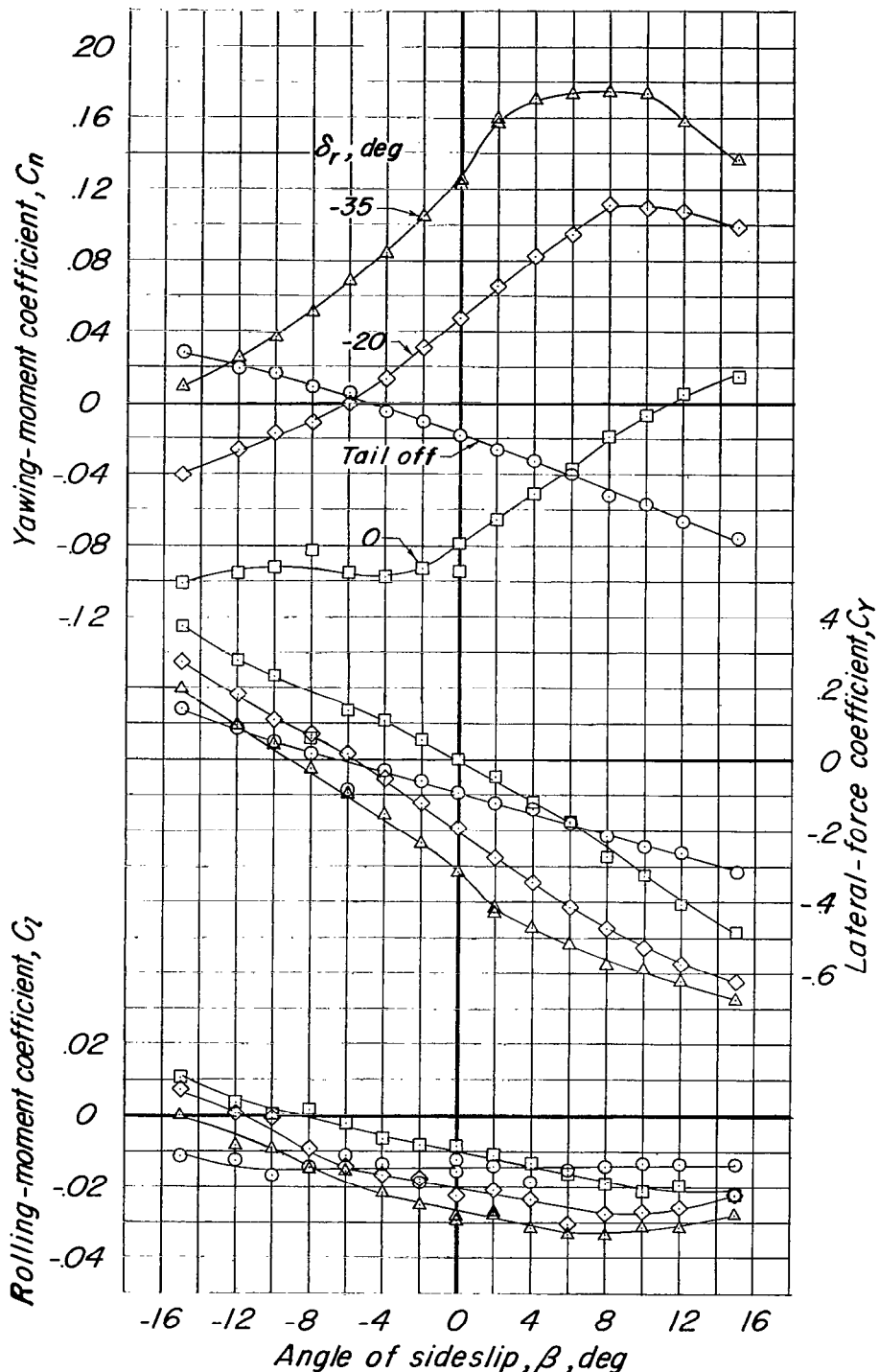
(c) Concluded.

Figure 25.- Concluded.



(a) $T_c = 0$; $q = 12$ lb/sq ft.

Figure 26.- Effect of rudder deflection on the lateral characteristics of the model in sideslip. Clean configuration; $\delta_f = \delta_a = 0^\circ$; $i_t = -2.48^\circ$; $\alpha = 10^\circ$.



(b) $T_c = 0.66$; $q = 8$ lb/sq ft.

Figure 26.- Concluded.

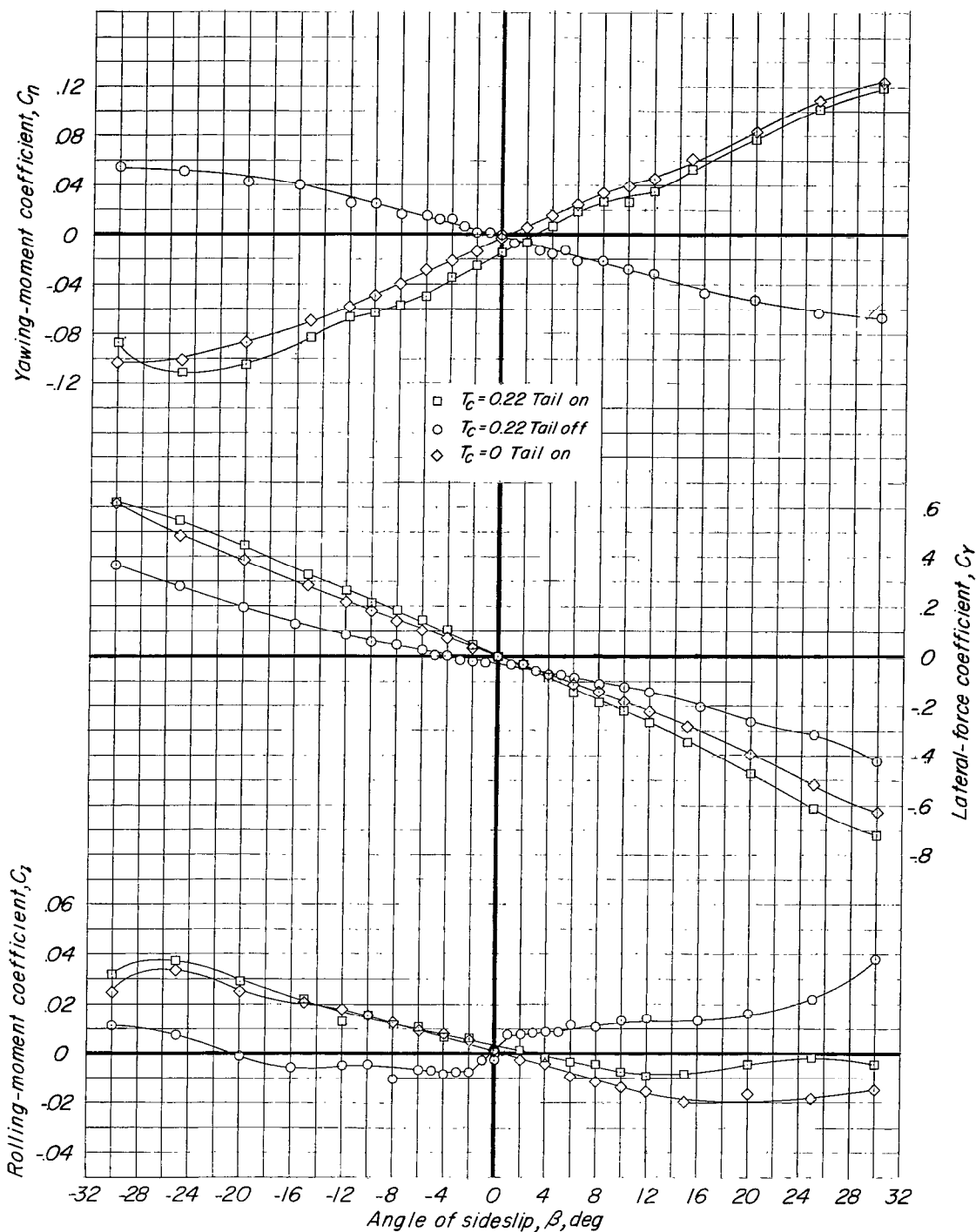
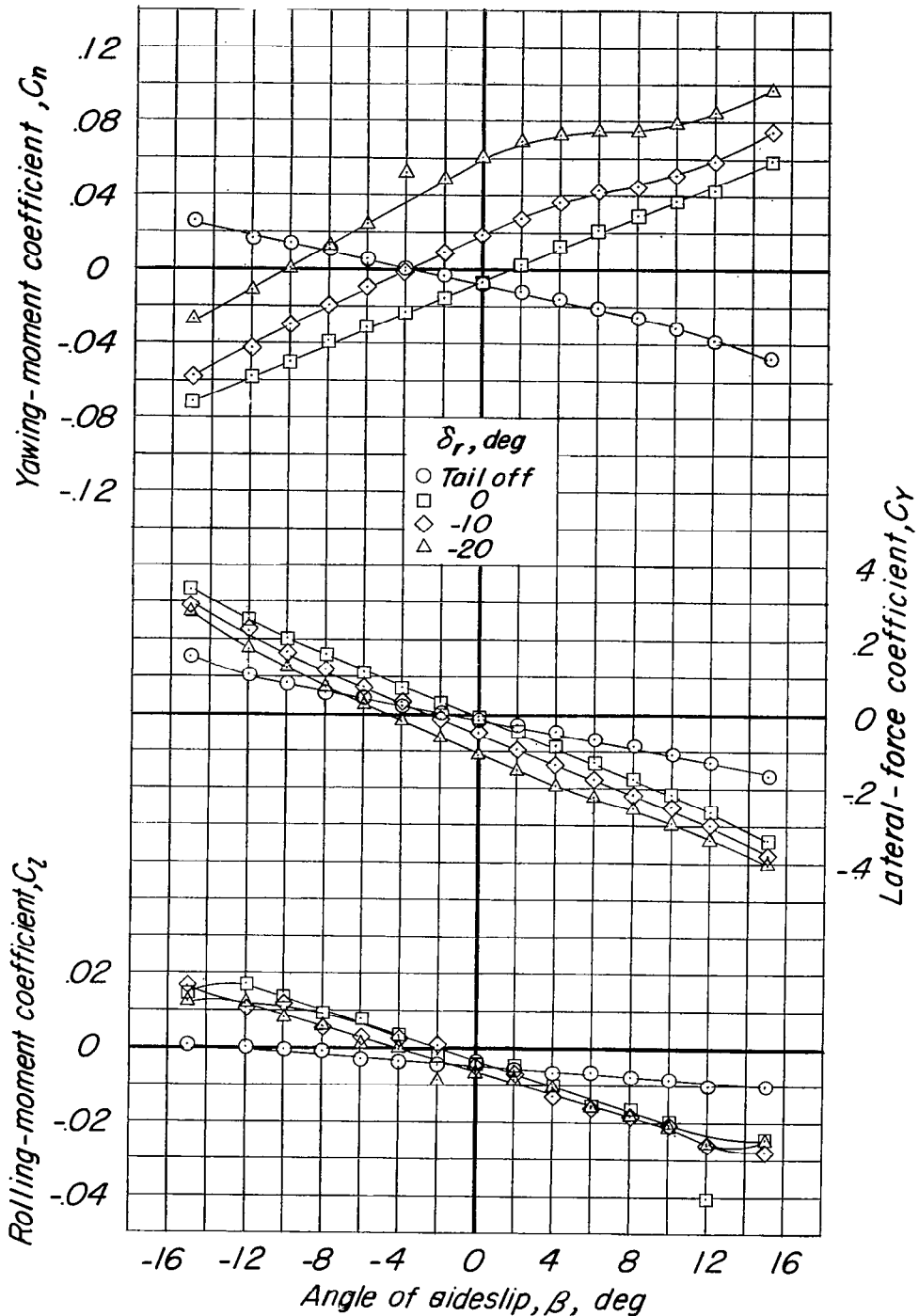
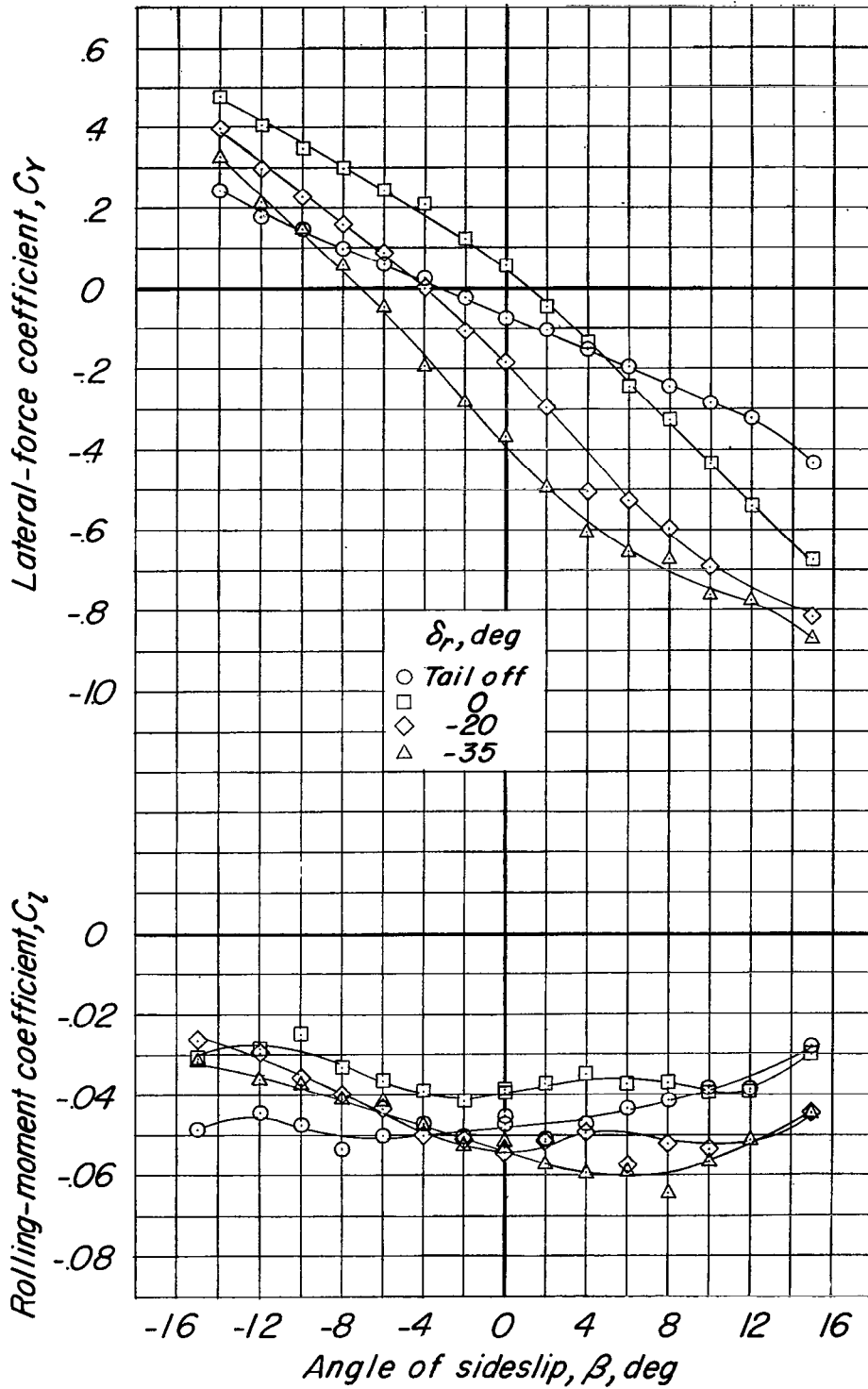


Figure 27.- Variation of lateral characteristics with sideslip showing the effect of the tail surfaces. Clean configuration; $\delta_f = \delta_a = \delta_r = 0^\circ$; $i_t = -2.48^\circ$; $\alpha = 3.6^\circ$; $q = 8$ lb/sq ft. Wing fence and leading-edge bulge off.



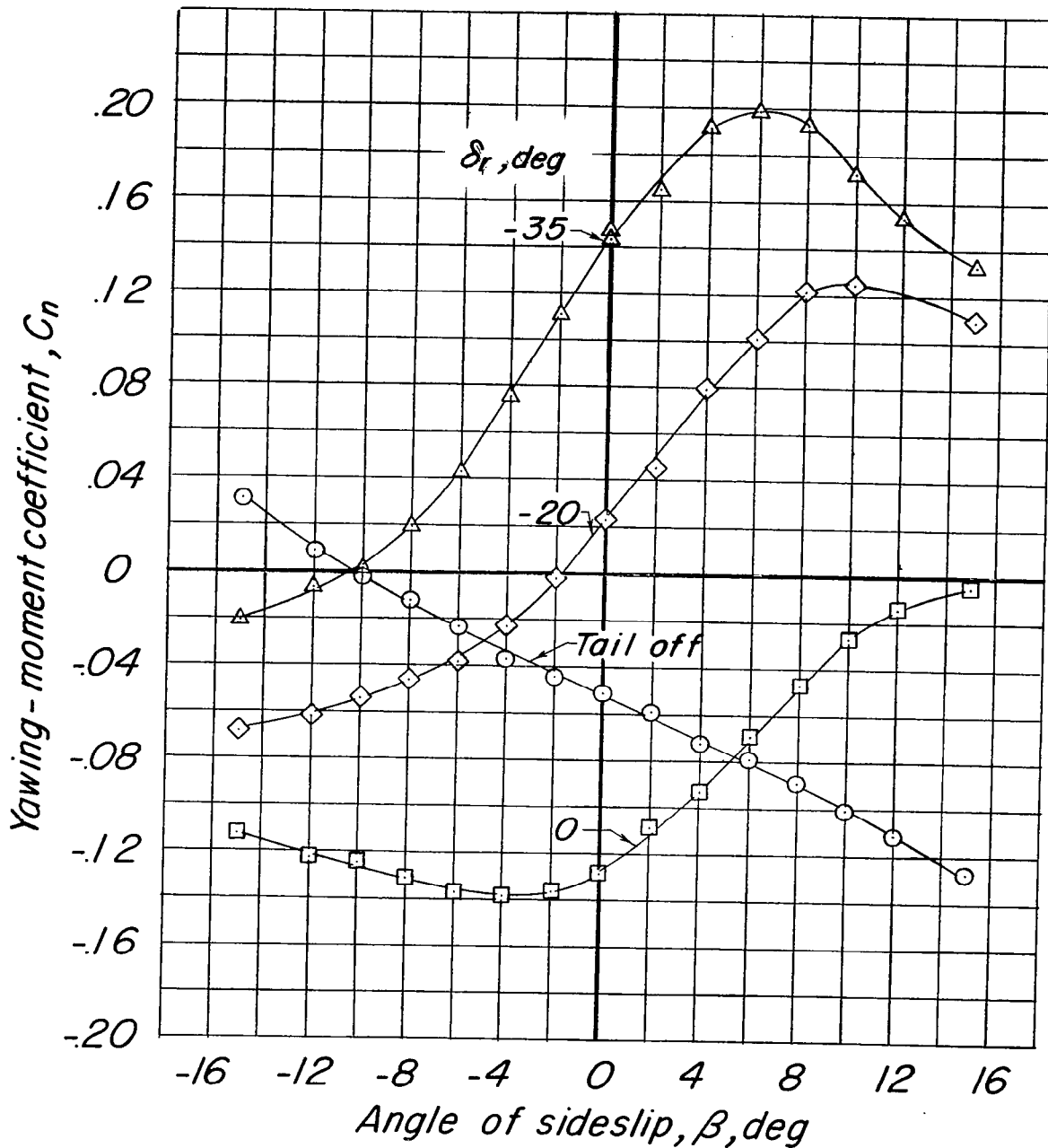
(a) $T_c = 0$; $q = 12$ lb/sq ft.

Figure 28.- Effect of rudder deflection on the lateral characteristics of the model in sideslip. Take-off configuration; $\delta_f = 20^\circ$; $\delta_a = 0^\circ$; $i_t = -2.48^\circ$; $\alpha = 11.3^\circ$.



(b) $T_c = 1.23$; $q = 6$ lb/sq ft.

Figure 28.- Continued.



(b) Concluded.

Figure 28.- Concluded.

~~CONFIDENTIAL~~

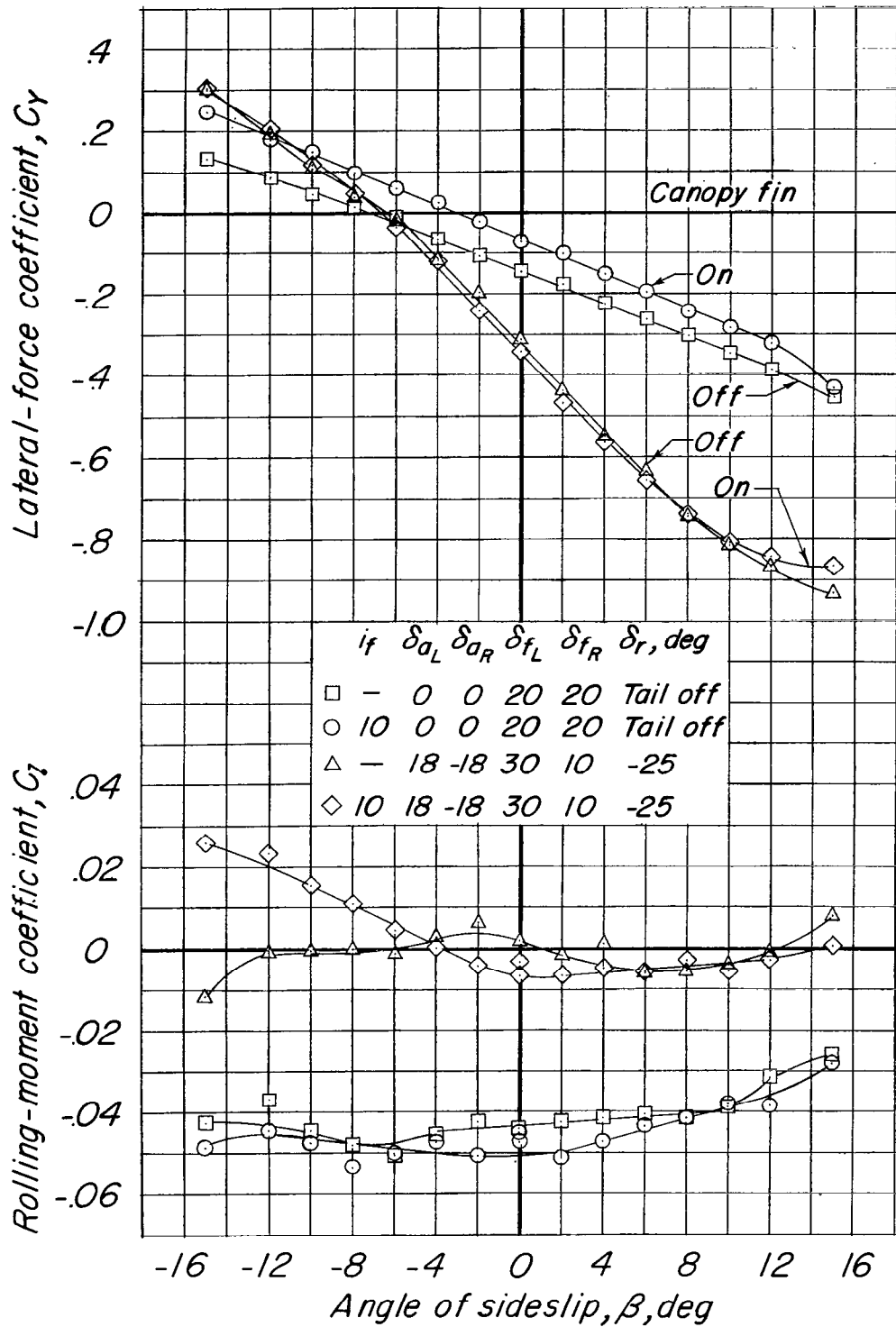


Figure 29.- Effect of the canopy fin on the lateral characteristics of the model with the propeller operating. Take-off configuration; $T_c = 1.23$; $i_t = -2.48^\circ$; $\alpha = 11.3^\circ$; $q = 6 \text{ lb/sq ft.}$

~~CONFIDENTIAL~~

	δ_{aL}	δ_{aR}	δ_{fL}	δ_{fR}	δ_r, deg	
□	0	0	20	20	Tail off	
○	10	0	0	20	Tail off	
△	-18	-18	30	10	-25	
◇	10	18	-18	30	10	-25

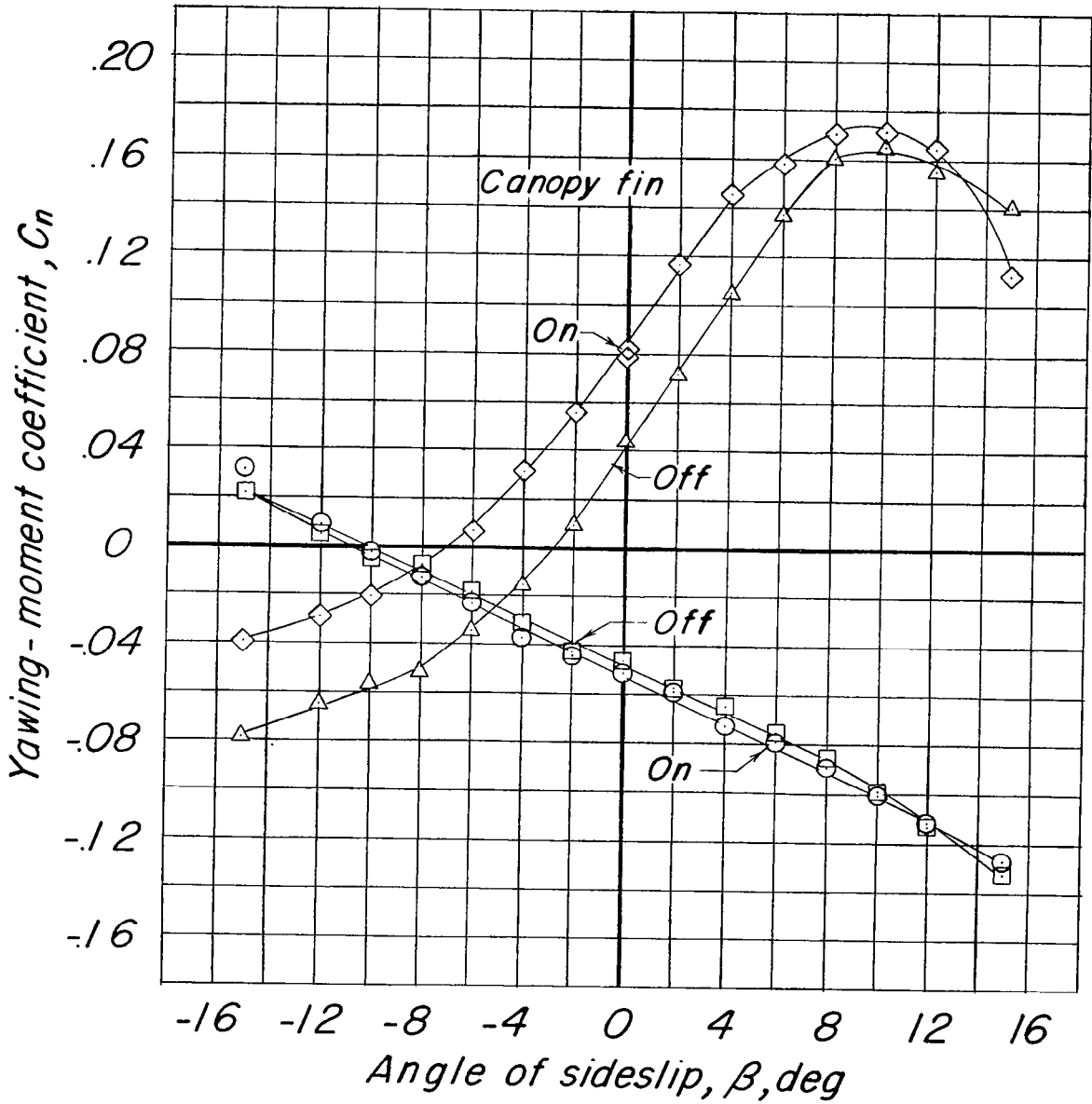


Figure 29.- Concluded.

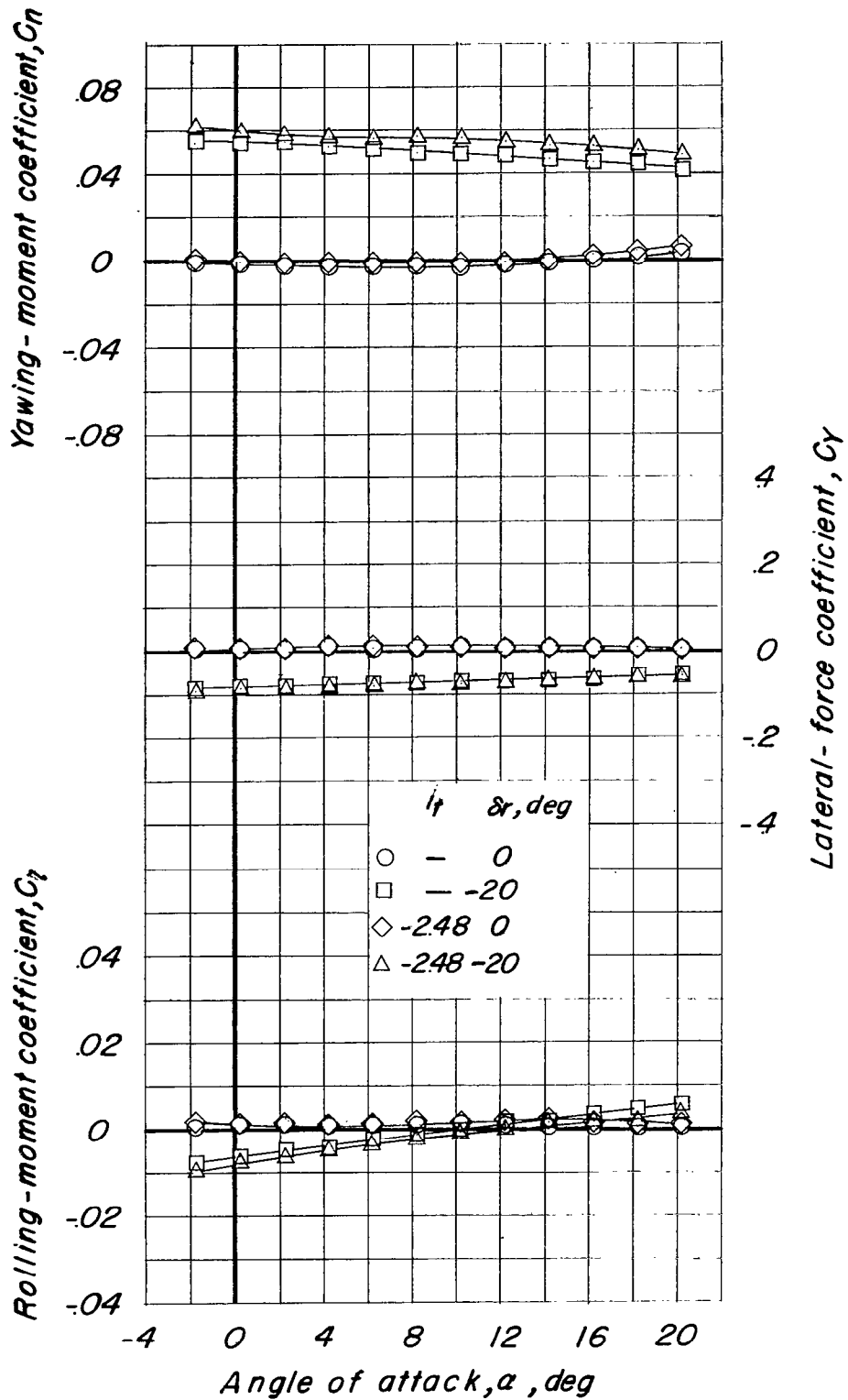


Figure 30.- Effect of the horizontal tail on rudder effectiveness at zero sideslip with the wing and propeller removed. $q = 40$ lb/sq ft.

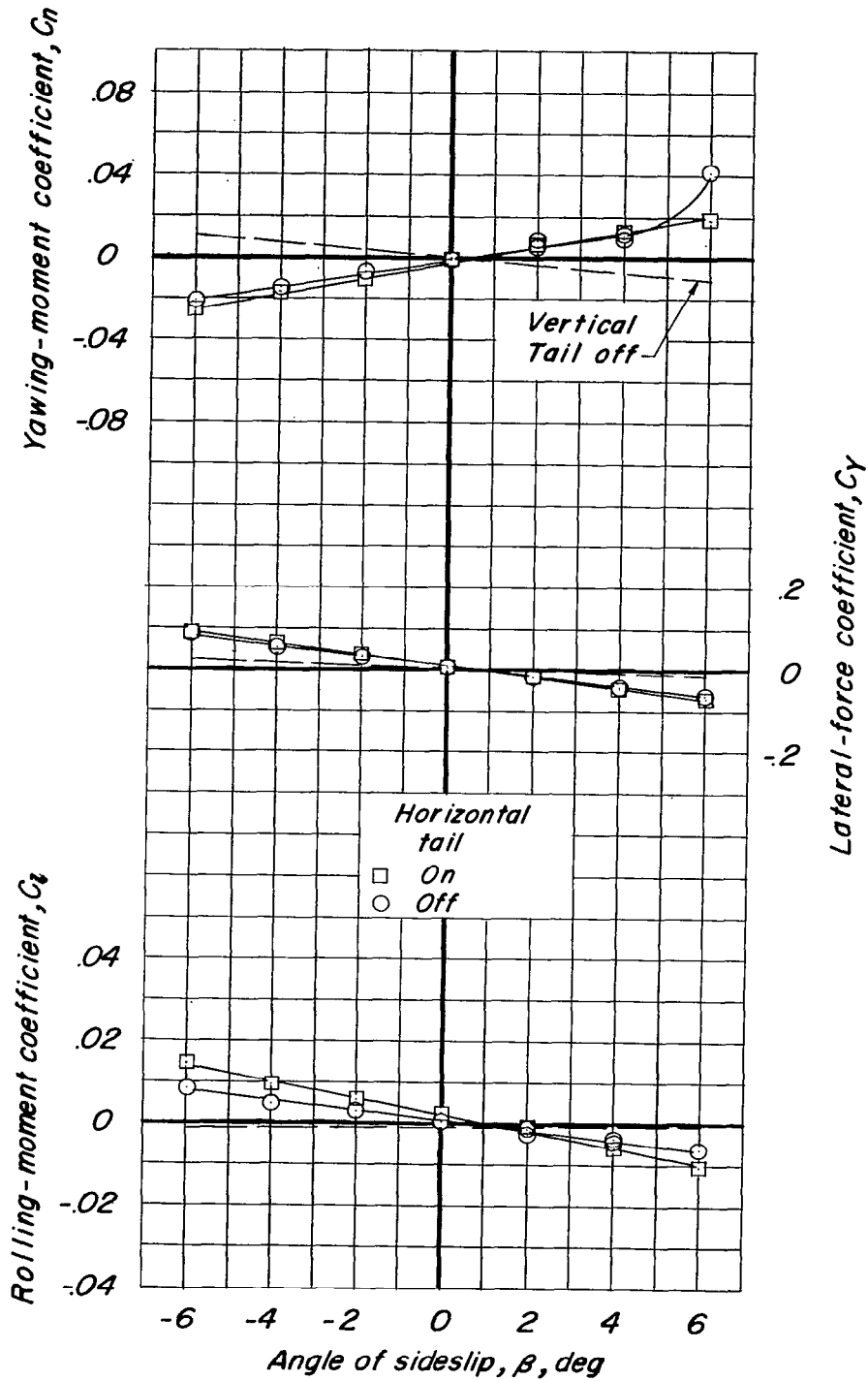


Figure 31.- Effect of the horizontal tail on the vertical-tail contribution in sideslip. Wing and propeller removed; $\alpha = \delta_r = 0^\circ$; $q = 40$ lb/sq ft.

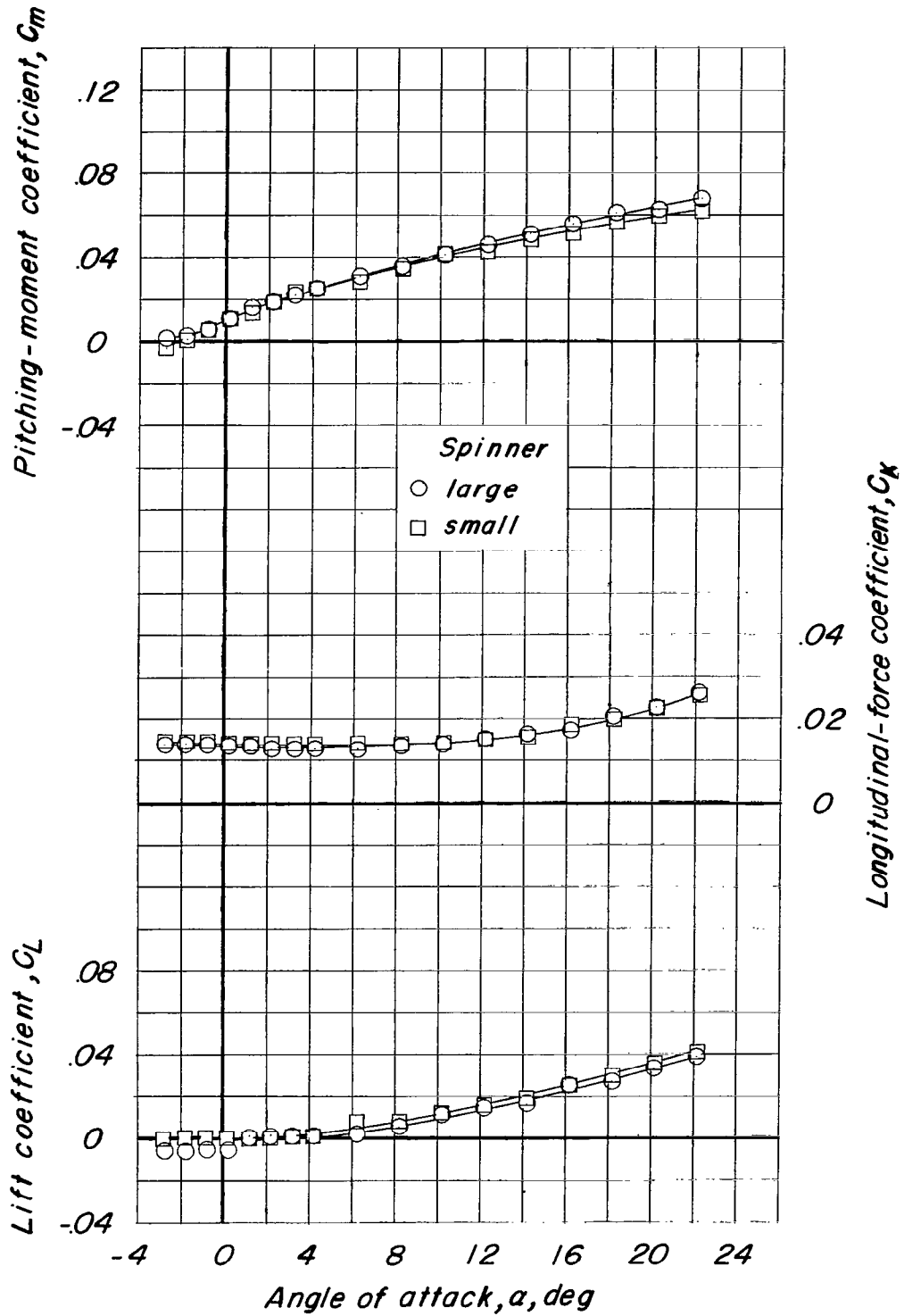


Figure 32.- Effect of spinner configuration. Large spinner is scale size and small spinner was used in all propeller-off tests. Wing, tail, and propeller removed; $q = 40$ lb/sq ft.

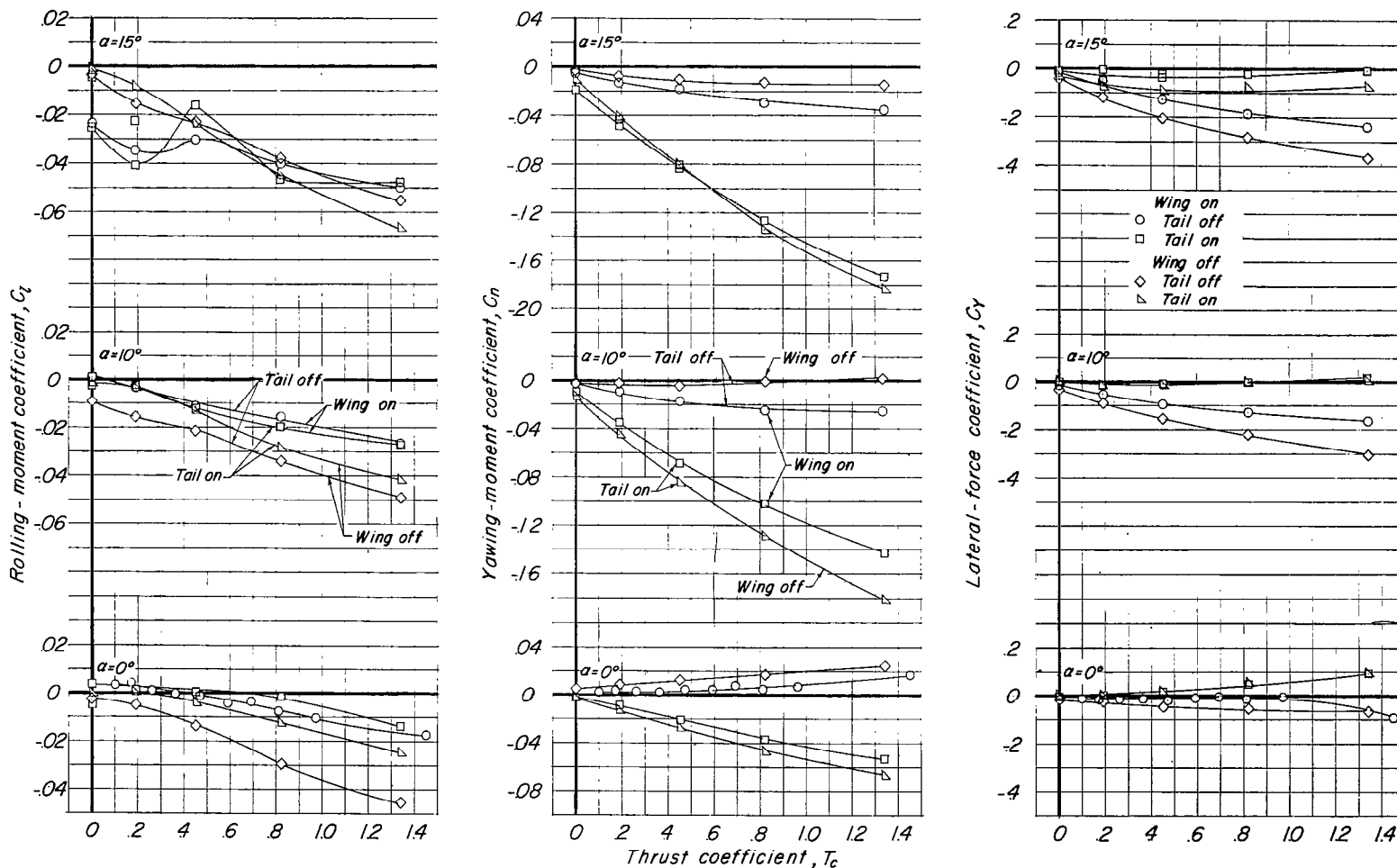
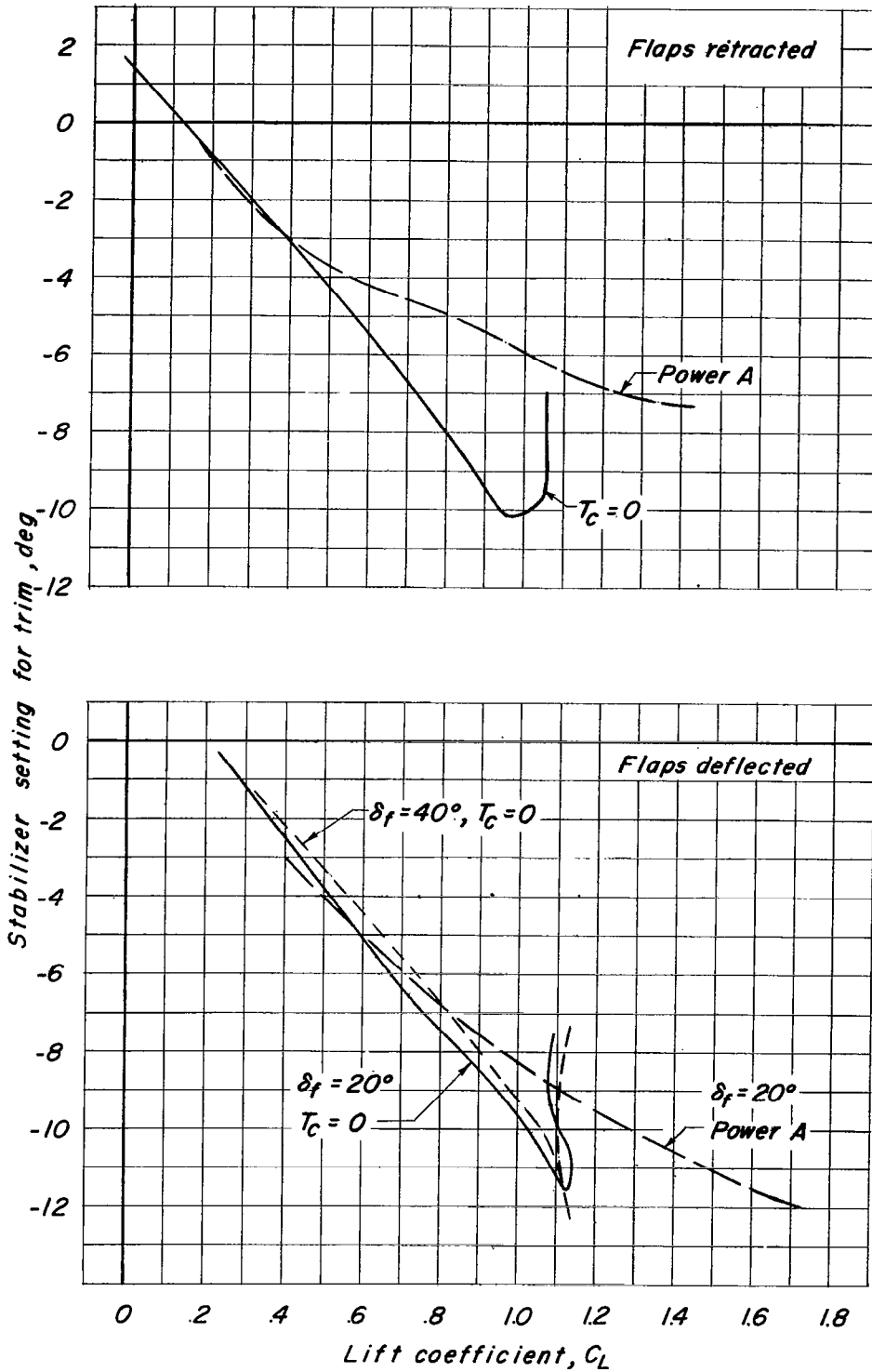


Figure 33.- Variation of lateral characteristics with thrust coefficient showing effects of the wing and tail surfaces. Clean configuration; $\delta_f = \delta_a = \delta_r = 0^\circ$; $i_t = -2.48^\circ$; $q = 6$ lb/sq ft.

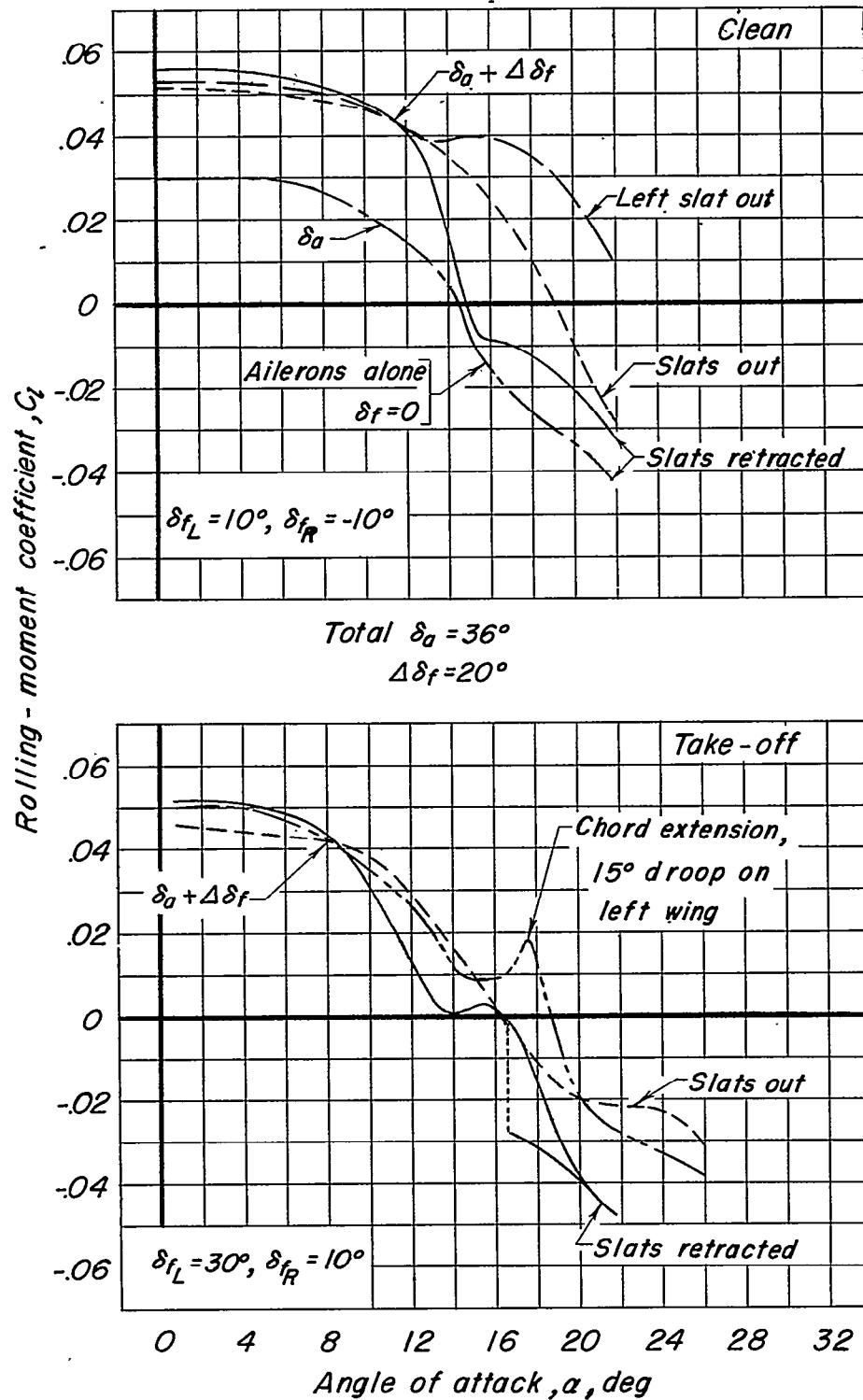
~~CONFIDENTIAL~~



(a) Longitudinal.

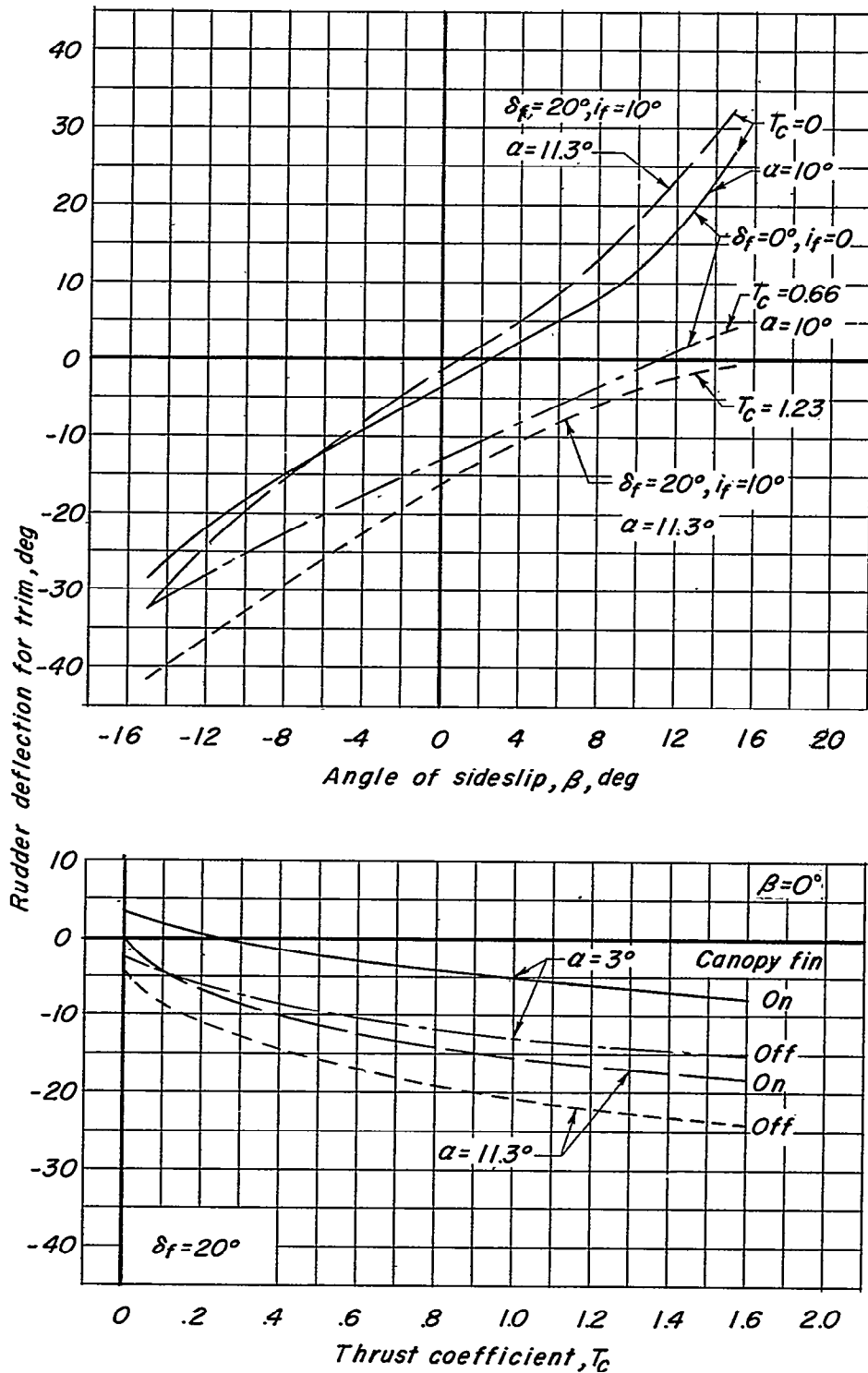
Figure 34.- Summary of model trim characteristics.

~~CONFIDENTIAL~~



(b) Lateral (full corrective control applied). $T_c = 0.81$.

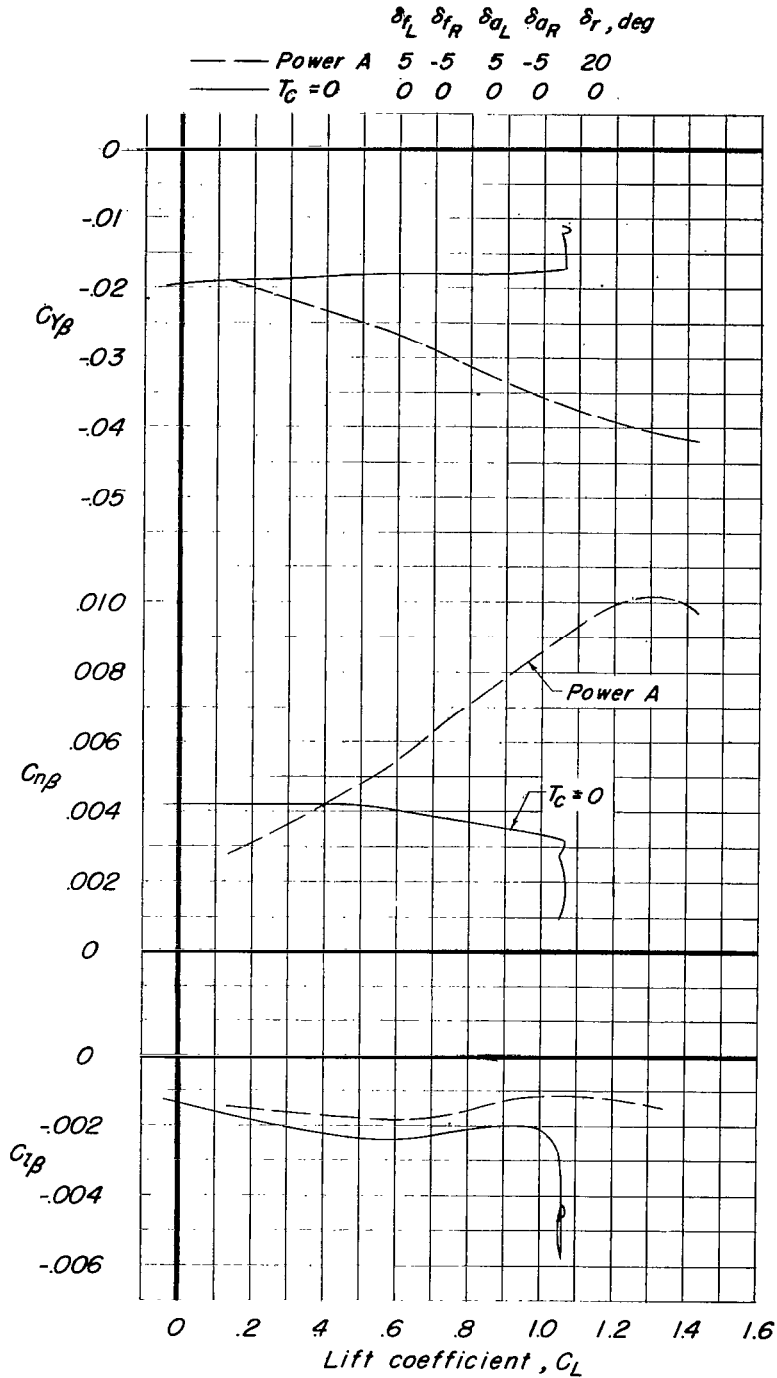
Figure 34.- Continued.



(c) Directional.

Figure 34.- Concluded.

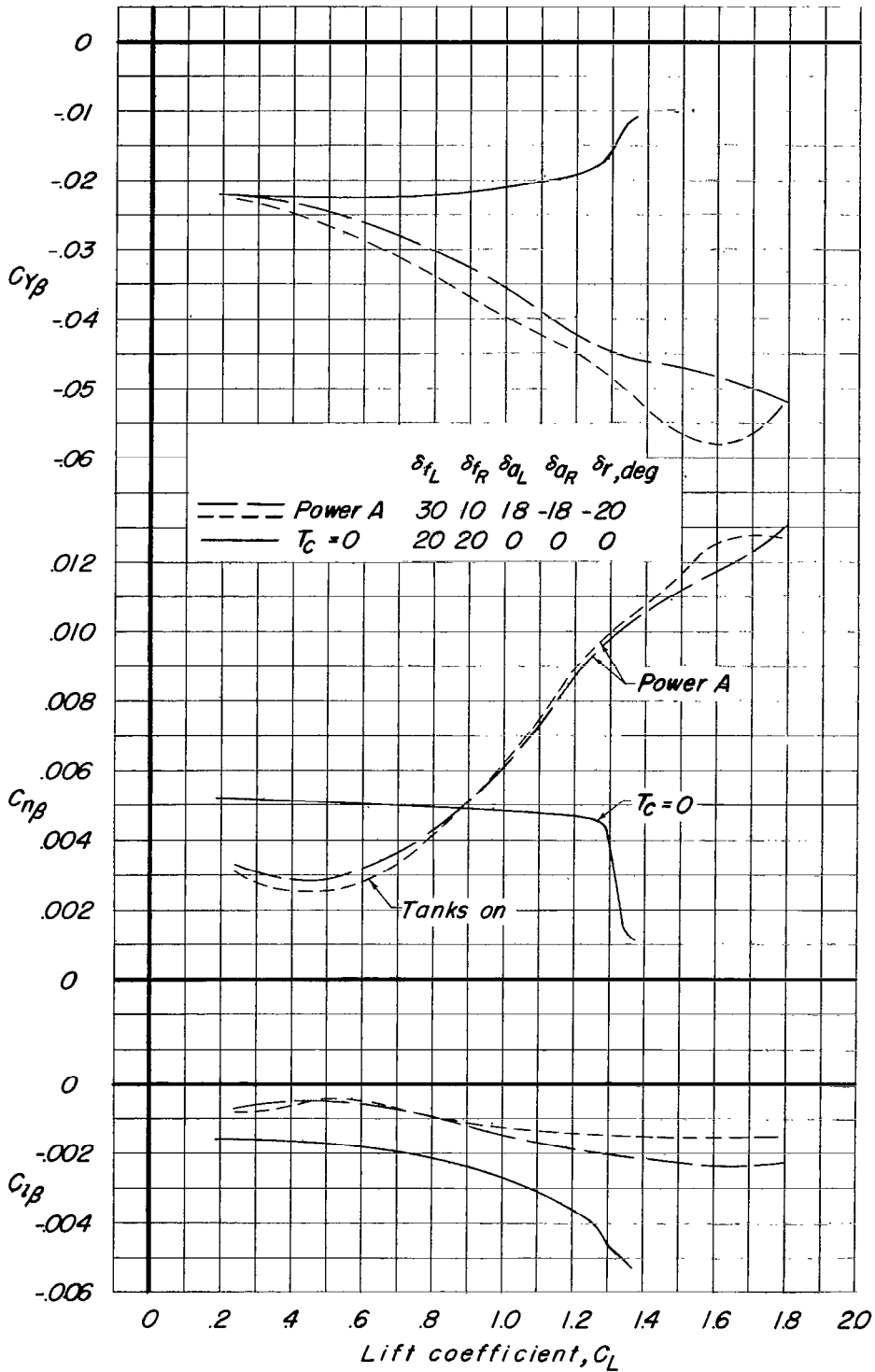
~~CONFIDENTIAL~~



(a) Clean configuration; 0° canopy fin offset.

Figure 35.- Lateral stability parameters obtained from tests at $\pm 5^\circ$ sideslip.

~~CONFIDENTIAL~~



(b) Take-off configuration; 10° canopy fin offset.

Figure 35.- Concluded.

SECU

NASA Technical Library



3 1176 01438 6644

MATION

~~CONFIDENTIAL~~